Acoustic Emission Monitoring

of Offshore Wind Turbine Support Structures for Detection and Localization of Fatigue Crack Growth

G.P.W. Lapoutre

TUDelft

Acoustic Emission Monitoring

of Offshore Wind Turbine Support Structures for Detection and Localization of Fatigue Crack Growth

by

G.P.W. Lapoutre

to obtain the degree of Master of Science
at the Delft University of Technology,
to be defended publicly on Wednesday August 23, 2017 at 9:30 AM.

Student number: 1361694
Project duration: September 1, 2015 – May 31, 2016
Thesis committee: Dr. ir. R. De Breuker,   TU Delft, committee chair
Dr. C. Kassapoglou,   TU Delft, supervisor
Dr. ir. P. L. Pahlavan,   TNO, supervisor
Dr. ir. O. K. Bergsma,   TU Delft

This thesis is confidential and cannot be made public until August 23, 2017.

An electronic version of this thesis is available at `http://repository.tudelft.nl/`.

TUDelft

Preface

This thesis is the result of my efforts at the Technical University of Delft, and is a demonstration of the level I have achieved. The process of writing the thesis has been one with ups and downs, but ultimately has resulted in a report of which I am proud.

This thesis could not have been completed without the help of a number of people. First, I would like to take this opportunity to thank my supervisor at TNO, Pooria Pahlavan, who supported me along the way and always was willing to help out when I got stuck. My mentor at the TU Delft, Christos Kassapoglou, who encouraged me, supported me, and helped me achieve my potential. Rob Jansen from TNO, and Gerrit Blacquière who supervised the project at TNO. I would like to thank Ger Hagen and Erwin Boer for their support during the many experiments I have performed.

I would also like to thank those that helped me, made me laugh, or were there whenever I needed them. My study time would have been a lot more boring without them. In no particular order: The Formula Student Team Delft, in which hard work, great pleasure and a lot of learning go hand in hand. Force Elektro, where I could always clear my mind after a long day of graduation work. Erwin, with whom I have spent many hours drinking coffee, beers and glühwein while discussing the important (and less important) matters in life. Thijs, who is always in for whatever idea you propose, such as a BBQ in January. My group of high school friends, A2, with whom I share many joyful moments. Vierkant voor Wiskunde, where I get to have a week of fun while helping out students and let them enjoy the wonderful world of mathematics. My parents, brother, sister, for always supporting me and raising me up to the person I now am. And last, but not least, Iris, who motivated me and makes me smile every day.

Contents

List of Figures

List of Tables

1

Introduction

The climate is changing, and the global average temperature keeps on rising. The Paris Climate Agreement aims at keeping the increase in temperature below $2°C$ above pre-industrial temperatures. This requires the use of renewables, of which wind energy is one of the major components. Wind energy has been associated with high costs, and in order to drive the costs down substantially, extensive research is being done on various aspects of design and operation of wind turbines. Fatigue is one of the major mechanisms that causes degradation of the structural strength, and visual inspections are currently performed to assess the structural health. This is especially important for offshore wind turbines as they are subject to heavy repeated loading, in a harsh environment with limited access. Mainly due to lack of experience with offshore wind turbines, rapid developments in this area, and assumptions on loading and structural degradation, some wind turbines are wearing down more rapidly than anticipated. This wear can come in the form of fatigue crack growth, which is a slow process, but can rapidly increase prior to failure, thus requiring periodical inspections. Replacement of conventional non-destructive inspection methods with quantitative structural health monitoring techniques could contribute to cost savings in the operational phase. Acoustic Emission monitoring is a potential candidate for this and allows for remote monitoring of fatigue crack growth, and can determine when and where fatigue crack growth is occurring. This can eventually reduce the need for periodical visual inspections and allow for a more cost effective maintenance strategy.

Acoustic Emission monitoring of offshore wind turbine support structures is a complicated multi-dimensional subject, which has not yet been sufficiently investigated. Complicating factors are mainly the generation of the acoustic emission signals when crack growth occurs, the leakage of signal into the water, and the different types of noise present on site. The different factors that influence the operation of the Acoustic Emission monitoring are schematically shown in figure 1.1. One of the key characteristics of the monitoring system is the coverage area of a sensor node. The coverage area can be calculated once the attenuation of the signal, the source signal amplitude, and the surrounding noise level are properly understood. In this thesis the attenuation rate of acoustic emission signals is studied using numerical simulations. The most restrictive sources of noise have been identified. Furthermore, the sources that were found to be most restrictive have been measured, using a setup in the laboratory or by performing field measurements, in order to predict the capabilities of the monitoring system in the field.

Before one starts installing acoustic emission monitoring systems on each and every wind turbine, it is important to determine whether it is worth the effort. This brings us to the main goal of this thesis: evaluate the feasibility of Acoustic Emission monitoring on offshore wind support structures. To reach this goal, a number of questions need to be answered. Operators would be mainly interested in the cost and benefits of such a system. The benefits depend on the savings that can be obtained by reducing the amount of inspections and by improvement of the operations, while the cost depends on the cost of the several components and the coverage area of the sensors. This thesis presents the steps that have been taken to find an answer to these questions and is followed by recommendations on the next steps.

The thesis starts with an introduction to the global wind energy market in chapter 2. The future plans are analyzed, showing the potential of (offshore) wind energy globally. The current situation and future
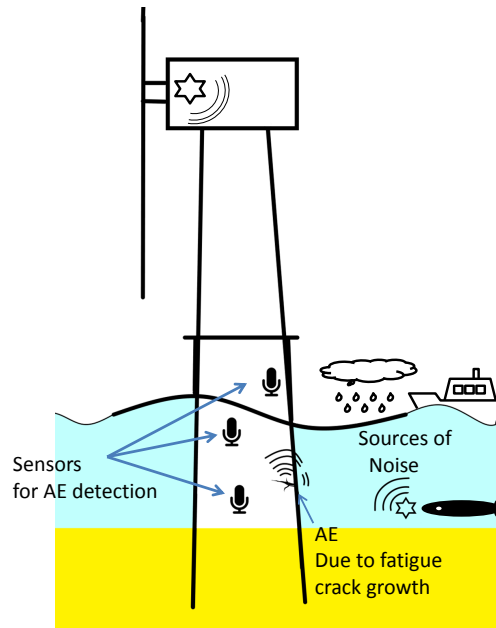
Figure 1.1: A schematic representation of an acoustic emission monitoring system on an offshore wind turbine foundation. When fatigue crack growth occurs, an acoustic signal is emitted, which can be picked up by the sensors. By analysis the source location can be determined when the signal is detected by 4 sensors. Noise, coming from the environment or from within the wind turbine, can limit the capabilities of the monitoring system. A combination of literature study, numerical simulations, and measurements provide the answers required for determining the capabilities of the acoustic emission monitoring system.

plans for the Netherlands are discussed in more detail. This shows the great potential that (offshore) wind energy has globally, and the necessity of further development and cost reductions in wind energy. The chapter finishes with a description of the different offshore wind turbine support structures. The fundamentals of acoustic emission are treated in chapter 3. In chapter 4, the current developments in acoustic emission monitoring are discussed as well as different simulation methods that can be used for the modelling of elastic waves in fluid-solid-media. The attenuation rate of acoustic emission signal is determined using Spectral Element Method (SEM) simulations in chapter 5. The attenuation rate helps in determining the coverage area of a sensor. A number of experiments have been performed, studying the localization accuracy, autonomous implementation of the analysis, noise in water and on wind turbines, the effect of curvature and surface quality of the structural members, and the behavior of a T-joint section which had fatigue crack growth occurring. The results and setup of these experiments are given in chapter 6. With the results from the experiments and the numerical simulation, an estimate is made for the coverage area of sensors. For scenarios of monitoring of a single wind turbine and monitoring a wind park, the costs and benefits are discussed in chapter 7. Ideas regarding the results and their reliability are shared in section 8, together with recommendations for further research. Chapter 9 concludes this thesis, and summarizes the results and conclusions that have been obtained during the research.

2

Wind Energy and Offshore Wind Turbines

Wind energy has been in use for many centuries. Initially it was used for transportation of boats over longer distances or operating machinery such as saws and water pumps. As electricity became more popular during the 20th century, wind energy became also a source of electricity production. During the past three decades wind energy has seen an exponential growth. This chapter treats what the wind energy market currently looks like, and takes a look towards the future of wind energy, in the Netherlands as well as globally. Next to that, the current developments in offshore wind turbine design are treated. This information can be used to establish the expected benefits from improved monitoring and maintenance, and to determine an acceptable cost for advanced defect monitoring systems.

Wind Energy

Wind energy started out as a source of electricity, mainly in remote areas and as a source of electricity for idealistic people and operators. They desired to be self-sustainable, which became more obvious after events during the seventies. As of the first and second energy crisis, in 1973 and 1979 respectively, it became clear that being dependent on fossil fuels was not desired. As of that moment, the wind energy market started to develop rapidly. Denmark was the first country to start a subsidized system in 1979, which has led to a wind energy market share of 12% in the year 2000 and up to 39% in the year 2014 [1]. The goal set by the Danish government is to have 50% of electricity production from renewables in 2020 and to have 100% of electricity consumption and heating based on renewables by 2035.

With its large share of wind energy, Denmark is unique in the world. The global energy production totals 22,668 TWh [2], while wind energy totals only 520 TWh [3], a share of 2.2%. The growth of wind energy production has been exponential from 1990 until 2010, as can be seen in figure 2.1. The wind energy market is maturing, and the rapid growth is starting to stabilize, as the growth in yearly installed capacity is slowing down, as shown in figure 2.2. It has to be noted though, that this decline does coincide with financial crisis. In order to keep costs down, wind turbines should be installed at locations with favorable wind conditions. As the wind energy market develops, more and more of these locations become occupied. The capacity factor (defined as the ratio of actual electricity production over theoretical maximum production) for onshore wind turbines typically lies around 20%. The capacity factor for offshore wind turbines might give a capacity factor of up to 60%. The Danish offshore wind farms have a capacity factor ranging from 19% up to 52%, while the average capacity factor reached 46% between October 2014 and September 2015. Unlike more conventional sources of electricity, wind energy is only available when there's wind, and may vary from hour to hour. This dependence on an uncontrollable resource has caused some concern regarding the reliability of the energy grid. The large share of wind energy does not cause notable issues regarding grid reliability in Denmark. There is no consensus on whether a large share of renewables Europe-wide would cause grid reliability issues.

Wind energy was first used for electricity production in Europe and the United States. Nowadays, the former developing countries are greatly investing in wind energy, with China taking 48.5 % of newly

3
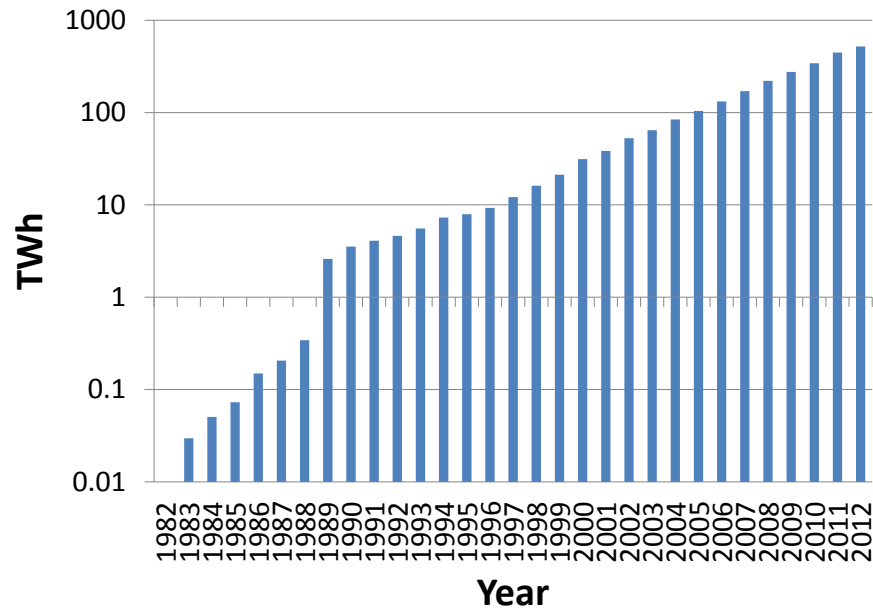
Figure 2.1: Global electricity production by wind (TWh) showing the growth of total electricity produced by wind turbines until 2012. On average, the increase in capacity is 40% per year from 1983 until 2012, or 26% per year from 1990 until 2012. [3]
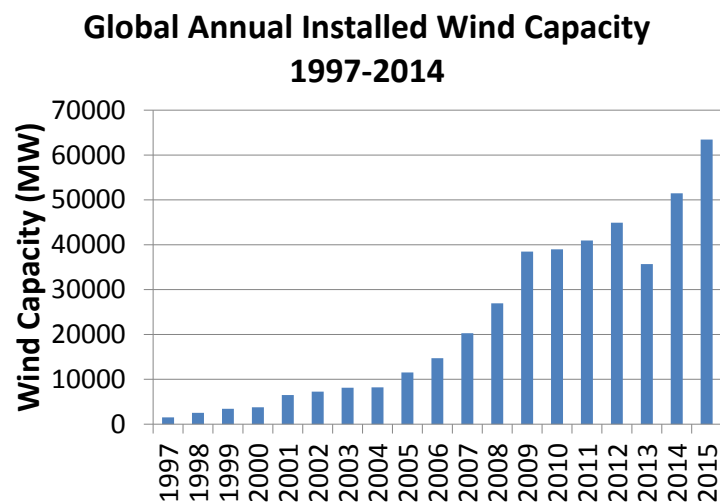
Figure 2.2: Total wind energy capacity installed annually, showing a rapid growth until 2009, becoming more of a constant growth during recent years. [4]

Top 10 Cumulative Capacity (end 2015)
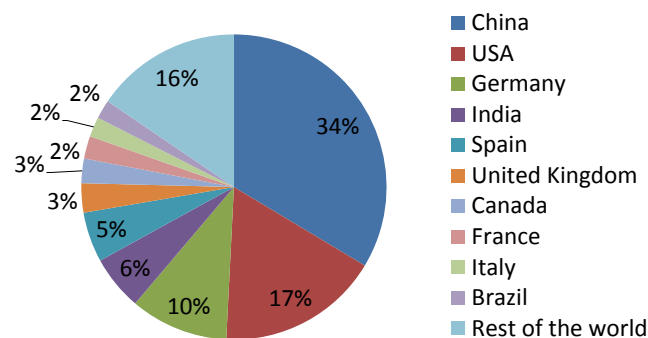
Figure 2.3: Distribution of installed capacity in top 10 countries with largest installed capacity. Total capacity installed worldwide is 432 GW. [4]

Top 10 New Installed Capacity 2015
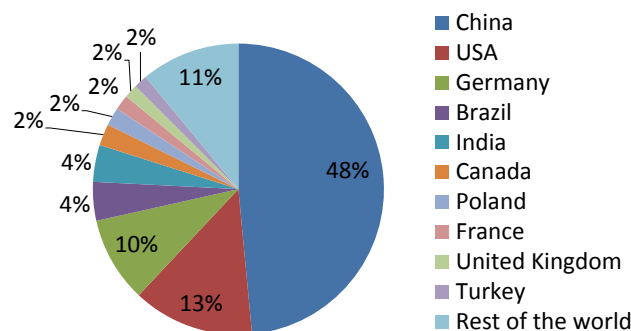
Figure 2.4: Distribution of added wind energy capacity in 2015. Total capacity added globally: 63 GW. [4]

installed capacity in 2015, as can be seen in figure 2.4. China has reached their position by large investments, which also shows in the list of largest wind turbine suppliers in figure 2.5. The continuous growth in installed capacity can be achieved by installing more wind turbines, and/or by installing larger wind turbines. The average capacity of the wind turbines that have been installed in 2014 was equal to 1958 kW [5]. This growth in average installed wind turbine size is not yet expected to level off, as turbine capacities go up to 7.5 MW. Development of more energy efficient techniques, such as direct drive generators, are also taking an increasing share of wind turbines, of up to 28 % in 2013. In order to reduce the use of land space, more wind turbines are being built offshore. The percentage of newly installed capacity offshore has increased from 1.5% in 2004 up to 12.6% in 2014 [6]. Most of the offshore capacity is currently located in Europe, while China has just surpassed Europe in 2015 in having the largest onshore capacity. Wind energy is expected to increase, both onshore and offshore, greatly in the coming 35 years, as can be seen in table 2.1

Before these wind turbines are built, someone has to pay for them. China's plan to build up to 1 GW by 2050 is estimated to cost 1.9 trillion dollars [7]. Europe has plans of a similar level of ambition, but focuses more on offshore wind energy. The European Wind Energy Association estimates that between 367 billion Euro and 591 billion Euro is required over the period 2015 until 2030. Plans are to install an equal amount of wind energy capacity both onshore and offshore. Currently, the cost per installed capacity for offshore wind turbines is twice that of an onshore installed wind turbine. This difference in price is expected to remain as accessibility and construction of an offshore wind turbine are more difficult than that of onshore wind turbines. The cost of wind energy for the time period 2030-2050 has been estimated by extrapolating the numbers. The USA expects to spend 70 billion dollars

Top 15 wind turbine suppliers in annual global market 2015
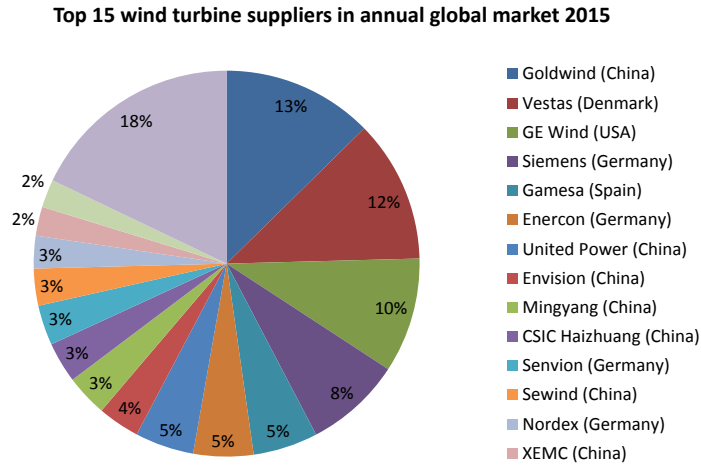
Figure 2.5: Market share of top 15 wind turbine suppliers in 2015 [4]

Table 2.1: Ambitions on future wind turbine capacity. All numbers are given in GW

Region	2014	2020	2030	2050
China Near Offshore	0.7	30	60	150
China Far Offshore	0	0	5	50
China Onshore	113.9	170	335	800
China Total	114.6	200	400	1000
USA Onshore	66	110	202	318
USA Offshore	0	3	22	86
USA Total	66	113	224	404
EU Onshore	120	190	250	460
EU Offshore	8	40	150	460
EU Total	128	230	400	920

Table 2.2: Investments required to achieve previously stated ambitions. Numbers are in billions

Region	2010-2020	2020-2030	2030-2050	2010-2050
China Total				$ 1 900
USA Total				$ 1 800
EU Onshore		€ 158	€ 400	
EU Offshore	€ 120	€ 316	€ 890	
EU Total		€ 474	€ 1 290	

per year on wind energy by 2050 [8]. Repowering and operational expenses are included in the cost figure given for the USA, while this is not included in the numbers given for Europe or China. It is estimated that the difference between including or excluding repowering would be approximately 40%. Assuming that the investment grows linearly from 2013 to 2050, and with an investment of 36 billion dollars in 2013, the total investment in wind energy during this period would total 1.8 trillion dollar. The total expected investment up to 2050 for the three largest wind energy markets, being China, Europe and USA, is expected to be approximately 6 trillion dollars. The estimate is based on current ambitions stated by these governments, and can be subject to adjustments depending on global developments in opinion and technology. Historical estimates on the development of renewables as a source of energy production have always greatly underestimated the developments. The International Energy Association estimated in 2000 that by 2010 solar and wind energy would achieve a installed capacity of 25 GW in North America. In 2010 the actual installed capacity in the United States alone reached 59 GW, a difference of more than 50 %. Although the wind energy market is maturing and becomes more predictable, the estimated numbers for 2050 can still be off by a margin of 50 %.

Future Dutch Wind Energy

So far, a rough estimate about the global future of wind energy has been given. This also gives a view of what can be expected in Europe as a whole. In order for this to be achieved, every member state has to do its share. In this section, the Dutch situation is further analyzed; what are the plans regarding wind energy, what locations are appointed for wind energy developments, and what are the costs associated with these plans. The information that has been used is of 2015 and currently accurate, however, developments can go very rapidly and governmental plans may get readjusted frequently.
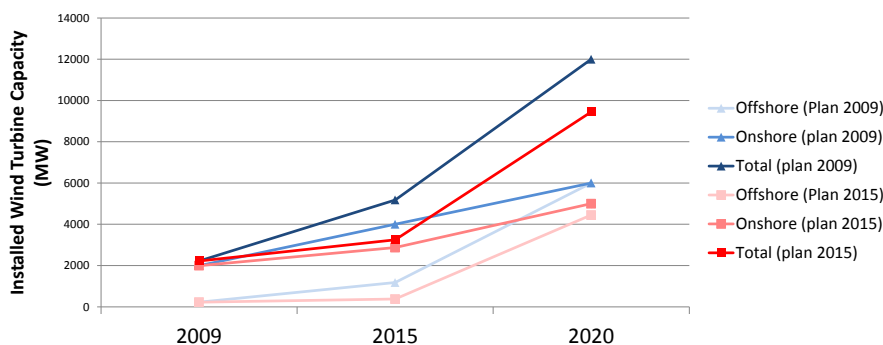
Figure 2.6: The difference in plans regarding wind energy in the Netherlands after 6 years. Ambitions of 2009 have not been met, and future plans have been decreased with respect to the original plan [9] [10] [11] [12]

In figure 2.6 and table 2.3, it can be seen how the projections have varied between 2009 and 2015 and what actually has been achieved of the initial plans. Initially, the goal of the government was to have a total of 6 GW installed by 2020. Although all provinces have given their cooperation to this plan, not all of them are on track with meeting the numbers. When the 6 GW of onshore power is achieved, the plan is to maintain this capacity until 2050. Any further increase in wind energy production should
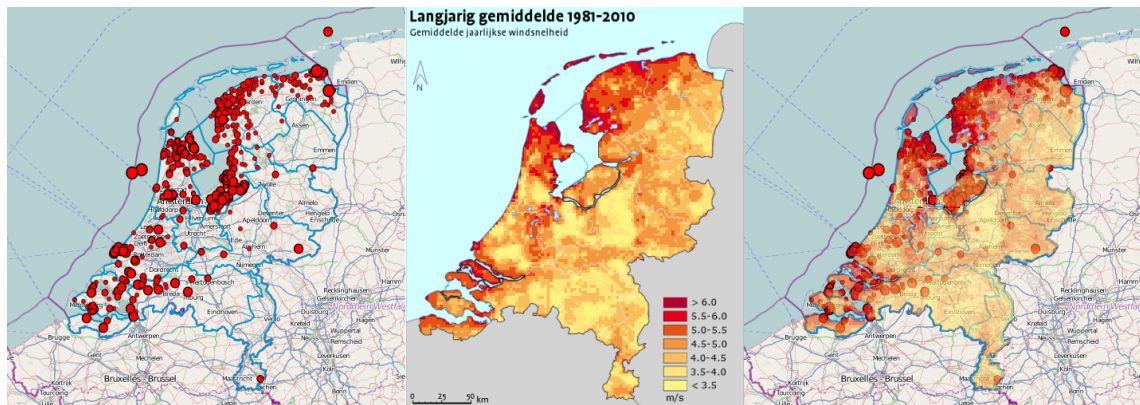
Figure 2.7: The current locations where wind turbines have been installed is shown on the left, size of the dot corresponding to the capacity. In the middle the corresponding wind velocities can be seen. By combining both images it is clear that most of the wind turbines are located at 'windy' locations and the available wind potential is used as much as possible.

Table 2.3: The currently installed capacity per province in the Netherlands Versus the planned capacity for 2020 (offshore: 2023)

Province	2014 Capacity [MW] [13]	Planned Capacity 2020 [MW] [14]
Friesland	171	530.5
Groningen	379	855.5
Drenthe	14	285.5
Overijssel	33	85.5
Gelderland	46	230.5
Flevoland	839	1390.5
Noord Holland	354	685.5
Utrecht	19	65.5
Zuid-Holland	301	735.5
Zeeland	351	570.5
Noord-Brabant	118	470.5
Limburg	19	95.5
Total Onshore	2645	6001
Offshore	228	4450 (by 2023)

then come from offshore wind. This is also reflected in current installed power as well as the plans, which distinguish between goals set for 2020 and offshore wind energy goal set for 2023. An overview of the wind turbines that are currently installed is given in figure 2.7, showing a good correlation between average wind speed and installed wind turbines. This is to be expected, as the output of a wind turbine is higher at higher wind speeds and therefore typically more profitable. Another factor that plays a role in the location of a wind turbine is the cost of land and the number of people living in the vicinity of the location. By 2014 there were only 2 offshore wind parks in use, the "Princess Amalia windpark", rated at 120 MW, and the "Windpark Egmond aan zee", which is rated at 108 MW.

It can be seen from table 2.3 that there is still a lot to be done. In order to achieve 6000 MW of onshore wind power by 2020, the capacity onshore needs to be doubled, while in 2014 only 5% of offshore wind energy had been realized. Area's for large scale wind energy production have already been appointed. There is one 600 MW wind farm currently being built and expected to go online by 2017. Starting in 2016 the government is tendering five offshore wind projects, each 700 MW in capacity. The infrastructure offered for these 700 MW wind farms should be standardized. If there are no delays, the offshore capacity should reach 4450 MW by 2023. The locations that have been appointed for onshore and offshore large scale wind energy are shown in appendix A. The standardized infrastructure should result in cost savings of approximately 3 billion euro's, according to electricity transmission operator TenneT [15]. For the long-term future, governmental ambitions regarding the share of renewables in the energy production would require a total of 26 GW of offshore wind turbines installed by 2050.

In order to successfully build these wind farms as planned, the costs to build them have to be

covered. The cost gives an estimate of the size the wind energy industry that could be obtained, and the cost of future energy production.

To calculate the total cost of building and operating the offshore wind farms for the period of now until 2023 and from 2023 until 2050 some assumptions have to be made. One of the assumptions is the distribution between capital expenditure (CAPEX) and operational expenditure (OPEX). In the current offshore wind energy projects, the distribution between CAPEX and OPEX over the total lifetime of a wind turbine is estimated to be approximately 70:30. It is expected that this ratio will remain the same for coming offshore wind energy projects. The estimated lifetime of a wind turbine is 20 years, over which the OPEX will be spread. The CAPEX can be estimated more easily based on data that is available today. The price per kW of installed capacity for current wind parks is 3500 €/kW. The installation cost can fluctuate; the Gemini wind farm delivers 600 MW at an installation cost of 2.8 billion euro, resulting in a cost per kW of €4667. On the other hand, it is expected that the Borssele wind farm, with a capacity of 1400 MW requires €4 billion to be built; a cost of 2900€ per kW. The Gemini wind farm is expensive, but there are two reasons for that: 1) it lies at 85 km off the Dutch shore 2) it is a first in its kind in the Netherlands, and as such also a demonstrator of technology.

The government aims at reducing the cost of offshore wind energy by 2023 by 40%. Assuming that the cost of installing wind energy remains the same until 2023, and after 2023 is reduced by 40%, the cost for installing 3500 MW of offshore wind energy between now and 2023 equals 12250 million euro. Using the assumptions, the OPEX for the year 2017, when 1100 MW should be in operation, can be expected to be 82.5 million euro per year, which increases to 334 million euro per year by 2023 when the installed capacity has reached 4450 MW. The expected cost for operating a Dutch offshore wind farm is slightly lower compared to the UK, where operational expenses are expected to reach 2 billion pound, with a total installed offshore capacity of 23.2 GW [16]. The offshore wind locations in the UK are at a larger distance and the environmental conditions are slightly worse compared to the Netherlands. Compared to OPEX estimates by ECN and the National Renewable Energy Laboratory, the 82.5 million euro per year is lower than expected. ECN estimates an OPEX of 125 thousand euros per year per MW [17], while the estimate by the National Renewable Energy Laboratory ranges from 68 thousand dollars up to 239 thousand dollars per year per MW, with a central value of 136 thousand dollars[18].

A part of the OPEX comes from inspecting the wind turbine in the field. It is estimated that an average sized monopile type foundation requires 20 man-hours a year, while a jacket type foundation requires 60 man-hours a year [19]. It is expected that by implementing an Acoustic Emission monitoring system, the man-hours spent on inspection can be reduced, and thereby the OPEX. The monitoring system can ideally be placed at critical locations and used to estimate the remaining life time more accurately, and by more accurately monitoring the state of the structure preventing unplanned maintenance [19]. These measures could result in savings of up to 0.8% on monitoring and up to 4.4% by improving operations and maintenance[20]. Translated to a 'typical' wind farm of 134 MW, this equates to annual savings of 80 thousand euro in monitoring and up to 440 thousand euro by improved operations and maintenance.

With these numbers the cost up to 2023 can be estimated, by simply adding the OPEX and CAPEX spent until 2023. By 2023, a total of 4450 MW should be installed offshore, and the total cost to operate that over a lifetime of 20 years would be 22.25 billion euro. Using the same approach, an estimate for the period from 2023 until 2050 can be given. The goal is to have 26 GW of offshore wind energy by 2050. It is safe to assume that the 4450 MW will have to be replaced during that time span, as the expected lifetime of a wind turbine is 20 to 25 years, therefore the full 26 GW will have to be installed. As the offshore wind market is maturing, and the Dutch government expects to have a significant reduction in price of offshore wind energy, it is assumed that the cost for both CAPEX and OPEX will be reduced by 30% as of 2023. The total cost over the period from 2023 until 2050 is estimated at 90 billion euro.

These estimates are subject to a large uncertainty. The numbers that are given in this section have been compared with comparable numbers that are available for the UK market. In general the numbers found in this section appear to be smaller than those found in estimates for the UK. This can partly be explained by the location at which the UK wind parks are planned. Having them located at a greater distance from the shore and in a harsher environment makes the installation and maintenance more expensive. This can also be seen in the cost per MW of currently installed wind turbines, as the installation cost for UK offshore wind turbines is significantly higher than that of an offshore wind turbine placed in the Netherlands [21]. Based on today's numbers, the OPEX is estimated between 75 thousand euro's per MW per year and 125 thousand euro's per MW per year. A permanent monitoring system at crit-

Table 2.4: Approximate CAPEX & OPEX, used in order to obtain total cost of wind energy in the Netherlands

	Cost per MW	Units installed	Total cost
Up to 2023			
Installation cost	3 500 k€	3 500	12 250 M€
OPEX per year	75 k€	4 450	334 M€
OPEX sum of 20 yrs	1 500 k€	4 450	6 675 M€
2023 - 2050			
Installation cost	2 450 k€	26 000	63 700 M€
OPEX per year	52.5 k€	26 000	1 365 M€
OPEX sum of 20 yrs	1 050 k€	26 000	27 300 M€

ical locations in the turbine's foundation could result in savings in inspection and maintenance. The cost reduction is estimated at 0.8% of the actual OPEX, but there are other potential benefits too: an improved monitoring system may increase knowledge on the actual structural performance of the wind turbine design. This could increase the operational life of wind turbines or result in better future wind turbine designs.

Structural Components of an Offshore Wind Turbine

Every wind turbine consists of a number of parts, which all contribute towards extracting as much energy as possible from the wind in the most efficient way. As wind turbines increase in size, the loads increase as well, and the support structure has to support and withstand them for a period of more than 20 years. As the turbines are located in an offshore environment, they require a well-designed solution for the support structure. In this section, the different structural components of an offshore wind turbine are treated by analyzing the function each has to fulfill, as well as the loads it has to endure. Some structural components have a number of alternatives, with varying advantages and disadvantages. The different options for the foundation type that are most well-known are discussed.

Sizing and positioning of a wind turbine

When deciding on the size of a wind turbine, a number of factors play a role. The size of the wind farm, the wind velocity and profile, the surface, surroundings and accessibility, amongst others. Often, a wind farm of a designated capacity has to be placed in a pre-specified area. An operator aims at maximizing its profit, requiring the wind farm to be as efficient as possible. Rotor diameters and hub heights have been increased over the years, and have resulted in higher efficiencies. A larger rotor covers a larger area and is capable of extracting more energy from the wind. Having the rotor at an increased height also helps in producing more energy, as the average wind velocity is higher at greater heights, and as the wind shear is smaller at higher heights, as shown in figure 2.8. Hub heights as high as 90 meter are possible, and with increasing rotor diameter, will move even higher. As wind turbines grow larger and taller, the amount of materials needed increases at a higher rate than the gain in installed capacity; the mass of a $1.5MW$, a $1.8MW$, and a $2MW$ wind turbine are 164 tons, 267 tons, and 334 tons respectively [22]. A study has shown the per kW cost of wind turbines, as a result of doubling the capacity per wind turbine between 2001 and 2010, had increased by $234\$/kW$ or approximately 30% [23]. At the same time, the projected capacity factor increased from 27% up to 35% or approximately 30%. Due to other factors as well, the projected levelized cost showed a decrease of 7%. With current and future developments, the average size of wind turbines keeps increasing, there's no consensus yet on what the optimal size would be [24].

For a wind farm consisting of multiple wind turbines, the positioning of wind turbines can also influence the efficiency of the wind farm as a whole. The wind that passes by a wind turbine is affected, and may contain less energy and could also become turbulent. This results in a decrease in the per wind turbine energy produced when wind turbines are located in a utility scale wind farm compared with an isolated wind turbine. Having a high density of wind turbines, results in a larger decrease in efficiency in comparison to a lower density of wind turbines with the same total capacity, as shown in figure 2.9. The individual positioning of wind turbines can also affect the overall efficiency of a wind farm. The gain that can be expected from optimizing the wind farm layout, starting from a regular grid is in the order of 0.1% up to 1%, as is shown in figure 2.9.

wind speed vs altitude
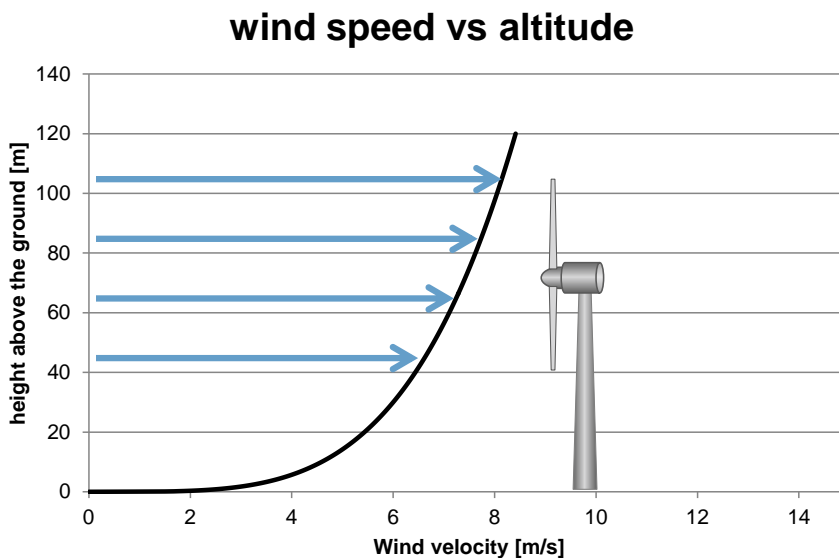
Figure 2.8: At a higher altitude, the average wind velocity is higher. At the same time, the wind velocity gradient is smaller, resulting in a smaller difference in wind velocities between the top and bottom of a wind turbine rotor. The smaller difference results in smaller bending and/or fatigue loads on the wind turbine.

Efficiency vs Installed Power per km^2
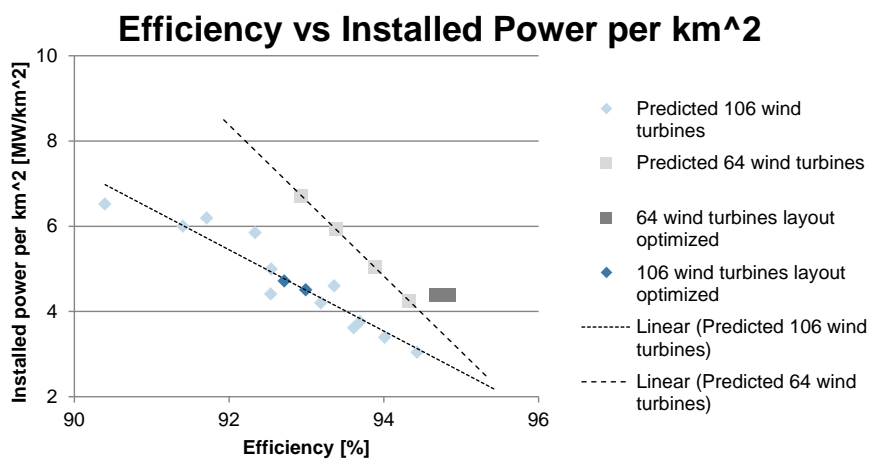
Figure 2.9: A comparison between two simulated wind farms of similar total capacity. The light colored shapes represent a matrix-like layout, while the dark shapes represent an optimized layout. It can be seen that by packing the wind turbines in a smaller area, i.e. a higher power density, the efficiency decreases. It can also be seen that the efficiency of the wind farm overall can be increased by installing fewer wind turbines of higher capacity. [25]

Table 2.5: Market share of different foundation types that are used at offshore locations as foundation for wind turbines

Type of structure	Depth range	Wind turbine capacity	Share
Monopile	0 - 30 m	< 8 MW	74.1%
Gravity	20 - 60 m	< 10 MW	16.3%
Tripod	10 - 55 m	< 8 MW	1.6%
Tripile	25 - 40 m	< 8 MW	2.5%
Jacket	20 - 70	< 8 MW	4.9%
Floating	30 - >600	< 10 MW	0.2%

Support Structure

A large part of a wind turbine consists of the support structure that is designed to keep the wind turbine in place under the conditions it endures during its lifetime. These conditions include wind, wind gusts, waves, and seasonal effects. The intensity of these loads can be severe while the loading itself is of the fatigue type. The support structure has to be designed with this in mind, and as such, there are several design requirements for it. In order to make sure that wind turbines are built properly, the design requirements are becoming more and more standardized. An example of such a standard is IEC 61400, which specifies typical design requirements such as the loads the wind turbine has to withstand. The wind velocity can reach up to 70 m/s once per 50 years, while the average wind velocity is 10 m/s. Even though the wind turbine will shut itself down at wind velocities above 25 m/s, the structure will still encounter such high wind velocities, and should be able to survive. The support structure typically makes up 25% of the total cost of a wind turbine.

Foundation

The foundation is the part that attaches the wind turbine to the seabed. It thus has to withstand and transfer the forces and moments that come from the wind turbine as well as other loads, such as currents around the foundation. There are different types available that can be used, each with its advantages and disadvantages, and there are several concepts in development for future use. An overview of the different foundation types is given in figure 2.10. Of these types, monopile, gravity based, jacket, tripod and tripile are commonly in use in different wind farms. The floating wind turbine is still under development and only used in a demonstrator. Not all foundation types are suitable at each location, as some have limitations regarding the depth or capacity at which they can be installed, as shown in table 2.5. Also included in this table are the market shares for each different foundation type. The information given is based on current state-of-the-art, and can change in the future. Developments in the wind energy market can increase the depth and capacity of foundations in the future, in order to enable installing even larger wind turbines and decreasing the cost of wind energy. The different foundation types are discussed separately in the next few sections.

Monopile

A monopile consists of a pile that is driven into the seabed. Although the concept is easy to understand, the challenge for monopiles is how to upscale according to the increase in wind turbine capacity. As the pile is driven into the seabed during installation, the pile is subject to severe compressive loads. In order not to buckle during installation, the wall thickness of the tube has to have a certain thickness. Typically, the wall thickness for monopiles is between 5 and 15 cm. Not only the monopile has to be able to withstand the forces during pile driving, but the installation equipment also needs to deliver the required installation force. Installation devices are also limited in terms of the maximum diameter of the pile that they can install. Current monopiles can be as large as 7 meters in diameter. The dimensions of a monopile are a result of the bending, axial, and shear forces exerted by the wind turbine during operation as well as the sea current and the installation process. The portion of the monopile that is below the seabed depends mostly on the sea depth at the location of installation, the composition of the seabed, and the wind turbine size. When manufacturing techniques and installation process are further developed, it might be possible to install monopiles at deeper locations and with larger dimensions. Although it could be possible to upscale current installation hardware, there are techniques under development that make use of a different method to drive the pile into the seabed. During operation, the factors that limit the functioning of the foundation are fatigue, corrosion and scour. During experiments, a scour depth of 1.75 times the monopile diameter was observed without scour

(a) Monopile   (b) Gravity Based Foundation   (c) Jacket

(d) Tripod   (e) Tripile   (f) Floating Foundation
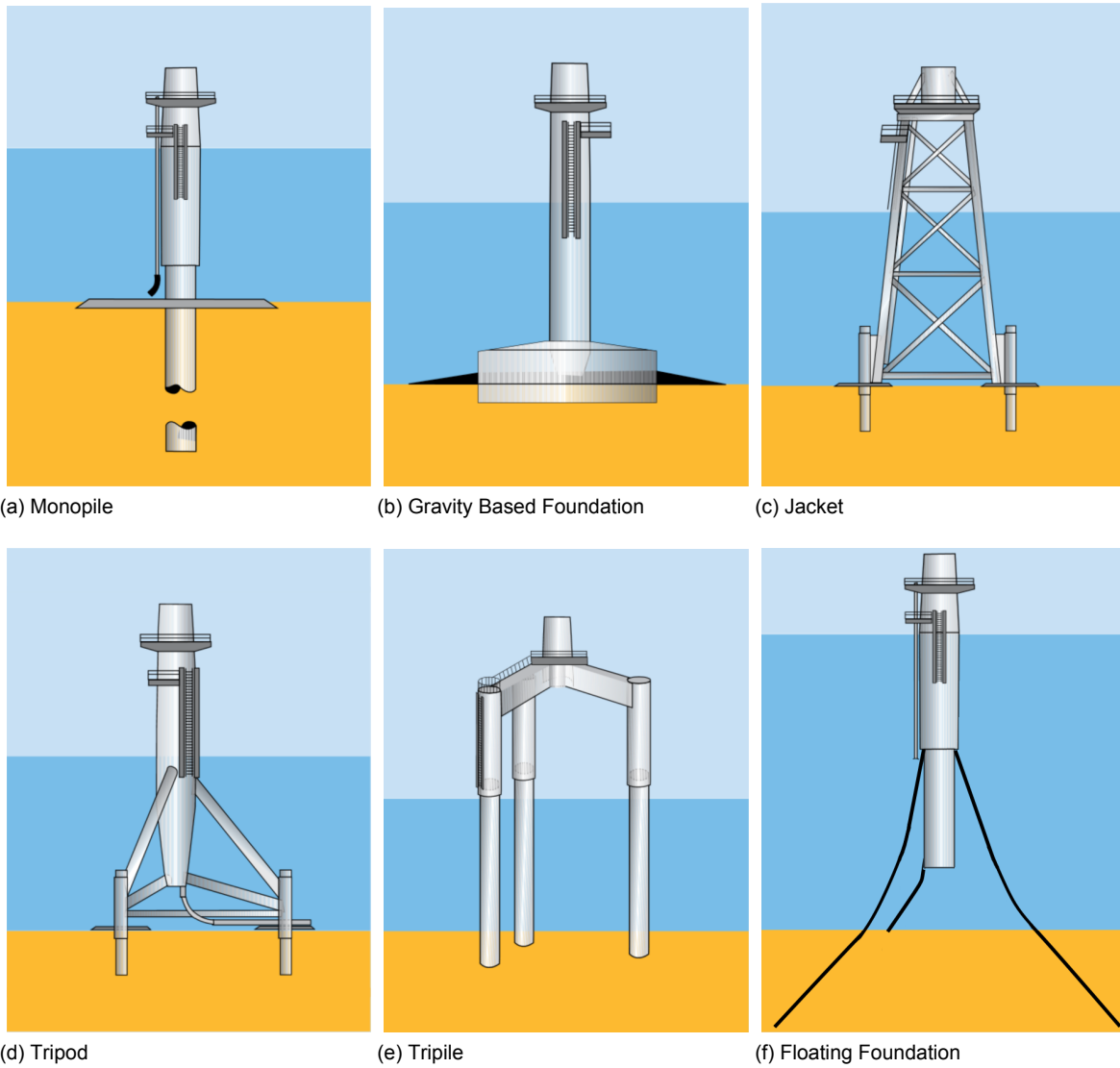
Figure 2.10: Different support foundation types that are being installed offshore. [source: EWEA]

protection [26]. Scour depends mainly on the seabed conditions, but can be reduced by reducing the current around the monopile as well as by preventing the soil from being taken away from the monopile.

Gravity

The gravity type foundation consists of a large concrete part, which is placed on the seabed and onto which the other components are attached. It can be built onshore, and then transported to the location where it has to be installed. Installation is done by deploying the foundation on the seabed. The seabed has to be inspected before installing the gravity foundation, to determine whether the location is suitable for a gravity type foundation. Recent cost reducing developments have reduced the number of lifting operations, by building the foundations on a barge or by towing them with a tug boat to the proper location. Although the installation process is relatively simple, designing and manufacturing of the foundation is more complicated compared with monopiles. Gravity type foundations are expected to last up to 100 years, which is 4 to 5 times longer than the wind turbine itself. It could therefore be a durable option, if future wind turbines are compatible and if no unexpected structural degradation occurs. As wind turbines are still increasing in size, the compatibility might be an issue, as well as salvaging at the end of life of the foundation. Gravity type foundations are less susceptible to scour compared to monopiles, but it might still occur, and has to be taken into account when designing for a gravity type foundation.

Tripod

A tripod consists of a structure that connects the wind turbine to three piles on the seabed. The piles that are used to attach the tripod to the seabed are typically around one meter in diameter. Instead of piles, it is also possible to make use of suction buckets. The tripod construction can be built onshore, and then transported to the location offshore and installed using the three smaller piles that are driven into the seabed. This can make installation cheaper, as smaller equipment can be used for installation. Designing the tripod is more complicated than designing a monopile, as well as its manufacturing, where the different joints have to be welded together. Scour is less of an issue with tripods; the foundation is using three piles that are smaller in diameter, resulting in less scour, and the piles are loaded predominantly in tension, thus the foundation depends less on sideways support of the seabed. The complex welded design is more susceptible to fatigue. Care has to be taken when designing a tripod with regard to fatigue.

Tripile

This foundation type sits somewhere between the tripod and the monopile, construction wise. It uses three piles of approximately 3 meters in diameter that are driven into the seabed. These piles are connected to the transition piece using a grouted connection, similar to a monopile. By using this method, the grouted connection is mainly loaded axially, while in the case of a monopile, the grout also has to transfer forces that are generated due to bending. The tripile is relatively heavy, but can become more weight-competitive in deeper water. This foundation type was first installed in 2008, intended to be an evolution of the monopile. According to the manufacturer, this foundation type weighs less than similar tripod or jacket type constructions (in water depths of 25 to 40 meters). As wind turbine sizes increase, so will the foundations. The tripile foundation type can still grow significantly with today's installation techniques, and therefore wind turbines of this type can still grow in size a lot before upscaling problems become significant.

Jacket

This type of foundation is common in offshore oil and gas, where it is frequently used to support platforms. This type of support has the advantage that it consists of many different members, creating redundant load paths. Having a redundant load path means that the support could have a local failure of some kind, without the structure collapsing. Such a structure can be designed relatively light, but designing such a foundation type is complex. Not only the design is more complex, but also manufacturing of such a foundation is more complex, as there are multiple joints, creating more locations at which fatigue or other defects could occur. The complexity also makes them expensive, but in return, the jacket foundation can be adjusted to most circumstances and allows for deeper locations.

Floating

The foundation types examined above are predominantly usable in water depths of several tens of meters. Foundations of the floating type are suitable for water depths of over a few hundred meters. This concept is fairly new and still under development. The costs are therefor high and not representative of large scale application. As there are more locations at which wind turbines could be located using this floating foundation, locations with better wind conditions can be selected, causing a further increase in the capacity factor, and thus profitability. As this concept is still under development, it is hard to say what its final form will look like, and what the associated disadvantages are.

Note

The foundation types that have been discussed are all the ones known and generally accepted today. It could be that one of these foundation types outperforms the others, or that the performance is similar and multiple types coexist, or that each type gets its own niche. Currently, monopiles are the dominant type, but some people expect jacket type foundations to grow in market share.

A potential issue that so far has not been looked at is what will happen at the end of life of a wind turbine. Only recently have wind parks reached their end of life, and knowledge on the decommissioning of wind turbines is therefore limited. Which of the foundation types is easiest to remove or recycle is therefor not yet fully disclosed, but could play a role in future decision making processes.

Transition Piece

The transition piece connects the foundation to the wind turbine tower. It can be part of the foundation, as for example in a tripod foundation. The transition piece serves multiple functions, not only it connects the tower to the foundation, but also serves as the entrance to the wind turbine for personnel. To do so, it is equipped with a boat landing, a ladder, safety measures, and a platform. It allows personnel to enter from a boat safely, and transfer to the wind turbine, while also having some room for any equipment that might be needed. As the transition piece is located within the splash zone, corrosion protection is required. A multilayer coating provides the corrosion protection on the outer surface and should also prevent any algae from growing. On the inner surface, corrosion could also occur, but this part of the structure does not encounter waves. The requirements for the inner surface are therefore less strict compared to the outer surface. Access to the wind turbine is usually gained via the boat landing. This procedure may cause a significant loading on the structure, which therefore should be designed to cope with this type of loading. Making use of the boat landing is only possible in calm weather, and access to the wind turbine is therefore not always possible. There are other access systems available and under development that might change the way access is gained to wind turbines. An example of an alternative technique is the Ampelmann-system. It makes use of a bridge which makes use of a hydraulic system that compensates for movements of the boat that it sits on. Such a system allows for a wider window of operation, and could allow access directly to the platform instead of via a ladder. It could therefore allow for a simplification in the design of the transition piece, reducing the amount of spots where fatigue damage could be induced and reducing the cost of the transition piece.

Grouting

Most wind turbines have a grout between the foundation and the transition piece. This grout is a layer that fills the gap between the two. This allows some margin in installation of the foundation, as misalignments between the foundation and the transition piece are corrected by the grout. The grout has to transfer the loads from the transition piece to the foundation. To do so, the grout not only needs to be flexible up to some extent, it also needs to be durable, as it is subject to dynamic loading for more than 20 years in an offshore environment. The grout has to be installed properly, otherwise the quality of the grout is not sufficient to last during the life span of the wind turbine. Installation can be done below the sea-level as well as above the sea-level. Before the grout is strong enough to carry the wind turbine, it has to cure first. The curing in time depends mainly on the temperature levels. The importance of the quality of the grout became clear in recent years, as in multiple wind farms the grouting has degraded and needed to be restored; a costly operation which could have been unnecessary when properly designed and installed. This problem became apparent after a few years of operation, and was a result of the stresses that were higher than previously anticipated. The deformations were larger than expected, and this resulted in excessive wear of the grout. To battle this problem, a number of changes to the grout have been proposed, which could solve this problem. The two most promising solutions
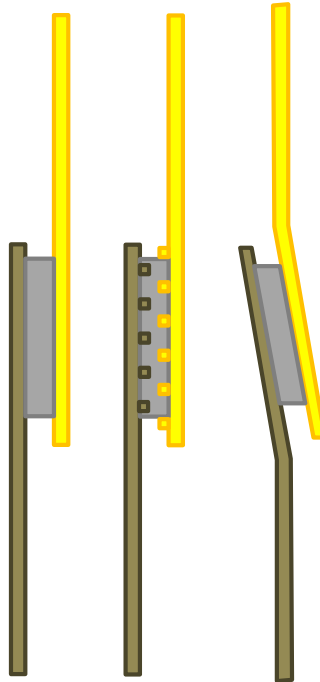
Figure 2.11: Different types of grouting connections. Conventional on the left, shear keys in the middle, conical shape on the right.

are usage of "shear keys" and a "conical shaped connection". These two concepts are shown in figure 2.11. The shear key concept makes use of a number of rings that are welded into the tube, and help in transferring the forces more effectively. The conical shaped connection is more effective in transferring the loads as well, but has another advantage: in case the grout would be degrading, it allows for some resettlement of the grout, thereby prolonging its lifetime. The conical shaped connection is more complex to manufacture, but requires less production steps, while the connection fitted with shear keys requires a number of extra welding steps. In order to assess the quality of the grout, it should be possible to inspect it. Apparently, this is not possible using conventional techniques. Alternative techniques for inspection of the grout are under development, using active ultrasound, which can assess the quality of the bond line by analyzing the transmission of the signal.

Tower

The tower connects the transition piece to the nacelle, which houses the actual wind turbine. The tower therefore has to transfer the loads from the turbine to the other parts of the structure. It has to do so at a high height. These loads include the wind blowing onto the turbine, vibrations from the turbine, and any imbalances, as well as the moment that is exerted during an emergency brake procedure. It also has to be able to withstand the wind load on the tower itself, every time a wind turbine blade passes the tower, i.e. the so-called 3P loading. Fatigue loading on the tower can be decreased by dampening as much of the vibrations as possible. This should then also have a positive result on the other parts of the support structure.

It is inevitable that future towers will grow in size; as the rotor diameters increase, so do the towers, due to the same or more clearance needed between the rotor and the ground. This growth can be accomplished in several ways: (1) upscaling every part, (2) using higher performance materials, (3) composite towers or (4) concrete towers. Scenario 1 can be considered possible, but requires everything else to scale up as well, including foundations, installation vessels, manufacturing plants. This scenario is not necessarily the most cost-effective solution. A variation on this scenario is option 2; by making use of high performance metals, the limits of current day design might be stretched further, thereby mostly delaying the first scenario. Using the second scenario, the weight could possibly be

reduced, resulting in lower transportation and installation costs. Scenario 3 entails production of a wind turbine tower mostly out of composites. The major advantages of a composite wind turbine tower are reduced weight/increased stiffness and the possibility to tailor the stiffness of the wind turbine to the individual needs of a specific wind turbine. The wind energy industry started using metal blades, which have been replaced with glass fiber reinforced plastic blades, with length of up to 75 meters. A similar development could also be made in tower design. The last scenario entails the usage of concrete as a building material for the tower. Currently, there is some experience with building concrete towers onshore, with the advantage that transport of large section of the tower is not required. Building a concrete tower can be performed onsite, or in small blocks that are assembled onsite. Concrete is well-known for its compressive strength and its durability, which could result in towers with an expected life span of well over 20 years.

Currently, a large portion of research tends to go to composite towers, however, whether this is the path that will be followed is still under investigation. Despite any outcome regarding the future of wind turbine towers, currently steel is the dominant building material for wind turbine towers. As the lifespan of a wind turbine is typically 20-25 years, steel towers will certainly be in use for the coming 25 years.

Conclusion

The global need for electricity has been increasing in the past, and is likely to keep increasing in the future. The share of wind energy in the electricity production has also been increasing during the past. The governmental future projections indicate that the share of wind energy in the total energy production will increase. This is aided by the upscaling of wind turbines and developments in the wind energy market. Although the wind energy market is maturing, the cost of electricity production of wind turbines is higher compared to conventional electricity production. Factors that contribute to the cost of a wind turbine are the location, maintenance, and the wind turbine itself. The parts within a wind turbine are subject to high loads, during the lifetime of 20 to 25 years, that may induce fatigue. Monitoring is required in order to determine the structural health of a wind turbine, and to perform maintenance before damage occurs. Offshore wind turbines are more difficult to access, and monitoring is costly. Costs may be driven down by a monitoring system capable of working autonomously, allowing for improved monitoring and maintenance schedules. Such a system could also lead to insights into the performance of offshore wind turbines and thereby improved designs that could further reduce cost.

3

Acoustic Emission

Acoustic emission is not something that has been invented by mankind, but has been discovered after observing several materials during casting or deformation. This chapter treats the discovery of acoustic emission, the working mechanism behind it, and gives a number of examples of where acoustic emission or similar techniques is being used.

History and Background

Although acoustic emission as a field of study started in the 1950's, there are examples known where it has been encountered before. For example, when a tree breaks, a loud cracking noise can be heard. Not all types of wood exhibit this behavior in the same way. For mining purposes, where the danger of a collapse is a threat, the acoustic warning prior to collapse of a wooden beam can help save lives. The sound is caused by the internal breaking of the structure. This happens at a large scale, as for example a tree or a beam, which can be heard by people, but happens at a smaller scale too. During tensile testing of a wooden coupon, acoustic emissions can be detected as the crack propagates [27].

The first metal that was discovered to emit a sound, without directly failing was tin. During the cooling down after formation, or upon deforming tin, a sharp chirping sound can be heard, which has been described by Jabir ibn Hayyan, who lived in the 8th century[28]. It was thought to be caused by the friction of crystalline particles within the material. In 1916, the first publication that linked twinning to tin and zinc was released by J. Czochralski [29]. Twinning is a possible source for this audible acoustic emission, but other scientists found different sources as well; formation of martensite in steel, or plastic deformation in aluminum under tensile loading[30][31][32]. In order to study this behavior more accurately, special instruments had to be built. One of the first tools specifically designed to do so consisted of a phonograph pickup, of which the resulting electrical signal had been amplified and recorded [33]. During bending of a wooden sample, it did record the audible cracking sounds, as well as a number of vibrations that were inaudible. Using a transducer made of quartz, ultrasonic emissions of the twinning of tin had been recorded in order to observe the movement of dislocations.

These discoveries and inventions resulted in an increased interest in acoustic emission. Initial research aimed at obtaining more knowledge on the fundamentals of acoustic emission, and the behavior of acoustic emissions for different materials under deformation. As the knowledge on acoustic emission increased, the focus of research went more into finding applications where this could be beneficial.

Working principle of Acoustic Emission

There are different sources that may cause acoustic emissions. The possible sources all have in common that the internally stored energy is released rapidly, resulting in a wave that travels through the structure. Breakage of fibers, closure of voids, plastic deformation and crack growth can all cause the rapid release of energy that can be detected as an acoustic wave [34]. It is also possible to cause an elastic wave, which is picked up by sensors, via other methods, such as tapping, friction or a leak. In this section the focus lies on acoustic emissions coming from fatigue. In order to get a better understanding of this, fatigue is briefly discussed first, followed by how this can result in an acoustic wave, and followed by how this wave can be detected.

Figure 3.1: An example of a bicycle crank that has failed due to fatigue. The crack started to grow in the black area, until at some point the remaining cross sectional area (light/silver) failed. Note that the lines in the crank indicate the size of the crack growth, and the lines have a larger distance in-between as the crack increased in size. [35]

Fatigue is a process that can occur when a structure is loaded repeatedly. Even though the applied load to the structure does not lead to the immediate failure of a structure, it can slowly degrade the structure's integrity. This can happen at loads that are significantly below the failure load. Even though the structure does not fail or yield, plastic deformation can occur locally. In order for this to happen, the applied load has to be higher than the so-called fatigue limit; a stress value below which the structure can withstand an infinite amount of load cycles. This can result in the growth of small cracks. As these cracks grow larger in size, the structure starts to degrade, and the failure load of the structure as a whole is decreased. This structural degradation does not show immediately in the load bearing capacities, as the structure is not loaded until failure, but the stiffness and the Eigen frequencies can change. The major method of detecting fatigue crack growth is visual inspection. As cracks grow in size, they can become so large that they can become visible.

Visual inspection is only possible after the crack has grown. However, every load cycle the crack will grow by just a fraction. The amount of crack growth per cycle can be determined using Paris' law as follows

$$\frac{da}{dN} = C\Delta K^M \tag{3.1}$$

where

$$\Delta K^m = (\Delta \sigma Y \sqrt{\pi a})^m \tag{3.2}$$

In this equation $\Delta \sigma$ is the maximum stress minus the minimum stress of a typical stress cycle. For a center crack in an infinite sheet, the value of Y equals 1, a is the current crack length, and C and m are material constants. Every time the crack grows by the amount previously calculated, a part of the stored energy is released [36]. This released energy can go towards increasing the crack surface, conversion to heat, induce plastic deformation, or propagate as elastic waves [37].

(a) Transverse wave   (b) Longitudinal wave

(c) Rayleigh wave   (d) Symmetric wave
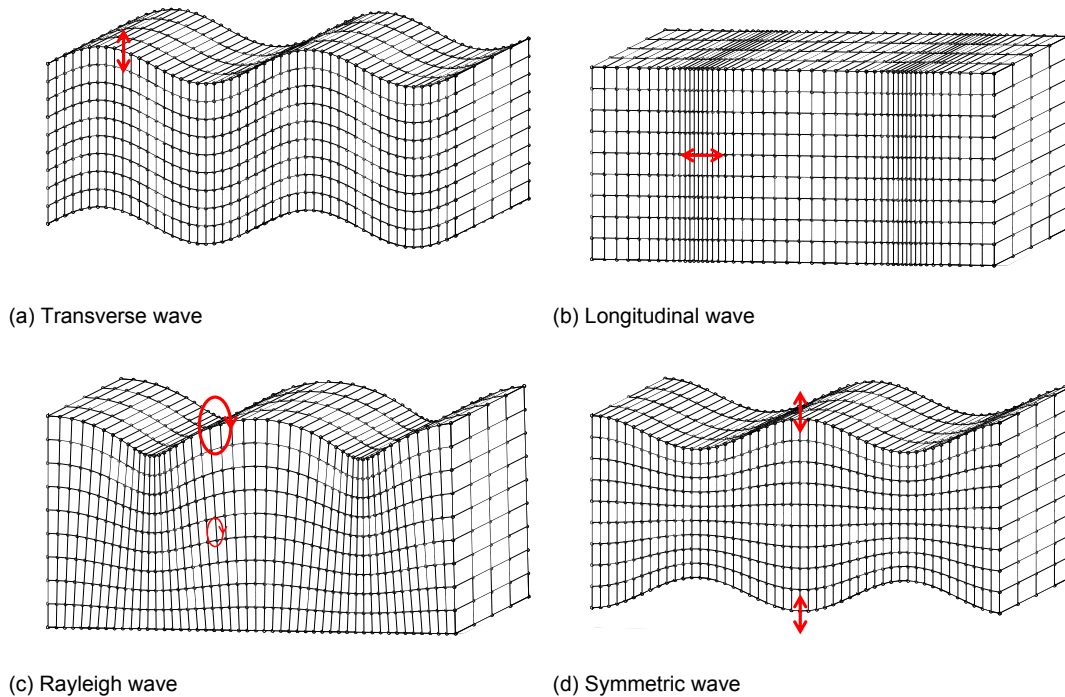
Figure 3.2: Different types of waves that can occur. Longitudinal and transverse waves are possible within a body when the wavelength is substantially smaller compared with the , as are longitudinal waves. When the structure is unbound at one side, i.e. it has a surface where it has an interface with a different medium, Rayleigh waves can exist. These waves contain both longitudinal and transverse waves, while it has highest intensity at the surface which dampens out as one gets further away from the surface. In the case of a plate transverse waves can exist in a symmetric mode as well as an asymmetric mode, as shown in the case of transverse waves. For all of the cases shown above, the movement of the particles within the structure is shown using the red arrow, while wave itself travels to the right. [41]

Propagation of AE signals

The elastic waves that are created in crack growth can travel through the structure. These waves are usually a combination of pressure waves and shear waves. When the medium through which the wave travels has a thickness larger than the wavelength of the elastic wave, only bulk waves exist. When the medium has a thickness that is smaller than the wavelength of the wave, Lamb waves can exist.

Bulk wave modes

Pressure waves are also known as longitudinal waves, compressional waves or primary waves (P-waves), and shear waves are also known as transverse waves or secondary waves (S-waves) [38]. The difference between these waves is in the movement of the medium within a wave. In a compressional wave, the medium through which the wave travels moves in the same direction as the wave. In a shear wave, the medium moves orthogonal to the direction of the wave. The difference is shown visually in figure 3.2. Not only is the direction of the medium through which the wave travels different, the velocity at which the wave travels is also different. For a given medium, the compressional wave is always faster than the shear wave, explaining the primary/secondary name-convention [39]. Another noteworthy difference between these two types of waves is that shear waves can only travel through a solid medium; shear stresses are nonexistent in gasses and fluids [40].

Guided waves

The longitudinal waves and the transverse waves can not only exist in bodies, but also in plates, or on the surface of a body. In the case of surface waves, they are often called Rayleigh waves [42]. Rayleigh waves consist of both longitudinal and transverse waves, but the intensity of these waves is higher at the surface compared with deeper in the structure. The resulting particle motion is elliptical in shape, as can be seen in figure 3.2c. Lamb waves occur in plate structures. Lamb waves can consist of

(a) Guided waves   (b) Body waves
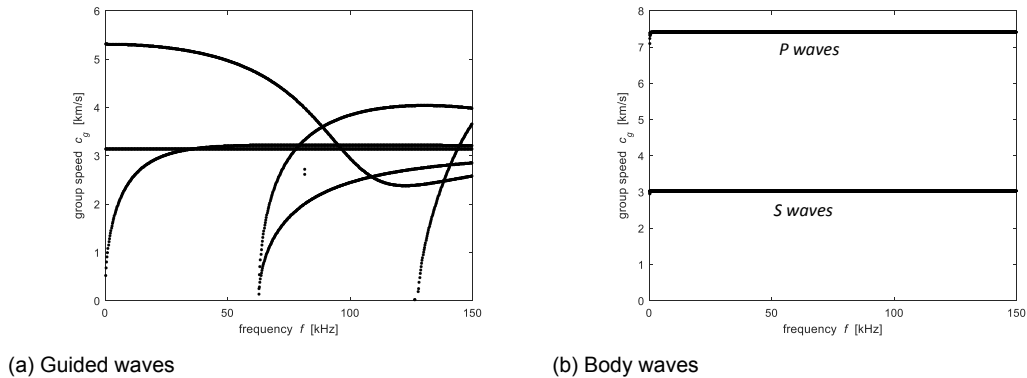
Figure 3.3: On the left, wave speed of different wave modes at different frequencies for a metal plate of 25mm thickness are shown. As the slope of the velocity increases, so does the dispersion. When there are multiple solutions for the wave speed, close to each other, determining the actual wave speed is more difficult compared to when the difference in wave speed is larger and there are fewer possible wave speeds. On the right, the wave speed for both the primary and secondary waves are shown in the case of a metal plate that has a thickness larger than the wavelength of the waves. The wave speed is independent of the frequency in this case, and no higher order wave modes exist.

both longitudinal and transverse waves. For the transverse waves, it is possible to have different wave modes simultaneously. At the same time, it is possible to have symmetric and anti-symmetric waves, indicated by S_x and A_x respectively, where symmetry is defined at the midplane of the plate. The lowest wave modes, S_0 and A_0, exist from $0 Hz$, while higher order wave modes only exist at increasingly higher frequencies. The wave velocity for each of the different wave modes can be different from one another, and varies with frequency and plate thickness. An example of the frequency to wave speed relation for a metal plate of 25mm thickness is shown in figure 3.3. The transmission of the signal through the plate can decrease over distance. This can be caused by absorption within the material, leakage of energy into the surrounding medium, dispersion, and geometrical spreading. This decrease in signal intensity over distance is called attenuation.

AE Transducers

The acoustic emission signals have to be detected upon their emission at the defect location. Ultra-sonic transducers are typically used for the detection of these signals. The transducers often feature a piezo crystal that creates a potential difference when a force is exerted onto it. By changing the properties of the crystal, the sensitivity and bandwidth of operation can be adjusted. For correct source localization, the wave velocity needs to be known. Using these transducers, the operational bandwidth can be chosen such that only S_0 and A_0 waves can be detected, this makes it easier to determine the source location. Once detected by the transducer, the output of such a signal is amplified in order to overcome the noise during transmission and is then received by hardware that records and stores the information when it passes certain threshold criteria. This is done in order to minimize data consumption, as the receiver typically works at a frequency in the order of MHz, and monitoring is performed continuously while the information of interest may only be a brief pulse. In this research transducers are designed to be placed onto the structure using acoustic gel and magnetic hold downs. Using this approach, the transducer is not able to detect any compressive waves within the structure, and can only detect the transverse waves. If the application should detect compressive waves as well, there are solutions available that can, but these make use of a different type of attachment, a chemical bonding for example. Most applications make use of four transducers to determine the source location. This can be done by comparing the difference in arrival time between the sensors, when the wave speed is known.

Analysis of AE signals

The waves that get detected are of interest to the user. They can help to provide a crack location, and can also be used to get a rough estimate on the crack growth. In order to do so, the signals have to be
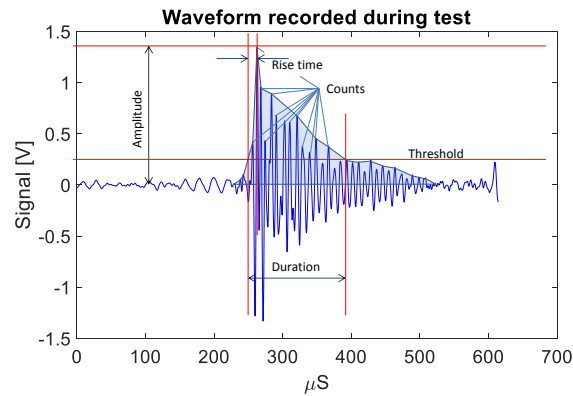
Figure 3.4: Some of the acoustic emission terminology explained using a waveform as recorded after a pencil lead break. By breaking a pencil lead on the surface, an acoustic signal is emitted similar to how acoustic emissions occur during fatigue.

analyzed.

Waveform Analysis

As an acoustic emission is usually a short burst of energy, it is not purely one distinct frequency. Acoustic emissions are typically represented as waveforms. A waveform is the detected response of the transducer to the elastic strain. This response, $R(\omega)$, is a function of the transfer function of the sensor, D, the coupling between the sensor and the structure and the path that has been travelled, W, and the source signal S, and depends on the frequency of the signal as described in the following equation:

$$R(\omega) = D(\omega)W(\omega)S(\omega) \tag{3.3}$$

An example of an acoustic emission is given in figure 3.4, together with some terminology that is conventionally used when treating acoustic emissions. Because the acoustic emission consists of multiple frequencies in thin-walled structures, the signal can get elongated as different frequencies travel at different velocities, see section 3.3.2. This phenomenon is called dispersion, and is a contributing factor in the attenuation of the acoustic emission signal. As damage accumulates in the structure, the waveforms that are emitted can change. These changes can include acoustic emission activity i.e. more hits per number of load cycles, the amplitude, the frequency, or the duration [43]. A single recorded set of waveforms is not enough to accurately monitor the development of the crack growth. Localizing a source of acoustic emission, i.e. fatigue, requires repeatedly detecting acoustic activity coming from a single location. When monitoring is performed over a longer period of time it may also be possible to detect the changes in the waveforms, as changes are often smaller than the scatter of the obtained data.

Parametric study

When monitoring for a longer period of time, the amount and complexity of data would be too much to cope with. The amount of data can be reduced by focusing on the most important parts of the data, such as amplitude and number of hits. Although this may be successful for some cases, it is not suited for every situation. Simplification to a limited set of parameters can result in neglecting small changes, or missing out on or misinterpreting signals. Also, this parametrification does not take all effects into account, such as path travelled.

Quasi-Beamforming AE

Detecting the emitted elastic waves can be done using AE Transducers, but in order to accurately determine the source location, the sensor placement is important. Good results have been obtained by making use of the Quasi-Beamforming (QBF) approach [44]. This method makes use of an array of at least four sensors that are placed close to each other, rather than placing the sensors far apart. By placing the sensors close to each other, effects that can cause inaccuracy in the results are minimized. Such effects are caused by non-uniformity of the material, spreading of the signal, attenuation of the

(a) Waveform at 0.5 meter   (b) Waveform at 2 meters
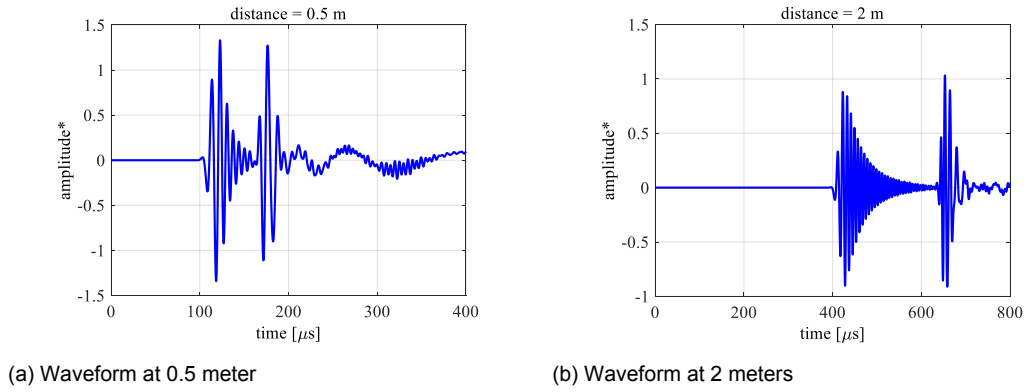
Figure 3.5: Due to attenuation, it can happen that the wave that arrives first remains just under the threshold and thus does not get detected, while the second wave to arrive does get detected. This secondary wave travels at a velocity which is lower than the first wave to arrive. In the example above, the same signal has been detected at a distance of 0.5 meter and at 2 meters. At 0.5 meter distance the first wave does get detected if the threshold is set at 1, while at 2 meters, this first wave does not get detected. If this is not corrected while estimating the source location, this can result in an incorrectly estimated source location, as indicated in figure 3.6.
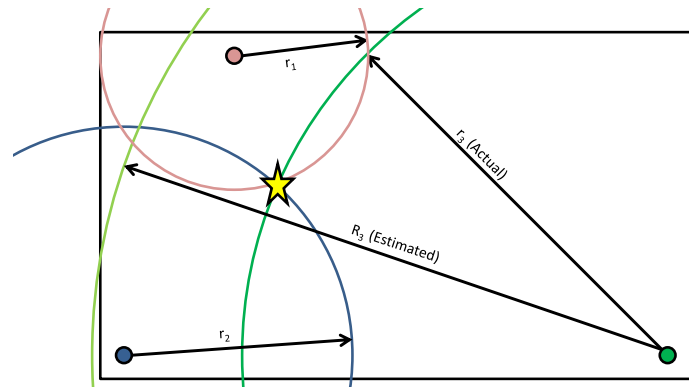
Figure 3.6: Due to an incorrect assumption in the velocity of the signal, the estimated source location does not coincide with the actual source location (indicated by the star).

signal, or disturbance as a result of geometrical features, as shown in figure 3.5. These effects can still influence the signal quality, but the chance of picking up a set of signals and interpreting it incorrectly is greatly reduced. An example of incorrectly interpreted signals is shown in figure 3.6

For a given structure, the dispersion curves can be calculated. These curves give the corresponding wave velocity for a specific frequency, see section 3.3.2. Once all four transducers pick up a signal within a predetermined time frame, the arrival times can be compared. The arrival time that is provided by the hardware, the threshold crossing, is not suited for determining the actual arrival time of the different wavemodes. The actual arrival time is determined by finding the time shift that results in the highest correlation between different wavemodes, as described by the following equation:

$$\Delta t_{ij} = \arg \max_{\tau \in \mathbb{R}} \left\| \int \hat{S}_j(t) \hat{S}_i(t + \tau) dt \right\|_\infty \tag{3.4}$$

In this equation, the signal detected at location j is represented by S_j, while $\|\cdot\|_\infty$ is used to indicate the maximum norm, and the hat sign indicated that a band-pass filtering has been applied to the signal. A band pass filtering may be applied to decrease the presence of signals outside the frequency range of interest. Finding the distance to the sensors can only be done when the wave speed is known. An algorithm is used to determine the wave speed, based on the frequency and characteristics of the waveform. With the difference in arrival time known, it is possible to estimate a distance of the source location with respect to each sensor. The source location is estimated by minimizing the error for the

calculated distances from the source location to the sensor, as follows:

$$\arg \min_{x,y,c_g} F(x_c, y_c, c_g, \Delta t_{ij}), \forall i,j \in [1, 2, \dots, n], \text{ subject to: } (x, y) \in \Omega \text{ and } c_g \in [c_{S0}(\omega), c_{A0}(\omega)] \quad (3.5)$$

In this equation, the location of the source is given by x_c and y_c, the wave speed of the dominant wave mode is given by c_g, while $c_{S0}(\omega)$ and $c_{A0}(\omega)$ indicate the wave velocities for the S0 and the A0 wavemode, depending on the frequency ω. The error function is represented by F, while the domain over which the calculations are executed is Ω. Using the QBF approach the estimated source location is more accurate.

By making use of the QBF approach it is possible to cover a greater area, as demonstrated in figure 4.4. It also allows to reduce installation cost, as sensors can be installed close to each other, requiring fewer operations.

Applications

Acoustic Emission Monitoring is currently applied in several applications. One of the most well-known applications is that of seismometry [45]. Seismometers can detect the movement of the earth's crust, and this can be used to detect the severity of an earthquake. Combining multiple seismometers at different locations, it is possible to estimate the location of the source of an earthquake, i.e. the hypocenter. Using the data from one location, the distance of the hypocenter to the seismometer location can be estimated based on the difference in arrival time of the P-wave and the S-wave. Combining the data from multiple seismometers, the hypocenter can be localized by the intersection of at least 3 of the estimated distances. If information about the decay of the signal over distance is known, this can also be used to estimate the energy released by an earthquake.

An application that has shown the capabilities of acoustic emission monitoring at an early stage is that of presser vessel monitoring [46]. Pressure vessels come in different sizes and uses, ranging from a small aerosol up to sizes beyond 80 meters in length and 10 meters in diameter. These pressure vessels are often used for storage of flammable gasses under pressure, and therefore the safety should be guaranteed. As these pressure vessels are often used for many years, and the varying pressure imposes a fatigue type load on the structure, a periodical inspection is required. Acoustic emission monitoring is a technique that is often used for this. By pressurizing the vessel while sensors are attached to the structure, the structural integrity can be tested. By tracking the pressure versus the amount, severity and source location of the acoustic emissions, it is possible to determine if a pressure vessel is undamaged and functions as designed.

A newer application is the monitoring of steel deck bridges [47]. As current day bridges encounter different load conditions than was anticipated for during the design phase, it is possible for bridges to show excessive wear, and the chance for failure to occur is increased. Determining the structural state of a bridge via visual inspection is costly and sometimes impossible to achieve. Acoustic emission monitoring gives the possibility to check for fatigue crack growth while the bridge remains fully functional. Over a long period of time, while the bridge encounters its typical loading, the acoustic emissions are monitored. The information that has been gathered can be used to determine the amount and location of the acoustic emission activity. Areas with high activity indicate fatigue crack growth. These areas can be inspected to further assess the crack development, repaired, and/or monitored for prolonged time.

4
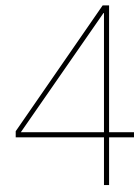
Literature Study

Introduction

This literature review discusses the current developments and difficulties in Acoustic Emission (AE), modeling of waves in fluid-solid combinations and the results of acoustic emission monitoring systems in current applications. AE has been used in several applications, but sometimes with mixed results [48]. Although its benefits seem to fit well with applications in monitoring of offshore wind energy support structures, it has not been applied yet [49]. The focus of this literature review lies on determining the source location of AE resulting from fatigue crack growth. This is done by establishing the state-of-the-art in current literature and applications, followed by determining which gaps need to be bridged in order to successfully implement AE. Before a system can be implemented, simulations determine the characteristics of the structure of interest. There are multiple methods available for simulating waves in structures, and the most promising are discussed in this review. Lastly, different techniques can be used in order to determine the location of the source. In the analysis part of the review, more detail will be given to how the literature is used. If knowledge is lacking, it is explained what has to be done in order to achieve the desired result. The review is closed by a discussion and conclusion, which treats the most important points from the review and what focus points require care during the MSc project.

State-of-the-art/Literature Review

This review aims at reviewing the literature that is required in order to successfully answer the research questions as proposed in the project plan. This review aims at reviewing the literature in the areas related to this research. By reviewing the different topics, the state of art in these topics is established. Next to that, the gap between the current literature and the knowledge required to design an offshore acoustic emission monitoring system can be established. This is done by first establishing the basics associated with AE. This is followed by an analysis of the available modeling techniques, such as differences in 3D and 2D modeling and different element types. Next, the localization techniques that are used for determining the source are discussed. Lastly, the noise level in the field is being studied, as there are a number of different sources that could influence the performance of an acoustic emission monitoring system.

Fatigue

Fatigue can be described as the weakening of a material by repetitive loading at a level below the failure stress of that material. The result of fatigue is that cracks start to grow in the structure, and the static strength of that structure is reduced. The relation between applied load and extension of the crack has been studied thoroughly, which has resulted in the well-known Paris-law [50] [51]. As the fatigue crack is growing, energy is being released at every growth event. The energy that is released causes an elastic wave that propagates through the structure [52] [53]. It is this elastic wave that has an ultrasonic frequency that is detected in Acoustic Emission Monitoring. Such a signal has certain amplitude at the source; the so-called source peak amplitude. Typically, a reference distance is used when someone is referring to the source peak amplitude. This reference distance is used, as when the distance to the

source is reduced to zero, the amplitude goes to infinity. In the case of ultrasonic acoustic emission monitoring, this reference distance is equal to 0.020m (NEN-EN 14584 , 2013). When measuring at a certain distance, the signal that is obtained is weaker as the distance increases. The decrease in signal amplitude over increasing distance is called 'Attenuation' and has multiple causes. The most notable causes for attenuation are geometrical spreading, energy loss into neighboring media, reflection or scattering of the signal and absorption [54] [55]. Although at the beginning of AE the understanding of the phenomenon was insufficient, a solid knowledge basis is available nowadays. As sensors have become more and more accurate over the years, the detection limit for fatigue crack growth is further improved. Although AE itself is well understood, the attenuation of a signal over a distance is a complex process [56], and is often determined via numerical simulation or by the use of experiments. The next paragraph will focus on different numerical simulation techniques that can be used to determine the attenuation.

Numerical Simulation

The behavior of the elastic waves in the structures is often analyzed using numerical simulations. Various methods have been applied, using different elements, different order of simulations, and different methodologies. Well known examples of different methods are boundary element method and finite element method. The modeling strategies that are used for simulation of acoustic emission are used in a very wide area of applications. Modeling is often performed in geology using 3D models [57] [58]. These 3D models can also be used in the modeling of elastic waves in metals, as both are of the Rayleigh type of wave [59] [60]. Two-dimensional techniques are used as well, as for example in [61]. Both the 2D and 3D appear to give good results in their own field, Although using a 2D technique to approximate effects in 3D can only give reasonable results if the right assumptions can be made. In the application of AE monitoring in offshore wind turbines, the attenuation of the elastic wave is required in order to determine the coverage area. The attenuation is depending on the properties of the medium through which the wave travels, as well as the surroundings. The surrounding water has a large effect on the attenuation of the signal and therefore has to be included in the model.

In modeling the behavior of elastic waves in the structure, different elements can be used. Approaches that are often used are using a FEM software package for modeling of AE signals, such as COMSOL [62] [63] [64]. The FEM method tends to be overly stiff, which results in less accurate results for high frequency vibrations. Although reliable, conventional FEM may suffer from worse accuracy as well as high computation cost. The Energy Finite Element Method (EFEM) is supposed to give more accurate results at higher frequencies [65]. This technique can model the energy propagation through the structure [66]. In the case of exterior acoustic problems, sometimes use is made of the Boundary Element Method (BEM); a method in which the domain can be unbounded, therefore the Sommerfeld radiation condition is satisfied at infinity [67]. The Sommerfeld radiation condition states that no waves should originate at infinity. This condition has to be met in order to obtain a unique solution. This condition can be applied by requiring the solution to satisfy the following equation (in 3D) [68]:

$$\lim_{r \to \infty} r \left(\frac{\partial u}{\partial r} - iku \right) = 0 \tag{4.1}$$

$$r = \sqrt{x^2 + y^2 + z^2} \tag{4.2}$$

Both the BEM and FEM can be combined, in order to make use of the BEM in the fluid part of the model and the FEM in the structural part [69]. In order to counter the 'stiff' behavior of the conventional FEM, a smoothed FEM is proposed by Liu et Al. [70]. This method results in more accurate results at no extra computational cost. And lastly, the spectral element method (SEM) has been proposed, which makes use of higher order terms during discretization in the computation. Furthermore, as the mass matrix is diagonal by design, operations are relatively simple. This results in accurate, yet not exact, solutions at a relatively low computational cost, i.e. the method is fast and can make use of parallelization [61] [71] [72]. When a more accurate solution is required, the order of the elements can be increased as well as the number of elements.

The different methods have not been compared with each other in an article. Statements on the computational cost are typically qualitative. Despite this lack of comparison between the different methods, it was found that in order to cope with the high frequencies typically associated with AE, not all methods work well. As mentioned already, conventional FEM requires large computational efforts in order

to obtain the desired accuracy. Although BEM/FEM and EFEM promise to have an increased accuracy at equivalent computational cost, due to the way that the 'overly stiff' behavior of FEM is compensated, using SEM with high order elements might give even better results. SEM has proven to accurately simulate the behaviour of waves in different media [61] and can also be parallelized, allowing for a further decrease in computational cost.

Localization of Source

Different methods of source localization can be used. The oldest method, Time Difference of Arrival (TDOA), is often used [73] [74] [75]. This method compares the time at which a signal is detected, and estimates the location by minimizing the error in time of arrival with the calculated time of arrival for the estimated source. This approach may work when the wave velocity is constant. When the wave is subject to dispersion, a different wave mode might be detected, resulting in an error due to using an incorrect wave velocity [76]. In order to correctly determine the location, a method has to be used to cope with the possibility of varying wave speed. Quasi Beamforming (QBF) makes use of an array of sensors that are placed close to each other. By using this approach the signal has travelled roughly along the same path, experiencing the same dispersion, and the wave mode that is detected is the same. By making use of at least 4 sensors it is possible to accurately locate the source, because the wave speed can be determined as the wave travels through the array [44]. This allows for a more accurate source location [77]. Another advantage of this method is that in such a layout, the cost can be decreased due to centralization of the hardware and an increase in coverage area, thereby reducing installation cost and complexity of the system [78]. This QBF approach is therefore preferred over the TDOA approach. Although its benefits are clear, the performance of this localization technique should be validated on the test setup in order to determine the accuracy in a more complicated structure. During operation of the monitoring system, a large amount of data can be created. For autonomous functioning of the system, the processing of data should be optimized. This can be done by filtering and processing the acquired signals in situ, reducing the storage needs at the location.

Noise

The AE phenomenon that has to be detected is very weak in signal strength. Although the sensors can detect signals with a strength as low as $20dB_{ae}$, noise can make it difficult to detect the fatigue crack growth. Noise can come from natural sources, such as rain, waves, and animals, or it can come from anthropogenic sources such as boats, sonar, and explosions. Furthermore, the noise can be tonal, meaning it has one specific frequency, transient (short bursts of sound from dolphins or pile driving) or plain noise, which has an irregular character, containing multiple frequencies that interfere with each other. The sources that lie outside of the wind turbine that are within the frequency domain that is also of interest for AE monitoring are mammals, acoustic deterrents, acoustic communication equipment, echo sounders, and ships [79]. The frequency of these sources interferes with the preferred frequency for AE monitoring. Although these sources can interfere with the frequencies at which measurements are taken, it is not expected to be continuously present during operation. It should therefore be sufficient to detect if a measured event is resulting from such an external source or from a source that lies within the structure. This process can be performed using guard sensors [80] [81], which indicate whether a signal comes from a source within, or it can be done using filtering based on the characteristics of the signal, such as arrival time, frequency, signal duration. Filtering of the signals becomes more difficult when the noise is continuous and wideband. Such sources are for example coming from moving parts inside the turbine, wind, waves or rain. The intensity of this type of noise is shown visually in Figure 4.1 and Figure 4.2. The maximum noise level as a result of rain or wind is equal to $112dB\ re\ 1\ \mu Pa^2$ [79]. Although initially it was thought that rain caused purely white noise [82], later research showed that this is not true. As sensors did get more sensitive and capable of measuring at more frequencies, it was found that the frequency spectrum of rain was as shown in Figure 4.3.

The noise level in the surrounding water is only one part, as the noise level within the structure as a result from rain or wind is what is required. There have not been found any sources that go into that much detail. Regarding ultrasonic noise that comes from rotating equipment within the wind turbine, no source was found that contained this kind of information. There was one source that included ultrasonic noise and its influence on bat species [83]. It found that the noise emitted was of low intensity and highly variable. It concluded that ultrasonic noise, and the effects of ultrasonic noise on animals has not been investigated well.
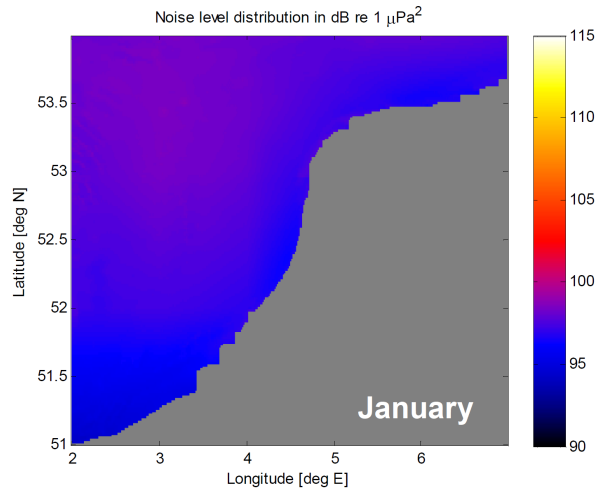
Figure 4.1: Noise in Dutch part of the North Sea as a result from wind, numbers given for the month with highest intensity. [79]
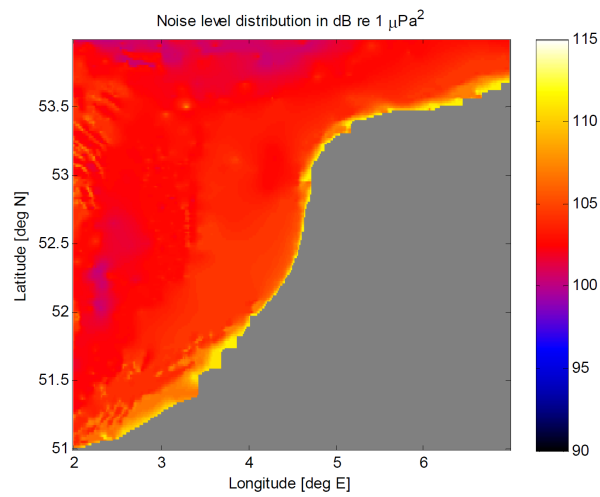
Figure 4.2: Noise in Dutch part of the North Sea as a result from rain at 10mm/h, with receiver at seabed. [79]
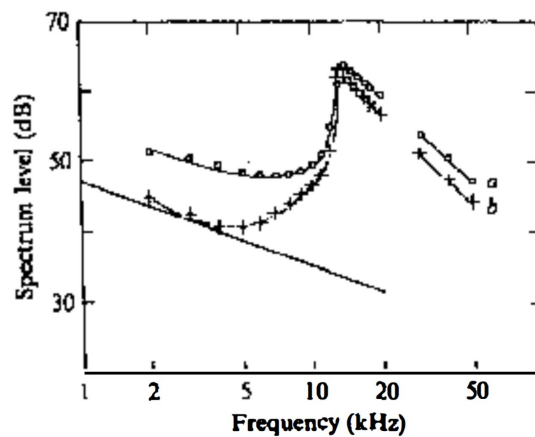
Figure 4.3: Rain causes noise which has a peak in intensity near 15 kHz, has a flat response below 10 kHz, and dies out at increasing frequencies. [84]
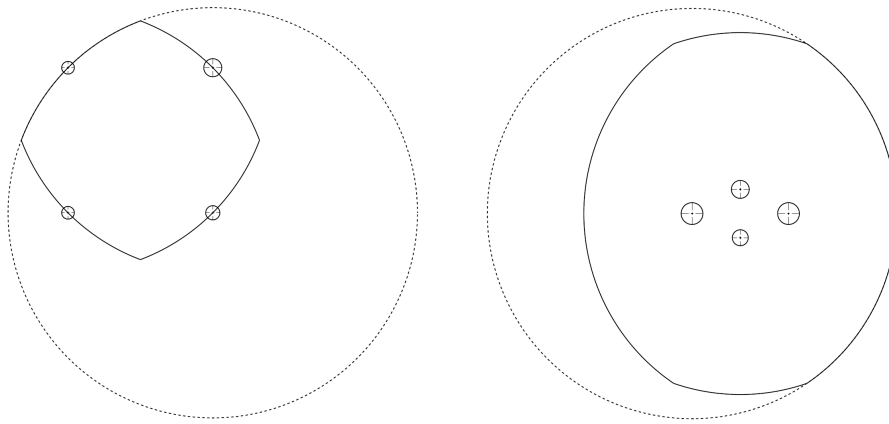
Figure 4.4: A schematical comparison between TDOA coverage area (on the left) and QBF coverage area (on the right). The dotted circle shows the coverage area of one single sensor, while the solid line shows the coverage area for the system as a whole, the sensors are displayed as small circles. The coverage area should be such that an event can be picked up by all 4 sensors. Therefore, the coverage area consists of all the points that lie within the maximum detectable range of each sensor. In the case of TDOA, the sensors are placed as far from each other as possible, resulting in a surface area that is almost as big as a square with rib length equal to the maximum detectable range. In the case of QBF, the coverage area approaches that of a circle with radius equal to the maximum detectable range of the sensor.

Analysis

Understanding of the AE phenomena has been established well already. When AE was discovered during breaking of wood, instruments were not very accurate. As the sensing equipment got more and more precise, the occurrence of AE was also shown in different metals, and the link to fatigue was made at an early stage. From the literature review, there appears to be no discussion on AE as a result of fatigue crack growth.

Modeling of the system by means of numerical simulation can be done in many different ways. Elastic waves are simulated in different applications, ranging from large scale seismic waves down to the scale of AE. Although the scale is different, the physics remain the same. Requirements for simulation are accuracy of the model and computational cost. Conventional FEM will have significant computational cost if the desired accuracy has to be met. EFEM and BEM/FEM perform a bit better, as both methods take measures against the overly stiff behavior of conventional FEM. The SEM seems to perform even better, as the method makes use of higher order elements in order to correctly model the elastic, high-frequency wave. By the design of the mass matrix, this method reduces the complexity of the system that is to be solved [61]. Further acceleration of the simulation can be achieved by using a 2D model instead of a 3D model. 3D models can be used when the geometry is complex, but come at the cost of increased computation time. For simpler geometries, such as in the case that is investigated in this thesis, 2D models do suffice. In this research project, the advantages of the SEM method in 2D modeling are significant, and therefore this is the method of choice.

The QBF Method has clear advantages over the TDOA methods in most structures. Its accuracy is at the same level as TDOA or better when TDOA fails to detect the correct wave velocity. The area that can be covered by the QBF Method is also approximately a factor of 4 larger. The TDOA method typically covers a square area with side length of less than the detection range of a single sensor. A schematic comparison is shown in figure 4.4. In case the grid is extended in the TDOA method, the area covered per number of sensors does get better, yet it can only approach the coverage area in case it is repeated a large number of times. The QBF Method covers a circular area with radius less than the detection range of a single sensor. As the sensors are located close to each other, requiring less actions during installation, installation cost should be less than that of TDOA. The accuracy of the QBF method is subject to the spacing of the sensors within the array; if the spacing is too large or too small, the quality of the signal might be affected, or the error in determining the time of arrival might become too large. In processing of the acquired data, different filters can be applied, and the allowable errors on different aspects can be modified in order to obtain more accurate results or to detect more events when quality of the signal is suboptimal.

Although there is some information on the noise level that can be expected in the field, this information does not directly translate to what signal will be picked up by the sensors. Next to that, the information only includes information on noise generated by waves and by rain. Noise as a result from rotating equipment, as well as waves hitting the structure cannot be found. The noise resulting from rain can be simulated in the lab, using a steel plate submerged in water. The results from this experiment can be used to link oceanic noise levels to noise that is being picked up by the sensor, as it is expected that the noise resulting from drops in fresh water is three to four decibel louder compared with salty water [85] [86]. The behavior of salt water differs from fresh water, which can be caused by the different chemical contents, as well as a slightly different density and wave speed. The differences in wave speed are in the order of 1 percent and can be neglected. Noise values for waves hitting the structure and noise resulting from rotating equipment in the tower are missing. In order to obtain accurate numbers, field measurements have to be performed. In order to accurately determine these values, a full year of observations should be performed. As this cannot be done given the time schedule for this thesis, having noise measurements from just one single day can be considered useful. At the same time the durability and resistance against environmental influences, such as waves, of the sensors could be tested. No problems have been reported on this aspect in [48] and [87], nor has anything been reported on the exact method of installation.

Discussions and Conclusions

During analysis of the available literature it seems that there is a good understanding of AE within the AE community. The understanding ranges from the microscale, being the phenomena of AE resulting from fatigue crack growth, to modeling of the behavior of structures up to large scale applications. Although it seems that this technique would be useful in many applications, the number of applications where it is used is limited. This could be due to the early days of AE when it was widely used without full understanding of the phenomena and how to correctly implement this technique, as well as the cost which used to be high. Nowadays, the phenomenon is understood, developments such as QBF may result in an increase of the capabilities, the cost of the hardware has come down, while the quality of the sensors has gone up. It thus seems like an ideal moment to study the feasibility of AE in structures, its performance and design a concept that could be used in monitoring of offshore wind turbine support structures.

The number of reports on (oceanic) noise is limited. Furthermore, the different types of noise that might be encountered offshore are only vaguely specified. Noise can come from natural sources, boat equipment, or rotating machinery from the wind turbine itself. Knowledge about the frequency spectra for different sources of noise is lacking, and this causes a risk for the design of an offshore acoustic emission monitoring system. To decrease the risk, experiments can be performed in order to establish the actual noise levels in the field. As the noise is partly weather-dependent, ultrasonic noise should be measured for a full season. With this knowledge, it is possible to accurately determine the operational boundaries of the system, and thus the capabilities.

It can be concluded that AE could be a suitable technique for monitoring of fatigue crack growth in offshore wind turbine support structures. In order to give a definite answer to this statement, a number of experiments are devised to support or reject this hypothesis. The detection range of a single sensor can be determined using numerical simulations. A 2D model using the Spectral Element Method can accurately model the attenuation of the elastic wave in the structure. Localization of the source can be performed using the Quasi Beamforming method, which provides superior coverage, increased accuracy and reduced cost by centralization, compared to other methods. If the calculations provide positive results, lab testing could deliver proof of the functioning of such a setup, bringing the application of AE in offshore wind turbine support structure monitoring one step closer.

5

Numerical Simulations

An important factor in determining the coverage area of the sensor is the attenuation of signal over distance. Via computer simulations a large number of scenarios can be tested without having to perform costly testing for all these experiments. This section starts with the goal of the simulation. Next, the theory of the Spectral Element Method (SEM) is discussed, followed by the implementation of this method for this subject. The results are validated using results from literature. Lastly, the results are discussed as well as what can be done by using these results in the context of acoustic emission monitoring of offshore wind turbine structures.

Goal of simulation

An important aspect in the performance of an acoustic emission monitoring system is the area a single sensor node can cover. This can be discovered empirically, but would require new measurements every time a parameter in the setup is changed. This is where simulations can provide an alternative to measurements, as many different scenarios can be tested without the need for many experiments.

In determining the coverage area of a single sensor node, the maximum distance at which a sensor can detect a signal plays an important role. The maximum distance at which a sensor can detect a signal depends on the source signal amplitude, the sensor transfer function, and the decay of signal over distance. Noise and other factors may also influence that maximum distance. The source signal amplitude and the sensor transfer function can be measured, but the decay of signal over distance is more complex. The decay of signal over distance consists of leakage to the water, dispersion of the signal and geometrical spreading. The geometrical spreading depends on the structure in which wave propagates and can be calculated analytically. The dispersion of the signal is a result of the velocity which is not constant with respect to the frequency of the signal. The velocity of the signal depends not only on the frequency, but on the thickness as well. The leakage to the surrounding medium depends on the frequency, thickness of the structure, density of the media through which the wave travels, and more. The simulation allows for adjusting any of the parameters such that it fits the situation, and the decay of signal over distance can be estimated based on these simulations.

These simulations are performed to find the attenuation of acoustic emission signal in offshore wind turbine foundations below the sea level. The parameters that are used should therefor resemble these conditions. The wall thickness that is chosen ranges from 12 mm up to 60 mm, as this range of dimensions covers the typical thickness of wind turbine support structures. The frequencies are chosen such that the $S0$ and $A0$ modes can be distinguished. Therefore, the frequency range has an upper bound and a lower bound. The lower bound is defined by the frequency where (near)-zero frequencies no longer have a disturbing effect. As can be seen from the dispersion curve in figure 5.1, the velocity drops below a certain frequency due to the curvature of the model, and this causes difficulties when determining the exact arrival time of the signal. The upper bound is defined by the onset of higher order wave modes. If higher order wave modes are present, it is difficult to determine which wavemode is being detected, resulting in less accuracy when it comes to source localization.

Quality of the results is ensured by validating the model against two different sources. Both of the sources provide a curve of the attenuation with respect to frequency or frequency times thickness for

the zero order anti symmetric wavemode. The simulation is performed for the case where the liquid medium is at one side only. The attenuation for the case where liquid is at two sides of the plate, is about twice that of the case with liquid at one side only, as long as the product of thickness and frequency is smaller than 3 MHz mm [88].

Theory

Numerical Simulations are often performed for various applications. Well-known are software packages that are used to analyze structures that are subject to loading, such as Abaqus, Ansys, and NASTRAN. The elastic waves for which the attenuation has to be calculated do have a small wavelength. The use of FEM for wave propagation simulation requires 6 to 10 nodes per wavelength [89], resulting in a high number of elements for this application. The time integration method is negatively affected by the number of nodes, resulting in high computation cost. SEM has proven to be efficient. The accuracy of the method is desirable, without the computational time to become excessive [61].

The method that is used for the simulations is based on work performed by Komatitsch, Barnes and Tromp [61][90] [91] [92] [93]. This method has proven to be robust, accurate and efficient. This section explains the key characteristics of this method

As the model consists of two parts, the solid and the liquid, the problem can be split up into two separate parts, that are joined together at the interface. Within the solid part, which is assumed to be isotropic, the wave equation is given as

$$\rho \ddot{\mathbf{u}} = \nabla \cdot \boldsymbol{\sigma} + \mathbf{f} \tag{5.1}$$

with $\mathbf{u}$ the displacement vector, $\boldsymbol{\sigma}$ being the symmetric second order stress tensor, and $\mathbf{f}$ the externally applied force. The density of the medium is expressed by ρ. Furthermore,

$$\boldsymbol{\sigma} = \mathbf{C} : \varepsilon = \lambda tr(\varepsilon)\mathbf{I} + 2\mu\varepsilon \tag{5.2}$$

The fourth order stiffness tensor is expressed by $\mathbf{C}$. In this equation μ and λ represent the Lamé parameters. The strain ε is given as

$$\varepsilon = \frac{1}{2}[\nabla \mathbf{u} + (\nabla \mathbf{u})^T] \tag{5.3}$$

For the liquid part of the model, the wavefield is defined using the conservation and dynamics equations as follows

$$\rho \dot{\mathbf{v}} + \nabla p = \mathbf{0} \tag{5.4}$$

$$\dot{p} + \rho c^2 \nabla \cdot \mathbf{v} = 0 \tag{5.5}$$

with $\mathbf{v}$ the velocity vector, p the pressure while the acoustic wave speed is indicated by $c = \sqrt{\frac{\kappa}{\rho}}$ in which κ is the bulk modulus of the fluid. If it is assumed that the liquid is homogeneous, the transmission of the acoustic wave within the liquid is irrotational, and the velocity of the acoustic wave can be written as $\mathbf{v} = \nabla \phi$, with ϕ the velocity potential. On the boundary between the two parts, continuity of traction and kinematic continuity are maintained as shown by the following equations:

$$\tau = \rho \dot{\phi} \hat{\mathbf{n}} \tag{5.6}$$

$$\hat{\mathbf{n}} \cdot \nabla \phi = \hat{\mathbf{n}} \cdot \dot{\mathbf{u}} \tag{5.7}$$

with τ the traction, $\hat{\mathbf{n}}$ the unit vector normal to the interface. An absorbing boundary could be used to mitigate reflections of waves at the boundary of the model. This would reduce the reflection to only a few percent of the original wave. For this application, no absorbing boundary is used, as the model size is such that the reflections do not influence the measurements.

The equations so far were all applicable to a continuous system. A computer can be used to solve the problem, but to limit the amount of calculations performed the system is split up into a predetermined number of elements. The first step towards this discretization is multiplication of the previous equations

with an arbitrary test vector $\mathbf{w}$ in the solid, and a test function w in the fluid part. The separate parts are integrated over the corresponding areas.

$$\int_{\Omega_s} \rho \mathbf{w} \cdot \ddot{\mathbf{u}} d\Omega + \int_{\Omega_s} \nabla \mathbf{w} : \mathbf{C} : \nabla \mathbf{u} d\Omega - \int_{\Gamma_i} \mathbf{w} \cdot \tau d\Gamma - \int_{\Gamma_{abs}^s} \mathbf{w} \cdot \tau d\Gamma = \mathbf{0} \tag{5.8}$$

$$\int_{\Omega_f} c^{-2} w \ddot{\phi} d\Omega + \int_{\Omega_f} \nabla w \cdot \nabla \phi d\Omega + \int_{\Gamma_i} w(\hat{\mathbf{n}} \cdot \nabla \phi) d\Gamma + \int_{\Gamma_{abs}^f} c^{-1} w \dot{\phi} d\Gamma = \int_{\Omega_f} w f d\Omega \tag{5.9}$$

The solid area is represented by Ω_s, the fluid area is represented by Ω_f, the boundary for the solid is Γ_{abs}^s, the boundary for the fluid part Γ_{abs}^f, and the interface between the two parts as Γ_i. In this equation, the externally applied force f has been placed in the fluid part, but this could also be placed within the solid part. In order to discretize the model, the domain Ω is meshed using n_{el} elements Ω_e. The elements that are used are Legendre spectral elements. Each element has a reference domain, which is described by $\Lambda = [-1, 1]^{n_d}$, with n_d the dimension of the model, which is two for this case. The link between such an element and the complete model is made via a reversible mapping function, specifying that $x(\epsilon) = F_e(\mathrm{E})$. On the reference element, a polynomial basis function of order N is applied. Each element has $N + 1$ Gauss-Lobatto-Legendre points in each direction. The Gauss-Lobatto-Legendre points are located at the roots of

$$(1 - \mathrm{E}^2)P_N'(\mathrm{E}) \tag{5.10}$$

with P_N' being the derivative of the Legendre polynomial with degree N. The basis function that is chosen is such that there is only one nonzero contribution at each of the Gauss-Lobatto-Legendre points. The integration of this approach is not exact, but the speed advantage obtained is worth it. With the discretization of the different elements completed, the system can be solved like a traditional FEM problem. The system is separated into a fluid part and a solid part as follows:

$$\begin{bmatrix} M_s & 0 \\ 0 & -M_f \end{bmatrix} \begin{pmatrix} \ddot{U} \\ \ddot{\Phi} \end{pmatrix} + \begin{bmatrix} D_s & A \\ A^T & D_f \end{bmatrix} \begin{pmatrix} \dot{U} \\ \dot{\Phi} \end{pmatrix} + \begin{bmatrix} K_s & 0 \\ 0 & -K_f \end{bmatrix} \begin{pmatrix} U \\ \Phi \end{pmatrix} = \begin{pmatrix} F \\ 0 \end{pmatrix} \tag{5.11}$$

in which M_f and M_s are the mass matrices for the fluid and the solid part, D_s and D_f are the absorbing boundaries for the solid and the fluid region, A is the coupling matrix, K_s and K_f are the stiffness matrices for the solid and the fluid part, U indicates the displacement in the solid, while Φ represents the velocity potential in the fluid. the force applied to the solid part of the system is represented by F. In order to discretize over time, an explicit Newmark scheme is used. For a second order system, such as

$$M\ddot{\mathbf{x}} + C\dot{\mathbf{x}} + K\mathbf{x} = F \tag{5.12}$$

the Newmark scheme states that

$$M\ddot{\mathbf{x}}_{n+1} + C\dot{\mathbf{x}}_{n+1} + K\mathbf{x}_{n+1} = F_{n+1} \tag{5.13}$$

and that $\mathbf{x}_{n+1}$ can be found as follows

$$\mathbf{x}_{n+1} = \mathbf{x_n} + \Delta t \dot{\mathbf{x}}_n + \frac{\Delta t^2}{2} \ddot{\mathbf{x}}_n \tag{5.14}$$

and

$$\dot{\mathbf{x}}_{n+1} = \dot{\mathbf{x}} + \Delta t \left[(1 - \gamma) \ddot{\mathbf{x}}_n + \gamma \ddot{\mathbf{x}}_{n+1} \right] \tag{5.15}$$

This scheme is conditionally stable, and second-order accurate when γ equals 0.5. This is used in the simulation and ensures that the results are accurate while computational cost remains low.

Validation

To make sure that the results of the simulation are of good quality, the model is validated against Watkins et al. [94]. This make use of numerical methods to calculate the attenuation of a steel structure that is in contact with water. The parameters of the simulation are set similarly to the ones used by Watkins et al and Zernov et al. as applicable. This is done to validate the model with a case that is similar, such that the potential for variations between the models is minimized. The dispersion curve for both curves is given in figure 5.1. The numerical simulations performed in both cases have been performed using the same settings, and should therefore result in similar results.
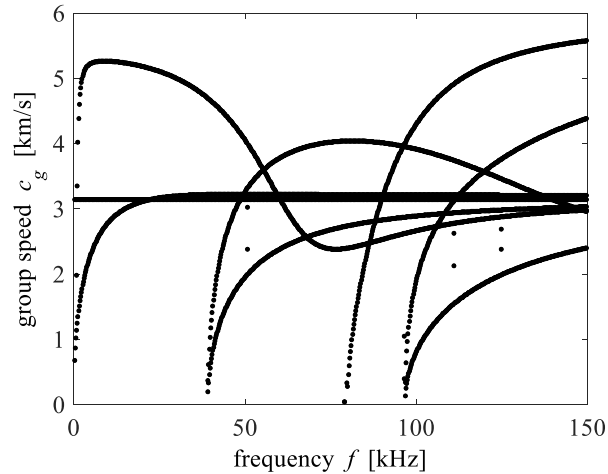
Figure 5.1: The dispersion curve corresponding to a steel metal plate with a thickness of 40 mm. This case is used for validation of the model. The decrease in group speed near the zero frequency is due to the curvature of the of the metal plate. This method is accurate for the zeroth order and first order wavemode. Higher order wavemode group speeds, present at 80 kHz and higher in this case, are not accurate.

Validation with Watkins et al.

Watkins et al. [94] have attempted to find the attenuation for the zero-order antisymmetric wavemode. The approach used calculates the power loss per distance travelled. The results indicate that the attenuation is dependent on a dimensionless parameter S, with

$$S = \frac{\omega b}{V_s} \tag{5.16}$$

With b the half-width of the plate, ω the angular frequency, and V_s the bulk shear wave velocity. The authors indicate that their approach is accurate up to ±5%, and only gives reasonable results when S is larger than the transition point, which is indicated by the peak attenuation. To be able to compare the results from this simulation to the results of Watkins et al., the results have been translated to end up with comparable information. The paper measured a loss of signal in decibel per wavelength as a function of the product of thickness and frequency, while the simulation calculates a signal loss in decibel per meter as a function of frequency only. To obtain similar units, the frequency-thickness product was divided by the 40 mm thickness that was used for the simulation. To get from the decibel per meter to decibel per wavelength, the wavelength had to be determined at every frequency, which can be done using the dispersion curve.

Comparison of the results from the spectral element method with those from Watkins et al. is shown in figure 5.2. Generally, there is a good agreement between the two methods. The decline from 20 kHz onwards is similar, as is the steep increase at low frequencies. The numerical simulation slightly overestimates the peak, and the decline starts a little later compared with Watkins et al. This is due to the finite bandwidth of the pulse in the numerical simulation, which is also subject to dispersion, while a monochromatic signal does not suffer from dispersion. At higher frequencies the effect of higher order wave modes results in an increase in attenuation. At frequencies above 40 kHz there are higher wave modes, which is unfavorable for the QBF approach, while the attenuation at low frequencies is too high to obtain a good coverage.

Results

After performing the simulations for the cases of 12mm, 24mm, 36mm, 48mm, and 60mm an estimate can be made regarding the attenuation of signal in an offshore monopile foundation below the sea-level. These results were obtained using the parameters as shown in table 5.1. The outputs generated by the simulation are the wavefield at any given moment in time, the progression of the waves over time at varying distance, the dispersion curves, and the attenuation. An example of the wavefield is
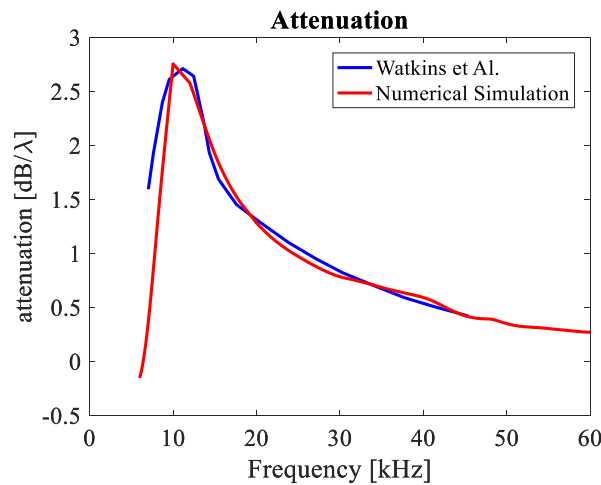
Figure 5.2: Validation of the spectral element model with numerical simulation by Watkins et al.[94]. The thickness for this simulation was set at 40 mm

Table 5.1: Simulation parameters as used in the simulations.

Young's Modulus solid	200 GPa	Length model	minimum of 2.160 m
ρ_s	7800 kg/m^3	time step	maximum of 0.2 μs
ν_s	0.3	time duration of simulation	minimum of 500 μs
G_s	$\frac{E}{2(1+\nu)}$		
Radius	3.5 m	mesh size	12mm, 24mm, 18mm, 24 mm, 30mm
ρ_l	1020 kg/m^3	Cp_l	1500 m/s

given in figure 5.3, while an example of the progression of waves over time is given in figure 5.4. The dispersion curves and the attenuation for each case are given in figure 5.5 and figure 5.6.

The results show that an increase in thickness results in a decrease in attenuation, and also a decrease in the frequency range that is suitable for acoustic emission monitoring. The frequency range that is considered usable is where attenuation is low, while there are only fundamental wave modes present, while the frequency should be higher than the frequency at which peak attenuation is obtained.

Using these results it is possible to make an estimate of the coverage area in a certain situation. By knowing the coverage area of a sensor array, it is then possible to determine the amount of sensor arrays required for a certain application. This information is used in section 7 to determine the estimated costs of an acoustic emission monitoring system.
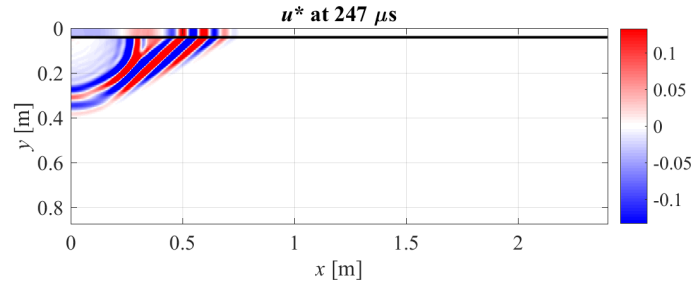
Figure 5.3: The wavefield as simulated at $247\mu s$ after application of input. It can be seen that the wave travels through the solid (top part) and leaks into the liquid. Because the wave travels faster through the solid, an oblique wave front is formed in the liquid. An omnidirectional wave front is also present, as a result of the input at x = 0.
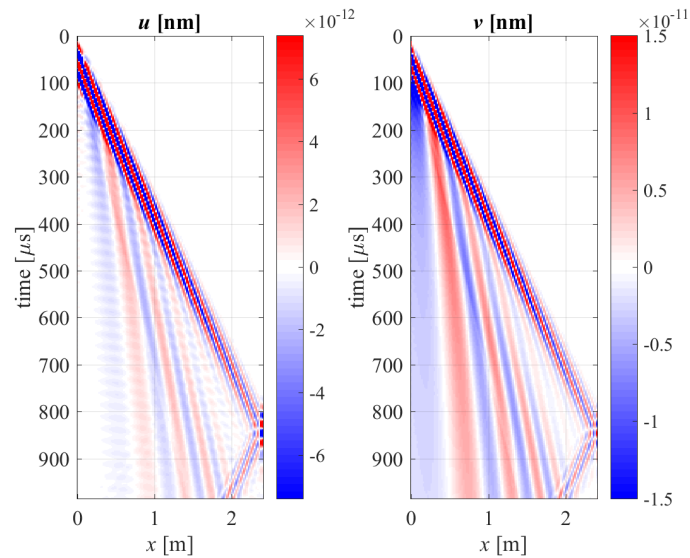
Figure 5.4: The progression of the wavefield (near the solid-liquid interface) over time is shown. Both inplane (left) as well as out of plane (right).

Figure 5.5: The dispersion curves and attenuation curves for a steel plate with thickness of 12, 24, 36 and 48mm submerged in water (one side). The curves are similar in shape, but the exact values are different. The dispersion curves are not accurate for higher order wavemodes.
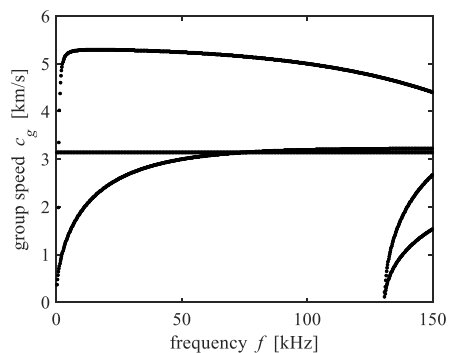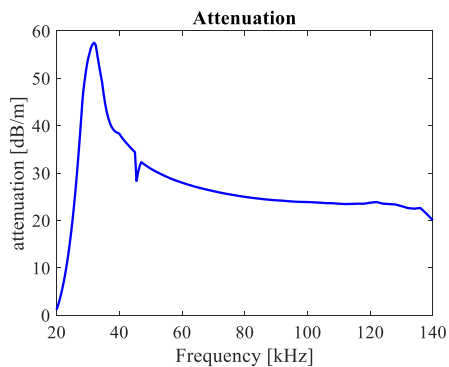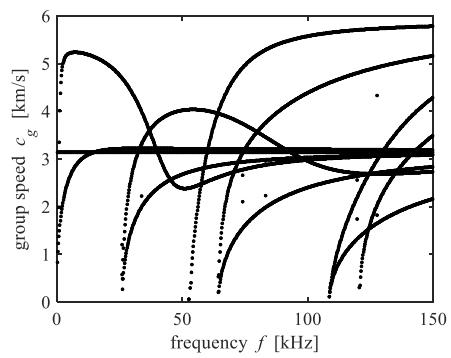
(a) Dispersion curves for 60mm wall thickness
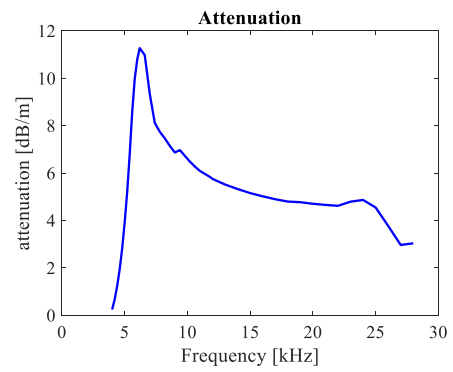
(b) Attenuation of signal for 60mm wall thickness

Figure 5.6: The dispersion curve and attenuation curve for a steel plate with thickness of 60mm submerged in water (one side). The curves are similar in shape, but the exact values are different.

6

Testing

If an acoustic emission monitoring system has to operate remotely at an offshore location, various aspects become important. Acoustic emission monitoring has been implemented in a bridge deck [44], which is by approximation a two dimensional structure. Wind turbines differ from bridge decks in the sense that the surface is curved, the noise they are subject to is different, and (offshore) wind turbines are often located at remote locations. In order to determine the consequences of the differences, a number of tests are executed. These tests provide small pieces of knowledge that could help determine the potential of an acoustic emission monitoring at an offshore wind turbine. Each test is designed to make use of a setup or situation where only one unknown is studied, to isolate the effect and functioning of a certain parameter or setup. As the amount of knowledge on the functioning of parts of the setup is increased, the complexity of the test can be increased too. Problems that are encountered along the way are analyzed to find the root cause of the problem. This is done to determine the limitations that may be encountered during the implementation offshore, before operation, such that effective countermeasures can be implemented.

This chapter starts at a low complexity level, adding different aspects of acoustic emission monitoring on offshore wind turbine foundations every section. The first test was used to verify that the software that is used for analysis of acoustic emission signals is capable of functioning remotely at set intervals. The geometry in that test is a two dimensional rectangular plate. Since wind turbine foundations generally consist of tubular steel, the effect of curvature on the transmission of the signal is studied using a flat plate and two tubular samples with different diameter. The tubular samples are showing surface corrosion at some areas. The effect of this surface corrosion is studied, showing the effects of surface corrosion and the necessity for surface treatment. With the effect of the curvature known, and having shown the functioning of the acquisition setup, it is time to move forward to a three dimensional part. A T-joint sample is used at TNO for fatigue testing. Before the sensors are tested during the fatigue tests, the localization performance is tested. With the accuracy and functioning known, the system is set to monitor as the sample is subject to cyclic loading and a fatigue crack develops. A possible factor that may limit the usability of an acoustic emission monitoring system is noise. Noise can be caused by a number of different sources, as shown in section 4.2.4. Two sources of noise that are expected to be dominant in an offshore environment are mechanical noise caused by rotating machinery and environmental noise caused by rain. An onshore wind turbine is monitored to get an estimate for the mechanical noise that is to be expected. The noise resulting from rain is studied in the laboratory by simulating rain. By combining the information gathered in these experiments, an estimate can be made as to how such a system would perform offshore. This can then be used to determine if further development of this system is deemed useful and what the next steps need to be in order to achieve a functioning monitoring system.

QBF Source Localization

During acoustic emission monitoring in an environment with noise, a big amount of data is being generated. A large portion of the data may be noise. By removing the noise from the data, the data storage requirements or requirements of the wireless transmission system can be reduced. This requires the
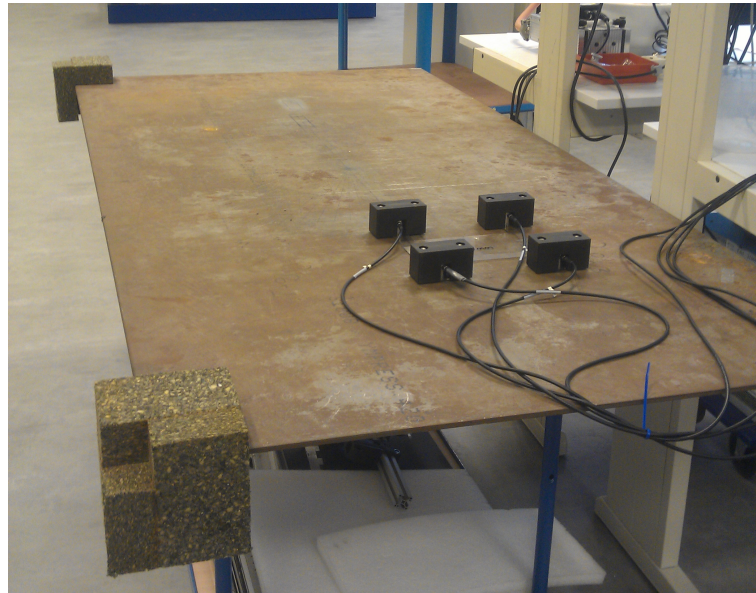
Figure 6.1: The setup as used during the first set of tests. The sensors are positioned in a two by two array, with dimensions 200mm by 200mm.

data to be processed on location at set intervals, which is performed by an add-on to the QBF localization software. The functionality of this add-on is tested to make sure that the software indeed eliminates noise while saving data that results in a source location estimate, so that it can be further analyzed onshore.

Test Setup

The test is performed at the ultrasonics lab of TNO at the Leeghwaterstraat. Use was made of an 8mm thick steel plate, with length of 2m and width of 1m. The sensors that are used are Physical Acoustics PK6I, with specifications as shown in appendix B. The sensors are placed in an array with width and length 200mm. Physical Acoustics' USB AE nodes, specifications in appendix D, are used to connect the transducers to a desktop, running the data acquisition software, which saves each detected waveform. A pencil lead, with hardness HB and a diameter of 0.5mm, is used to simulate an acoustic emission source. A picture of the steel plate and layout of the sensors is given in figure 6.1

Test Procedure

This test is performed to check whether the automation module can start the QBF software and analyze the data with a set interval. By doing this the data storage is minimized by storing only the information that does result in an estimated location for the source of acoustic emission activity. The software is set to analyze the data two times. The first time is after 30 seconds, and the second time is after 60 seconds. During each interval, a number of pencil leads are broken on the surface, at various locations, as a source of acoustic signal. At the same time noise is introduced by moving a finger over the surface, which does not result in a short emission of acoustic activity and has to be discarded during the processing. The pencil leads are approximately 5mm long, and the pencil is held at a $45 \deg$ angle to the surface.

Results

During the test, 600 waveforms have been recorded. Most of these waveforms can be considered as noise, resulting from movement of the finger over the surface. Out of the 600 waveforms, 8 sets of waveforms passed all the criteria and resulted in 8 estimated source locations, as shown in figure 6.2. A set of waveforms that have passed the criteria is shown in figure 6.3. For comparison, a set of waveforms that did not result in a location is shown in figure 6.4. In the first case, the signals after band pass filtering are shorter in duration, and the arrival time and rise time and peak can more easily be distinguished. By shifting the signals such that the correlation is highest, the difference in arrival
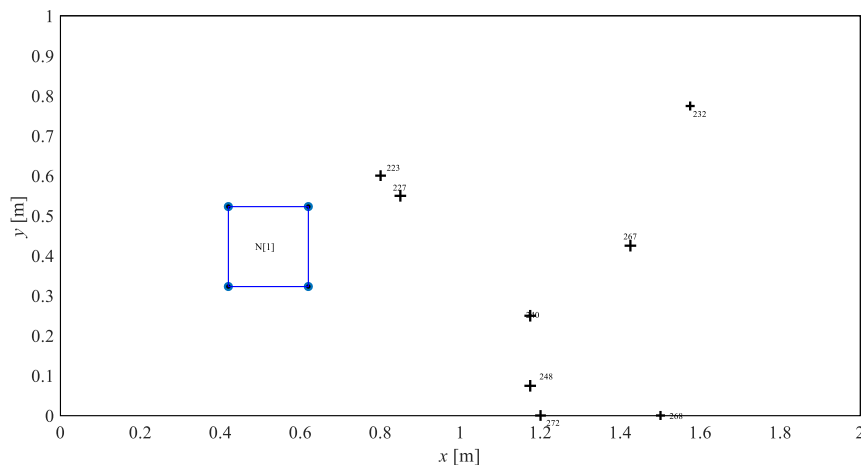
Figure 6.2: The estimated acoustic emission source locations during a test in which the QBF software is set to run at set intervals. The plate thickness is 8mm and a total of 10 pencil lead breaks were applied to the surface at various locations, over a time period of approximately 1 minute, while the QBF software was set to analyze the results every 30 seconds.

time is calculated. This difference in arrival time, together with the velocity of the signal, results in an estimated location. For the second case, the filtered signal after matching of the signals does not result in a good correlation between the signals or a time difference between the signals that could result in a location. The recorded waveforms are therefore deleted.

Conclusion

The test was performed to prove that the QBF software can be implemented in an online processing manner, over a prolonged time with set intervals. The test that has been performed, showed that over a time period of 60 seconds, a total of 8 source locations were estimated out of 10 pencil lead breaks. The missing source locations are likely to be caused by reflections of the signal on the edge of the plate, resulting in not meeting the criteria, being discarded, and not using any more disk space. The localization accuracy has not been assessed in this test, but this is done in section 6.4. It can be expected that by making use of the QBF software at set intervals, the requirements for storage of the data can be reduced, or wireless transmission of the data from a remote location might be a possibility. This enhances the capabilities of QBF acoustic emission monitoring system.

Curvature Effect

Wind turbine foundations, whether the monopile type or the jacket type, make use of curved steel. Having a surface that is curved might affect the signal transmission from the foundation to the transducer. To determine this effect, a test is performed in which 3 samples with different curvature are tested. This test shows the attenuation as a function of curvature, and thus whether the functioning of an acoustic emission monitoring system is limited as a result of the curvature. Together with the curvature test, the difference between a corroded surface and a clean surface is tested. The effect of corrosion on the transmission of signal shows if surface preparation is in practice needed, and what the effect on the accuracy of detection could be.

Test Setup

In order to test the effect of curvature on the transmission of signal, three samples with different curvature are chosen. Sample 1 is a flat steel plate with dimension 2000 mm by 1000 mm by 8 mm. Sample 2 is a steel tube with outer diameter of 272mm and a wall thickness of 9mm. Sample 3 is a steel tube with outer diameter of 356mm and a wall thickness of 8mm. Only one sensor is used, as localization is not the goal of this test. The exact same sensor is used for each sample, as to eliminate any differences that could result from imperfections within the sensor. The sensor used in this test is a PA-PK6I, with specifications as shown in appendix B. The surface quality is not controlled, but visually inspected, cleaned, and chosen to show a similar level of corrosion and surface roughness for all test
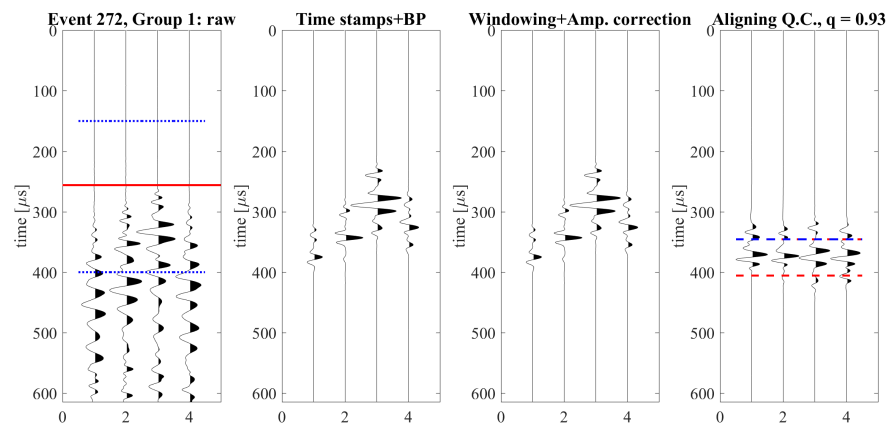
Figure 6.3: In this figure the different waveforms are shown along the process of being analyzed. The first on the left shows the waveforms as they are actually recorded on each individual transducer. In the second figure, the waveforms have been shifted according to their arrival times, and a band pass filtering has been applied. The third figure includes amplitude adjustments, and a windowing is applied. In the fourth figure, the waveforms are matched to maximize the correlation between the different waveforms. When the correlation is maximized, the time shift is used to calculate the acoustic emission source location. In the event shown above, a high enough correlation is obtained and a source location is calculated.
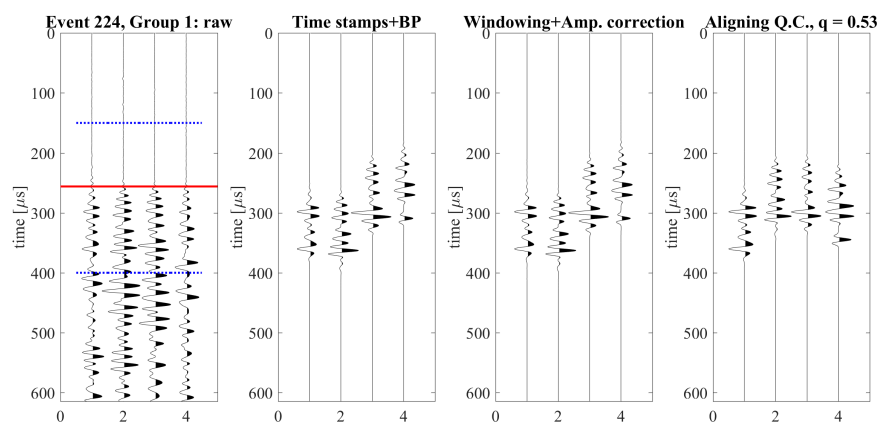
Figure 6.4: In this event, 4 waveforms have been recorded. The waveforms are not as pronounced as in the previous figure, and it was impossible to determine a source location for this set of waveforms. The waveforms are therefor discarded. This signal may be caused by reflections of a previous signal within the plate.

Figure 6.5: A view on the location where the signal strength was measured. The sensor is connected to the metal plate using acoustic couplant gel, and the black block is used to apply a constant force on the sensor, by making use of two magnets which are attached to springs.

samples. Acoustic couplant gel is used in between the sample and the sensor to eliminate voids and to improve transmission of the signal. An example of the setup is shown in figure 6.5.

Test Procedure
The surface at which the measurements are taken is cleaned using water and a dry cloth. A drop of acoustic couplant gel is applied to the surface, such that there is clear squeeze out everywhere around the transducer. A magnetic hold down ensures that the transducer does not move and a constant applied force on the sensor. Pencil lead breaks are used as acoustic emission source. The pencil lead has a diameter of 0.5mm, a hardness HB, and are broken at 5mm length at an angle of approximately 45 degrees. The distance at which the pencil lead is broken is 30cm, and is kept constant for each sample, thus to eliminate any attenuation as a result of geometrical spreading. A total of 5 pencil lead breaks are applied at each sample, as to reduce the variation in signal amplitude.

Results
The pencil lead breaks applied to the surface resulted in almost identical waveforms for each sample. The signal to noise ratio of the measurements is around 60dB, while the source sound level lies around 80 to $85 dB_{ae}$. The detected waveforms for 5 consecutive pencil lead breaks on the flat plate are shown in figure 6.6. It can be seen that the signal is almost identical between the different waveforms. As can be seen in figure 6.7, the detected amplitude does decline as the curvature of the surface increases. This decline in amplitude is limited, and has a negligible effect on the detection of signal for the case of monopile type foundations as well as jacket type foundations.

Conclusion
The effect of curvature on the transmission of the acoustic emission signal is negligible. The measurements show a decrease in signal transmission of up to 2dB for a jacket type foundation, which is similar to the bandwidth of the measured signal amplitude itself.

Surface Quality test
The effect of surface quality may play an important role in the transmission of acoustic emission signal. To have an estimate of this effect, the results for a curved surface with a high quality is compared with a surface with rust on the same tube.
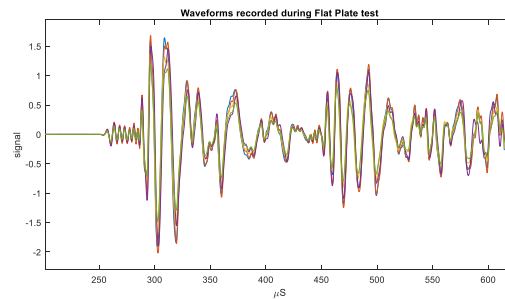
Figure 6.6: A series of five waveforms that were detected during testing for the effect of curvature on signal strength. It can be seen that the signal is repeatable and of similar amplitude, thereby being a representative source for the effect that is being studied.
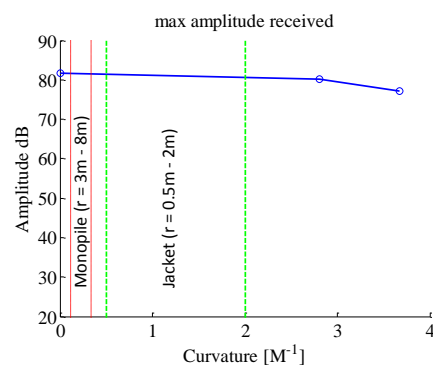
Figure 6.7: The amplitudes have been averaged, and the average is shown at the corresponding curvature. The effect of curvature on the transmission of the signal is limited to -4 dB for the smaller diameter.

Figure 6.8: The test setup at the smaller tube with rusted surface. The sensor is held in place using magnetic hold downs, and acoustic couplant gel is used to maximize transmission of signal between the surface and the sensor. The surface has been cleaned using water and dry cloth to remove any dust or debris, but rust is not removed.
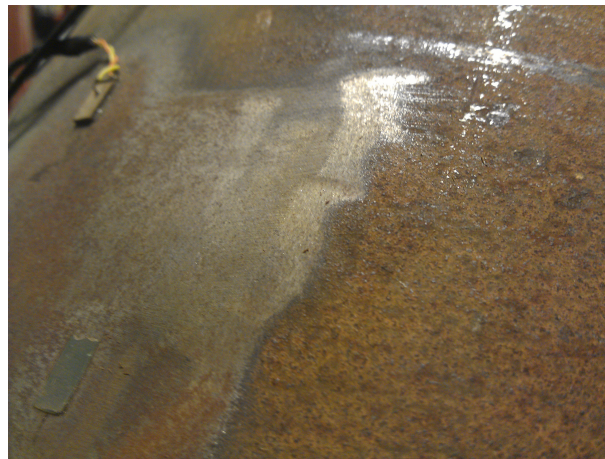
Figure 6.9: The larger tube, where a part has rust removed. Both the rusted part and the rust free surface are cleaned using water and dry cloth.

Test Setup

The effect of rust on the surface is tested, as most of the test sample tubes are covered with surface corrosion. To do this, both tubular test samples are used. Instead of using a surface that is as clean as possible as in the test for the curvature effect, the surface should be heavily rusted for this test. An example of one of the rusted surfaces is given in figure 6.8, and an example of a cleaner surface is shown in figure 6.9. The results from this test can be compared with the results from the curvature effect test. After comparison, the effect of a corroded surface In order to allow for a valid comparison, the same setup is used.

Test Procedure

The surface quality test is performed by comparing the results from the curvature effect test, which is performed on clean steel, with the same test performed on a rusted surface. In this way, the only variable is surface quality. Hence, the same procedure is followed as in section 6.2.2.

Results

The waveforms that were detected differed from the ones detected in section 6.2.3. Looking at the waveforms detected, shown in figure 6.10, the effect was more severe for the larger tube. In general, the largest effect is seen in the different peak amplitude values. A single waveform at the rusted surface is compared with a clean surface in figure 6.11, showing that difference. The difference in

(a) Tube with diameter 356mm
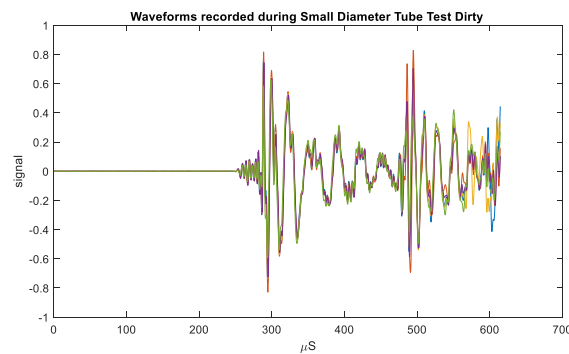
(b) Tube with diameter 272mm

Figure 6.10: Five waveforms that were detected at the tubes. The effect of rust was smaller for the tube with smaller diameter. Although the rust did not affect the signal as much as during the other test, it still had a negative effect.

peak amplitude values was 20 dB for the larger tube and 3 dB for the smaller tube. Not only is the peak amplitude affected, the characteristics of the signal are different too. A decrease in amplitude makes it more difficult to detect the signal for a given background noise, while the change in waveform characteristics could potentially result in more difficulties during matching of the different signals and determining the source location of a detected signal.

Conclusion
The effect of surface quality is significant. When the surface is not properly cleaned prior to application of the transducers, the detected signal can be decreased by as much as 20 dB. Not only does the amplitude decrease, but the characteristics of the signal change too, making the source localization less accurate. Before applying sensors to a structure, any rust should be removed at the location where the sensors are installed.

Localization on T-joint sample
In the previous sections, the functioning of the localization software has been tested, as well as the effect of curvature and corrosion on the transmission of signal. Offshore foundation structures are often tubular in shape, as for example in jacket type foundation. The effect of the curvature of such structures is negligible, but the effect of corrosion is not. The (potential) effects on signal transmission are summarized in table 6.1. After performing these tests, the next step is to test the localization accuracy using a pencil lead break. If this can be done successfully, the following step would be to perform a fatigue test at the lab and try to detect fatigue crack growth during cyclic loading.

Test Setup
For this application, a custom setup has been used, consisting of a simply supported T-joint setup. The brace is welded to the chord in this T-joint setup. The setup is shown in figure 6.12.
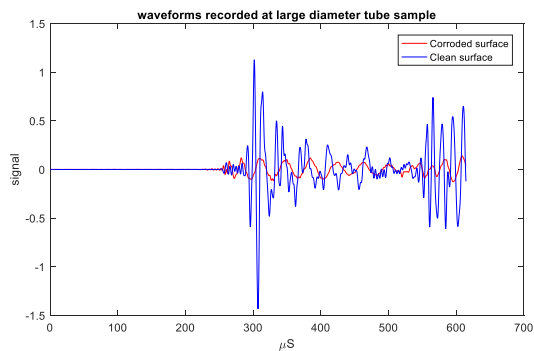
(a) Tube with diameter 356mm
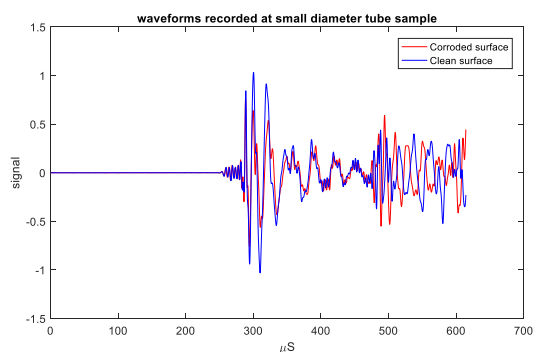
(b) Tube with diameter 272mm

Figure 6.11: The difference between corroded surface and clean surface is shown. In case of a corroded surface, the amplitude in signal is decreased, and the characteristics of the signal is changed.

Table 6.1: A summary of the different factors that are limiting signal transmission. The surface has to be treated properly in order to prevent signal losses of up to 20dB.

Effect	Result on signal transmission
Curvature	< 2dB
Surface quality	Up to 20dB
Leakage into water	13dB/m (wall thickness 24mm)
	5dB/m (wall thickness 60mm)
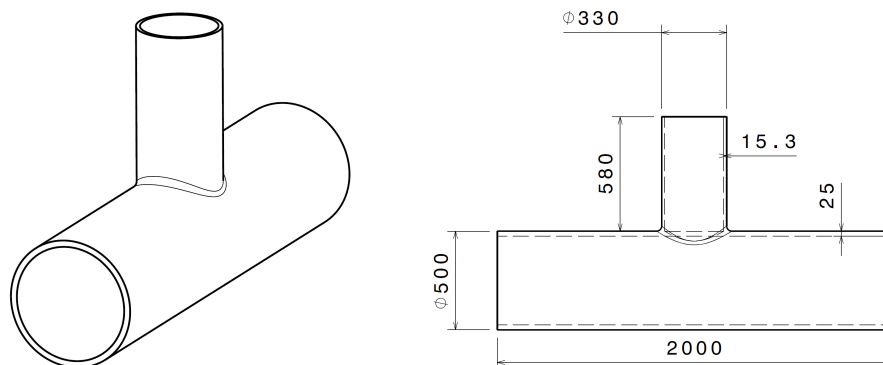
Figure 6.12: Dimensions of the test sample that is used, in millimeters.
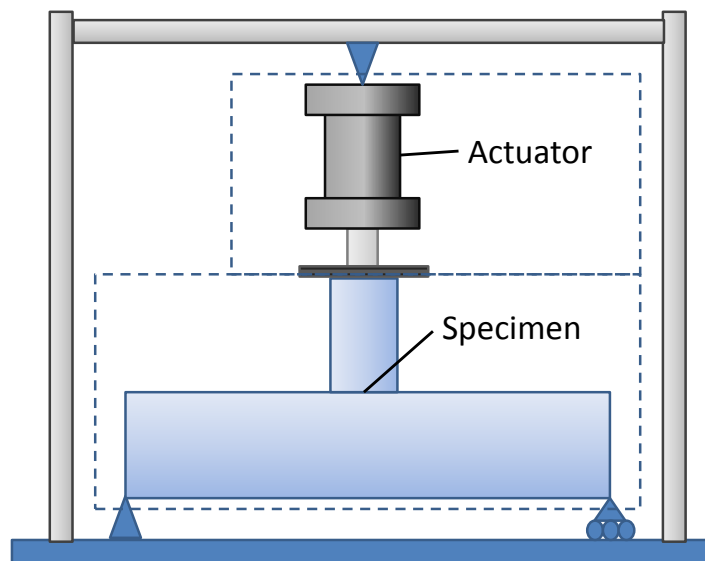
Figure 6.13: Schematic representation of the test setup. Specimen and the actuator are supported on one side using a hinge. The specimen has a roller hinge support on the other end, and is attached to the frame via a hinge. The actuator is attached to the specimen via a bolted connection. The actuator exerts a pulling force on the specimen, causing tension in the brace and the weld, which results in fatigue crack growth.

Table 6.2: QBF Software settings that have been used for processing the data that was gathered during monitoring of the T-Joint. These settings are such that most of the noise is filtered out and only a few events passed all the criteria, resulting in a most probable location.

C_{A_0}	3200 m/s	C_{S_0}	4500 m/s
dt	$0.2\mu S$	dt_{max}	$10\mu S$
Window Length	$250\mu S$	f_c	50 kHz
Band pass filter	$[20-90]kHz$	Minimum Correlation Coefficient	0.7

The test specimen was located at the TNO Structural Dynamics Lab. The material for the brace was S355J2H steel, and for the chord S355G13+N was used. The specimen was mounted in a frame, as shown in Figure 6.13.

The sensors are applied to the structure using a paper template, assuring that the location at which the sensors are applied is accurate. In order to have an accurate source localization, the positioning of the sensors is essential. The template used is a symmetric cross with height of 350mm and width of 200mm. The longest dimension of the template is aligned with the axis of the main tube, while the width is aligned with the radial direction of the tube. Figure 6.14 shows the setup used on the actual structure.

After the signals have been detected by the sensors, they are stored on a hard drive. The data then has to be processed in order to detect whether the recorded events might come from a detectable source, and if so, where that source is located. This is done by the QBF software. A number of settings in the software have to be set in order for the software to detect fatigue events correctly. The software settings used are shown in table 6.4. These settings are acquired by fine-tuning of the settings. The first attempt at processing is largely dependent on the geometry of the sample, and by shifting some of the criteria the number of successfully processed events can be increased or decreased. If during the fine-tuning process events are localized at a location at which no pencil lead break has occurred, the criteria needs to be more strict. If the number of successfully processed events is less than desired, the criteria can be weakened.

Figure 6.14: Sensors applied to the structure; the template has not been removed, as the holes cut into the template allow for maximum transmission.
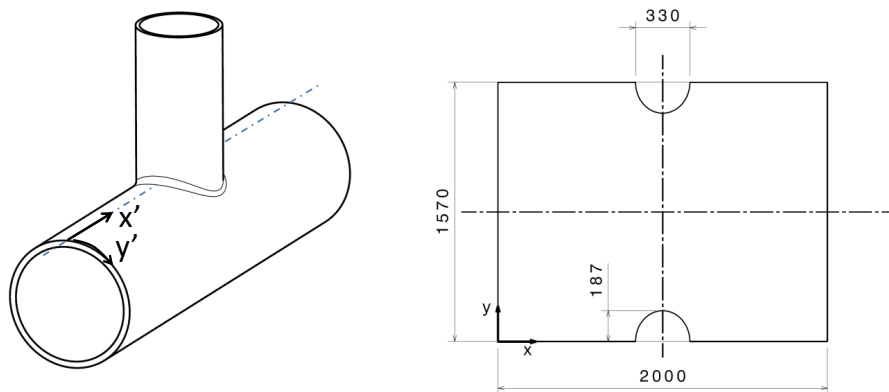
Figure 6.15: While the structure of interest is three dimensional, the guided waves travel through the tube wall, similar to how the elastic wave travels in a flat plate. The transformation from the three dimensional structure to the two dimensional source location map is done by assuming that the (larger) tube can be 'cut' along the top and unfolded to a two dimensional layout.

Test Procedure

The goal of the test is to determine the localization capabilities of the monitoring system on a T-joint. When the T-joint is loaded, fatigue crack growth is expected at the weld. This test therefore uses locations at the weld as input for the pencil lead break. The locations at which the pencil lead is applied are at a 45 degrees angle to the longitudinal axis of the larger tube. These locations were chosen because the fatigue crack can grow up to, and beyond this point, and it is expected to be representative for most realistic cases. The pencil has a hardness HB, and a diameter of 0.5mm. The pencil lead has a length of approximately 5mm, and is broken at an angle of 45 degrees with respect to the surface. By applying the pencil break at the weld, the emitted signal travels a similar path and experiences similar imperfections to those it would encounter during fatigue testing. At each location, a total of 10 pencil lead breaks are applied.

To analyze the results, the QBF software is used. This software is designed to work with waveguides. The T-joint is a thin-walled structure, and as such the software should act as a waveguide. In order to represent the gathered data, a two dimensional representation of the T-joint is used. This representation is obtained by assuming that the larger tube can be cut and unrolled, as shown in figure 6.15. The location of the sensors is shown in figure 6.16.
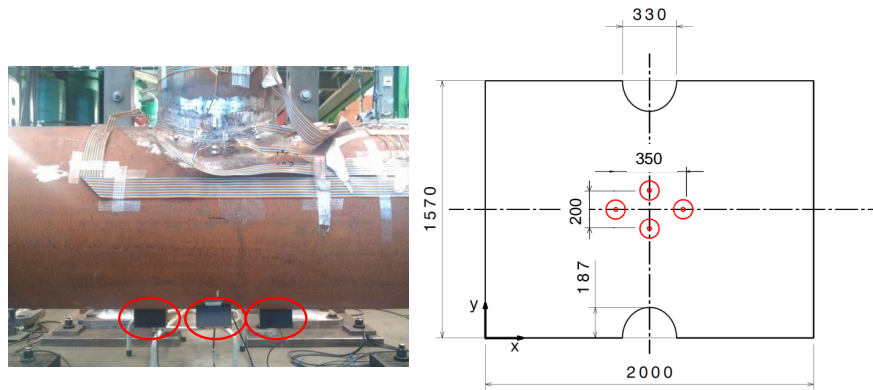
Figure 6.16: The sensors are placed beneath the smaller vertical tube. The width (along the length of the larger tube) is 350mm and the height is 200mm. In the two dimensional layout, there is symmetry around the vertical and horizontal axes.
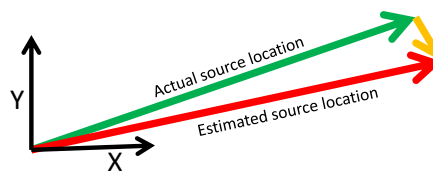
Figure 6.17: The error is defined as the length of the difference vector (orange) divided by the length of the actual vector (green). The difference vector is the difference between the estimated source location (red) and the actual source location (green), measured from the center of the sensor node.

Results

The goal of this test was to determine the accuracy of the localization on a T-joint test sample. The first part towards accurately mapping the source locations is detecting the signal. During the measurements not every pencil lead break has been detected. This is likely to be caused by reflections that disrupt the signal transmission just enough to prevent it from being detected or processed. Table 6.3 shows the number of events that have resulted in a location. As can be seen, the first test has one more event identified than has been applied to the structure, and the third and fourth test did not capture every event. The extra event that has been recorded is probably a result of the pencil touching the surface rather than the pencil breaking at the surface. While the QBF software is optimized for flat plate structure and this curved thin-walled structure may deteriorate the results, it could also be that reflections of the input within the structure, or other imperfections caused just enough disturbance to have the detected signals rejected. The criteria for signal detection may be alleviated in order to capture more of the events and estimate a source location to them. This is likely to come at the cost of a decrease in source localization accuracy, unless the maximum error is adjusted accordingly.

The error in localization of the source signal is defined as $error = \frac{|estimated location - actual location|}{|actual location|}$, this is visually shown in figure 6.17. The corresponding errors are given in table 6.3. The localization error is between five and ten percent, when dispersion correction is applied during processing of the detected waveforms. Although the settings were identical for each test, the outcome of the localization differed slightly between the different tests. The results from the second test are shown in appendix F, and as an example the results for test 2 are shown in figure 6.18 and figure 6.19. These figures show the different events that were identified as a location on the two dimensional layout of the T-joint, as well as the cumulative estimate. It can be seen that even though the location at which the pencil lead breaks have been applied, and the signal has travelled the same path, with similar characteristics, the QBF software does produce a slight variation in the estimated source location. In the third test, even though the averaged error was larger, and fewer events were detected, all of the detected events were estimated to come from the same location. During the fourth test, even though the settings for acquisition and processing were identical to the other tests, the processing failed to apply dispersion correction, resulting in an error in localization of 23 percent. By changing the settings for the QBF

Test series = 0 , dt = 0.2 μs, window = [150 400] μs, min. correlation = 0.7, (o) is S0, (+) is A0
max. Δt error = [8] μs, BP filt. coefs = [10 20 90 100] kHz, [c_{A0} c_{S0}] = [3200 4900] m/s,
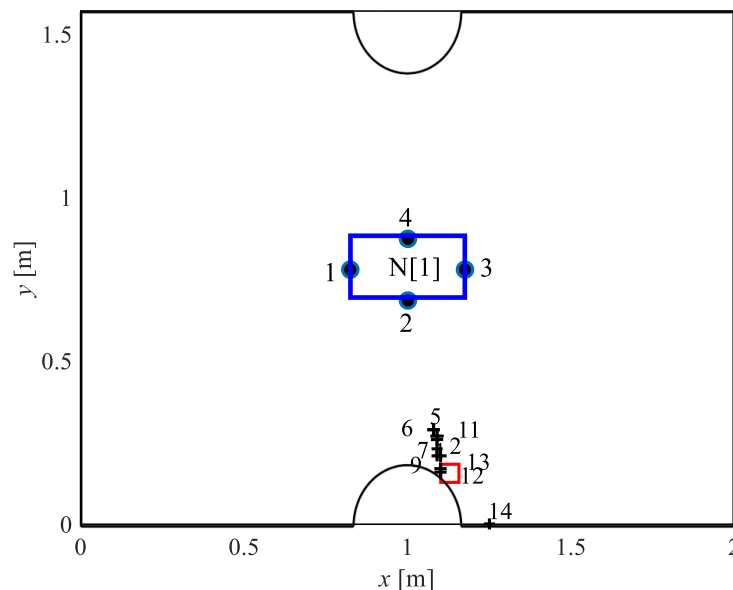
Figure 6.18: The estimated acoustic emission source locations are indicated using a '+' with a corresponding event number. The blue square in the middle represents the array of sensors used for detecting the signal, where the dots indicate the sensor location. During this test ten out of ten pencil lead breaks were identified. The location at which the QBF software estimated each event varied slightly.

software, these events did meet the criteria for dispersion correction, and the error was reduced to five percent. This was done by changing the center frequency f_c from 50 kHz to 60 kHz.

Table 6.3: Results from testing the detection and localization performance on a T-joint sample. Ten pencil lead breaks were applied at each of four different locations, of which the detection rate is given in the second column. For the events in which the QBF software managed to estimate a location, the estimated location is compared with the actual location at which the signal was applied. The relative error, in distance, is shown in the third column.

Test number	Number of events localized out of 10 inputs	Relative localization error
1	11	10%
2	10	5%
3	6	11%
4	7	23% (5%)

Conclusion
The test showed that using this setup, a large portion of the signals can be detected. For this specific test, 83% of the signals were detected, which should be enough to generate meaningful results. The accuracy of the localization has also been assessed. The location that was determined by the QBF software had an average error per test between five and eleven percent. Although the accuracy on a thin-walled two dimensional plate is better, this result is acceptable. The spread in estimated location was minimal, indicating that the results are repeatable and the signal quality was good. During monitoring, it may be possible that fatigue crack growth occurs at multiple locations, as occurs in the fatigue test. During the localization accuracy test this has not been tested, but based on research by Pahlavan et al. it is expected that monitoring of multiple fatigue cracks using one sensor node can be detected [44]. The acoustic emission activity is not constant, meaning that sometimes one location will be registered, while during another case the other location will be registered. If the signals interfere too much with each other, the data is discarded. Based on this test, it is expected that the monitoring system can be used during fatigue testing of this specimen, which is one step closer to the end goal of
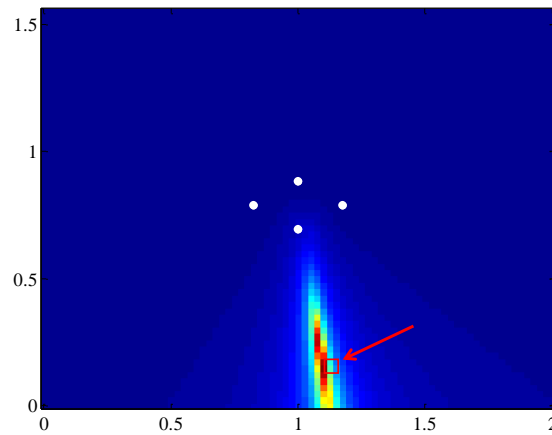
Figure 6.19: This figure shows the cumulative estimate for the acoustic emission source location. Distance shown in meters, and blue indicates a low probability of the source being located at that location, while (dark) red indicates a high probability of the source being located at that location. The estimate found during this test had a relative error to the actual source location, indicated by the red square and arrow, of five percent.

fatigue crack growth monitoring on an actual offshore wind turbine.

Fatigue test on T-joint sample

Fatigue testing is often performed in order to assess the properties of different materials, and to validate models. Such testing can be performed on simple specimens using a variety of tests. Fatigue can be tested under tension-compression, tension-tension, bending, or torsion. For each of these, the ratio of loading can be varied, with ratio defined as

$$R = \frac{\sigma_{min}}{\sigma_{max}} \tag{6.1}$$

with R the stress ratio, σ_{min} the minimum stress applied, and σ_{max} the maximum stress applied. Testing can be performed on different types of samples, these can be standardized test samples or custom test samples.

Test Setup

For this test, the same setup as in section 6.4.1 is used, with the addition of a load cell, which applies loading to the structure. The specimen is shown in Figure 6.12.

The load application is controlled via a Teststar IIs system, the hydraulic actuator is a MTS Series 204 model with a maximum applicable force of 979 kN, both in tension and compression. The hydraulic actuator is controlled using a valve from MOOG from their D076 series. The acoustic emission sensors are attached to a compact acquisition device: the USB AE Node, of which 4 are linked to each other, via UTP cables, and attached to a Dell Laptop via a USB connection. The specifications for the USB AE Node are shown in Appendix C. The software that is used to acquire the acoustic emission signals is AEwin, for which a specification is given in Appendix D. The sensors and the software are supplied by Mistras.

In order to determine an estimated location, the signals have to be processed by the QBF software. There are a number of variables that can be adjusted to fit the characteristics of the situation. The settings used during this test are shown in table 6.4.

Test Procedure

During the fatigue testing of the specimen, a constant amplitude fatigue loading is applied. The loading has a stress ratio of 0.1, with a maximum load applied to the structure via the brace of 556 kN and a minimum load of 56 kN, both in tensile direction. The tensile load is applied by the actuator as shown

Table 6.4: QBF Software settings that have been used for processing the data that was gathered during monitoring of the T-Joint. These settings are such that most of the noise is filtered out and only a few events passed all the criteria, resulting in a most probable location.

C_{A_0}	3100 m/s	C_{S_0}	4900 m/s
sampling interval	$1\mu S$	Maximum Localization Error	$49mm$
Window Length	$250\mu S$	f_c	47.5 kHz
Band pass filter	$39kHz - 56kHz$	Minimum Correlation Coefficient	0.5

Table 6.5: Data acquisition settings that have been used during continuous monitoring of T-Joint section. Settings were chosen such that events due to noise are limited, while loud events should be recorded.

Threshold Type	Fixed	Threshold	80 dB
Analog Filter Lower Limit	20kHz	Analog Filter Upper Limit	100kHz
Sample Rate	1MSPS	Pre-Trigger	$256\mu S$
Sample Length	1k		

in figure 6.13. The frequency at which the load is applied is equal to 1 Hz. The test is executed at the Structural Dynamics Laboratory from TNO, in dry conditions at a temperature of 20 °C. During the test, a crack will start growing in the sample, and the crack growth development is being monitored visually as well as electronically. The crack development can be compared with the measured acoustic emission activity.

As a result of the fatigue crack growth, acoustic emissions should be emitted from the crack. The software that is being used has to be set up properly to detect the signals that result from fatigue crack growth. In order to do so, the settings are set up according to Table 6.5. The file length was chosen to reduce the amount of data written to the hard drive, as this file length is enough to capture the signal produced by crack growth. The filter settings were chosen in order to only respond to signals that lie within the domain in which signals could be used for localization. The sampling rate was chosen both to accommodate the filter settings as well as to limit the amount of data written to the hard drive while still being more than sufficient to capture the frequencies of interest. The threshold was set at these values as the noise that is present in the test setup is constant and between 70 dB and 75 dB.

Noise mitigation

The settings that were selected resulted in large quantities of data being recorded. However, the noise that was present at the setup prevented fatigue crack growth from being detected. In order to reduce the noise level, the source of the noise had to be found. It was noticed that when the oil pressure, needed to operate the load cell, was reduced, the noise level also reduced with up to $60dB$, as shown in figure 6.20. By sampling at various locations it was found that the hydraulic valve, which regulates the pressure in the hydraulic cylinder, showed the loudest noise. Because the noise highest near the valve, the valve is most likely the source of the noise. If the noise at the sensors has to be reduced, the source of noise should be eliminated or isolated. It may be possible to replace the valve by a different valve, but this may not solve the problem and is very costly. Isolating the valve from the system by placing it at a remote location may reduce the noise too, but introduces lag to the system, requiring a recalibration, and is costly too. It was decided that a $1cm$ plastic layer was to be installed between the actuator and the specimen. This plastic layer did result in a small decrease in noise as shown in figure 6.21. The average sound level was reduced by $4dB$, while a reduction of $12dB$ was measured near $50kHz$.

Results during crack growth

During the testing, which started March 24th and ended May 26th approximately 500 thousand cycles were applied on the T-joint. The fatigue loading was stopped when the crack length reached 90 degrees of the circumferential and the crack depth reached 50 percent of the wall thickness. During the period of monitoring a crack has developed on both sides of the sample. The crack grows along the weld, as shown in figure 6.22. During most of the time, the monitoring did not result in any source location. This is a result of the noise which was too much, despite the attempt to mitigate the noise. The noise resulted in a reject due to exceeding the maximum timing error or due to not reaching the desired
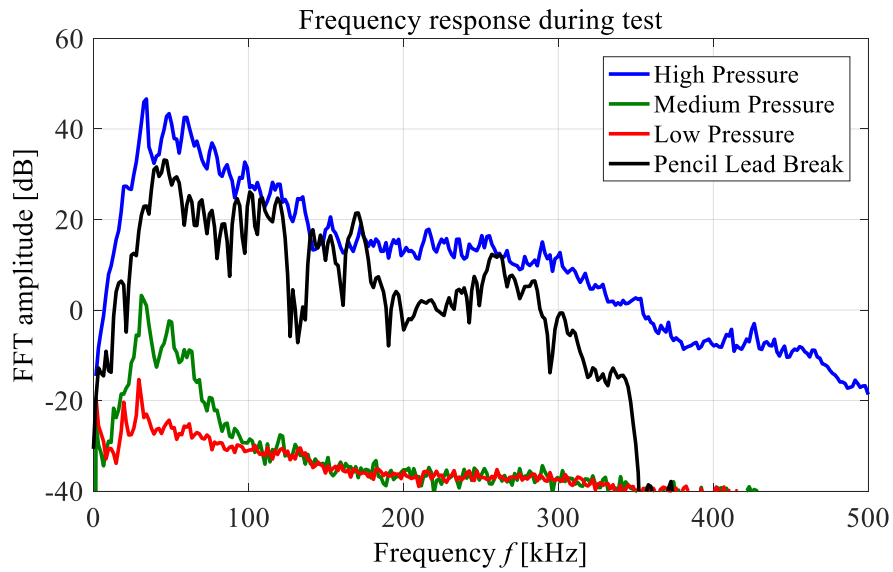
Figure 6.20: The noise level measured at various oil pressures. This indicated that the noise source came from within the system and was related to the hydraulic system. Also included in this figure is the frequency response of pencil lead breaks. It can be seen that the noise that is detected has a higher intensity than the signal of interest.
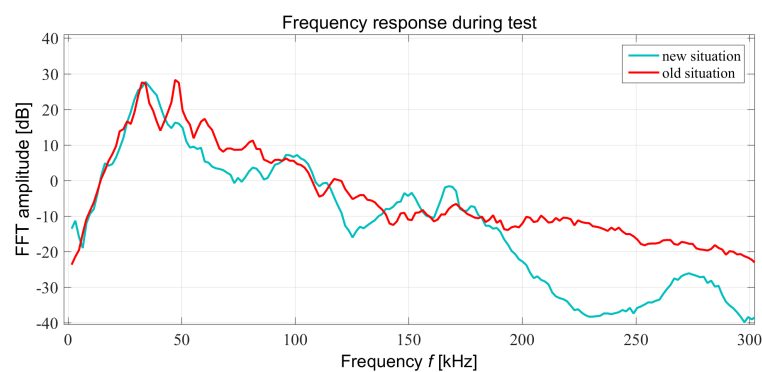
Figure 6.21: The placement of a $1cm$ plastic layer resulted in a small decrease of the noise values measured. The average sound level was reduced by $4dB$, and near $50kHz$ a reduction of $12dB$ was measured, but a peak near $40kHz$ showed zero reduction.
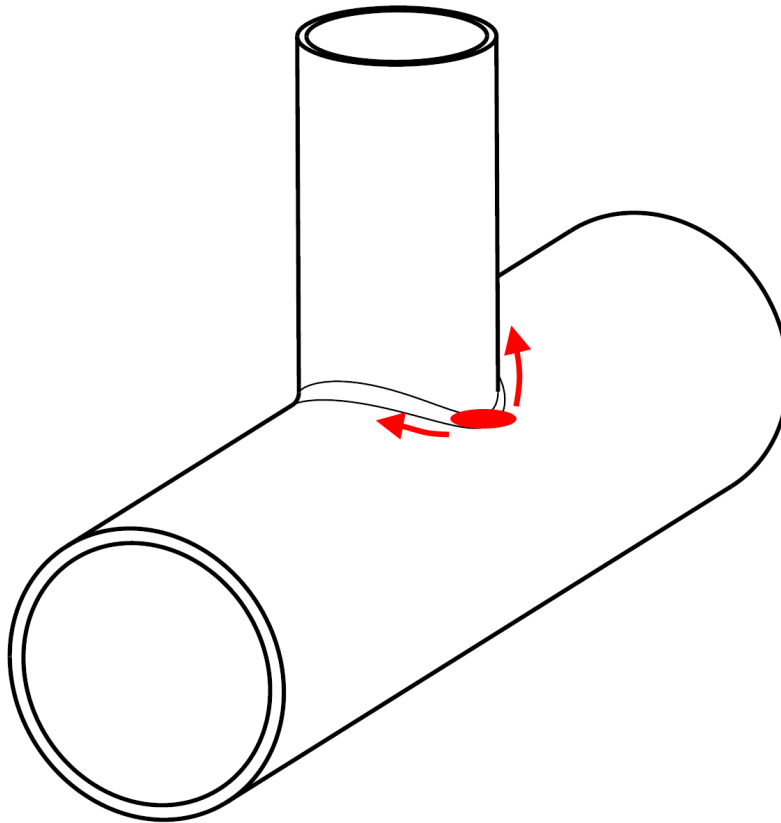
Figure 6.22: Fatigue crack growth typically starts on the sides of the T-joint, as indicated by the red area. As testing continues, the crack grows along the weld, as indicated by the arrows, while at the same time the crack deepens.

correlation between different signals. However, there were two time periods during which some signals were recorded. An audible sound could be heard during these time periods which were followed by accelerated crack growth. The source location estimates during these events were not all along the weld line. There are a couple of explanations for this: 1) the acoustic emission at the crack had sufficient sound level to be accurately picked up, but noise ruined the localization process 2) there is indeed crack growth at the locations as indicated 3) the signal is troubled by reflections, but still manages to result in an estimated location 4) there is another overlooked effect.

Conclusion

Although the localization was able to detect 83% with a localization error of between five and eleven percent, the effect of noise resulting from the hydraulics prevented detecting events for the most part. the hydraulic noise, even after an attempt to mitigate it, was too severe, and prohibited the fatigue crack monitoring as intended. The effect of noise cannot be overlooked and should be studied before an acoustic emission monitoring system is implemented. The setup of the experiment could only be partially modified, preventing more effective mitigation solutions to be implemented. Future fatigue crack growth monitoring testing should make sure potential sources of noise are eliminated, or isolate the source of noise. It is expected that in offshore conditions the noise would be less severe, and the monitoring system would be able to operate as intended, but further testing is required to provide proof.

Noise on Actual Wind Turbine from Rotating Equipment

One of the parameters that determines the usability of an acoustic emission monitoring system is the range of detection. This range is affected by the sensitivity of the sensors, the amplitude of the signal at the source, and the amount and type of noise present at the location of interest. The noise can be created by a number of different sources. Rotating equipment is one of the possible sources of noise.

Table 6.6: Software settings that have been used during measurement of noise. Settings were chosen to have as wide as possible filter limits. This was done to not miss out on any of the possible noise, while the sample rate was set as high as possible to accurately record any noise. Unfortunately this limited the options for sample length. The threshold was varied during the measurements to detect noise at different intensity levels; the ambient noise has a different intensity compared to more incidental noise that resulted from the turbine.

Threshold Type	Fixed	Threshold	Varying
Analog Filter Lower Limit	1kHz	Analog Filter Upper Limit	100kHz
Sample Rate	5MSPS	Pre-Trigger	$19\mu S$
Sample Length	1k		
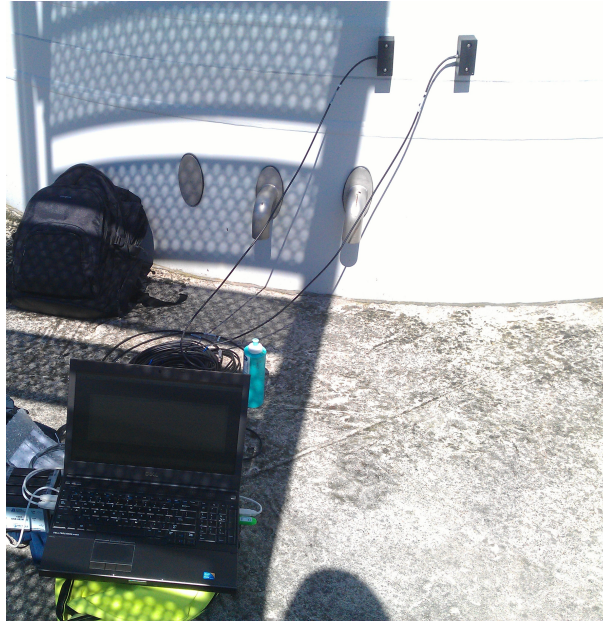
Figure 6.23: An overview of the test setup as used for determining the noise in an onshore wind turbine.

In order to get an indication of the noise that can be expected from rotating equipment, a wind turbine is monitored briefly.

Test setup

The tests have been performed on a Vestas V90-3MW wind turbine. This model is used offshore, as well as onshore. The turbine that was used for this measurements is located in the vicinity of Zoetermeer, at a distance of 15 to 20 kilometers from the sea. The wind speed reached scale 3 on the Beaufort scale; the average wind speed was between 3.4 and 5.5 meters per second. The cut-in wind speed of the wind turbine is equal to 3.5 meters per second. Further specifications for the Vestas V90 are given in Appendix E. The sensors that were used are the PK6-I sensors by Physical Acoustics, with specifications as shown in Appendix B. Two sensors were used as to have more reliable results compared with a single sensor. The sensors were attached to the Physical Acoustics USB-AE node, which was connected to a Dell Precision M4800 running Mistras' AEWin software. A picture of the setup is shown in Figure 6.23. The acquisition settings are shown in Table 6.6.

Results

During the measurements the head of the wind turbine was adjusted approximately once per minute. As the wind was relatively weak, the wind turbine rotated at the lower end of the 8.6 - 18.4 rpm range. An indication for both of these events can be found in Figure 6.24 and Figure 6.25. The threshold setting in these figures is $49dB_{ae}$ and $74dB_{ae}$ respectively. The signals that have been recorded have an amplitude of approximately $54dB_{ae}$ and $80dB_{ae}$.

Taking a closer look into the signals that have been acquired it is possible to extract more information and to determine its effect on the coverage area of a sensor node. During the measurements with
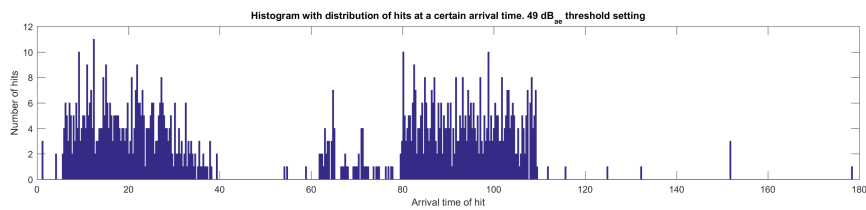
Figure 6.24: During monitoring of the wind turbine for 180 seconds, a number of events were recorded. The threshold was set to $49db_{ae}$. The intervals of increased activity can be linked to the yawing motion of the wind turbine head. The horizontal axis shows the time of the test, the vertical axis shows the number of hits at a specific time interval. The histogram consists of 600 bins; each interval has a length of 0.3 seconds.
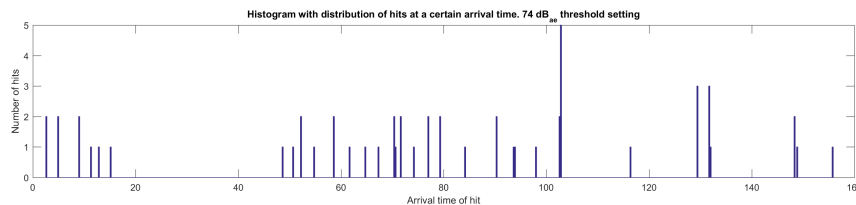
Figure 6.25: During another measurement on the wind turbine, the threshold was set to $74db_{ae}$. This time the effect of the yawing motion was not visible. Events occurred at an almost constant interval of 3 or 6 seconds between events.

a threshold setting of $49dB_{ae}$ it was seen that there was increased acoustic activity when the wind turbine head was adjusting to the wind direction. Furthermore, the noise that is recorded is wideband and the recorded signals show less similarity between each other, as shown in the left 2 subfigures of Figure 6.26. This type of noise, when present, is not likely to cause a problem for the operation of the monitoring system; the intensity of this type of noise is relatively low. However, it might reduce the coverage area of the monitoring system as the signal of interest has to be louder than any noise in order to be detected. The intensity of the signal dies out as a result of spreading and leakage into water. For the case in which the threshold setting was $74dB_{ae}$, there was no continuous noise. For this case, there were a number of events recorded. The number of events was limited, and only occurred every few seconds, as can be seen in Figure 6.25. When looking into the waveforms that have been recorded during this measurement, it can be seen that this noise differed from the noise measured at a lower threshold setting. Comparing figure 6.27 with figure 6.26, it can be seen that the (averaged) frequency spectra are different. Next to that, it can also be seen that the signal that was detected for the $74db_{ae}$ threshold setting looks similar for a number of events. This similarity suggests that there could be a source from which this noise originates. As only one wind turbine has been monitored, it cannot yet be said if this would be originating from a defect or whether this is emitted by default. Either way, it is expected that, although the intensity of the signal itself is relatively high, a monitoring system would not be limited in its operation by this noise. The operation would be limited if noise of this intensity would be continuous and could not be filtered out. In this case, the noise is not continuous, and as the signals seem quite similar, it might be possible to filter them out if necessary.

Conclusion

During the measurements on a Vestas V90 3MW turbine at different threshold settings an assessment of the noise in an onshore wind turbine has been made. This has been done in order to determine part of the noise that an offshore wind turbine will encounter. This information provides a clue as to what the coverage area for an acoustic emission monitoring system would be in an offshore wind turbine. It was found that for this specific wind turbine the highest incidental noise detected was at an intensity of $80db_{ae}$. This was not measured continuously and can probably be filtered out if necessary. The adjusting of the wind turbine head to the wind direction caused a continuous noise of $54db_{ae}$. This type of noise would be hard to filter out, but its intensity is not too high. It therefore limits the coverage area of the monitoring system, but the remaining coverage area is still enough to work with for this application.
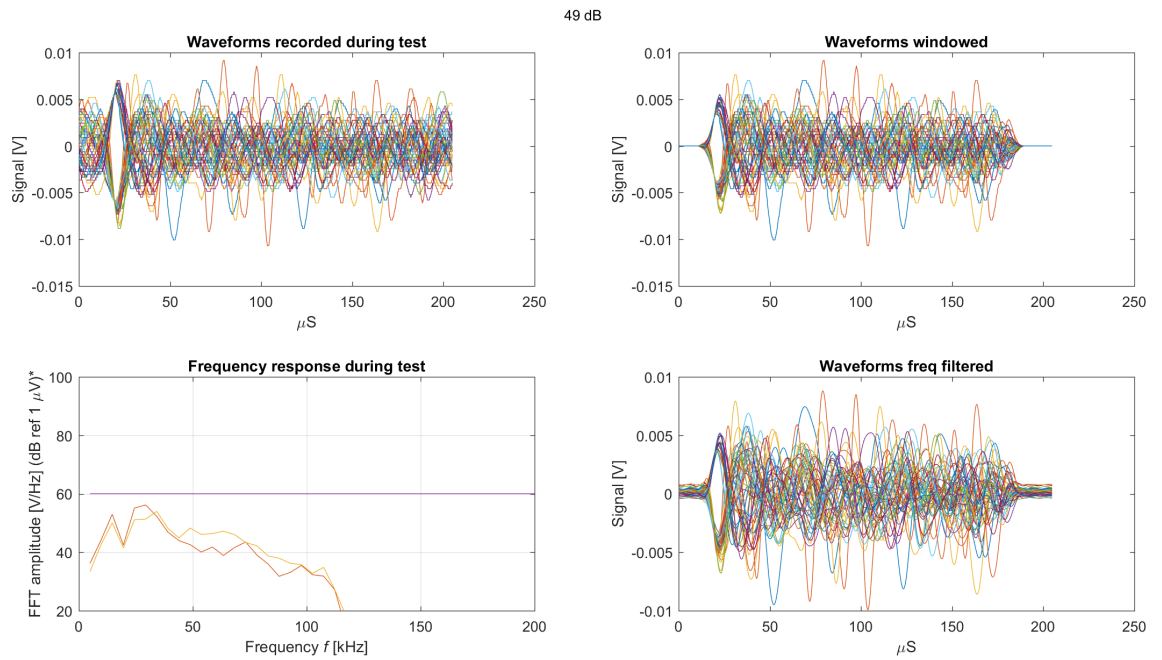
Figure 6.26: During another measurement on the wind turbine, the threshold was set to $49db_{ae}$. This time the effect of the yawing motion were visible. Even though the amount of events is increased, the intensity of these events is small.
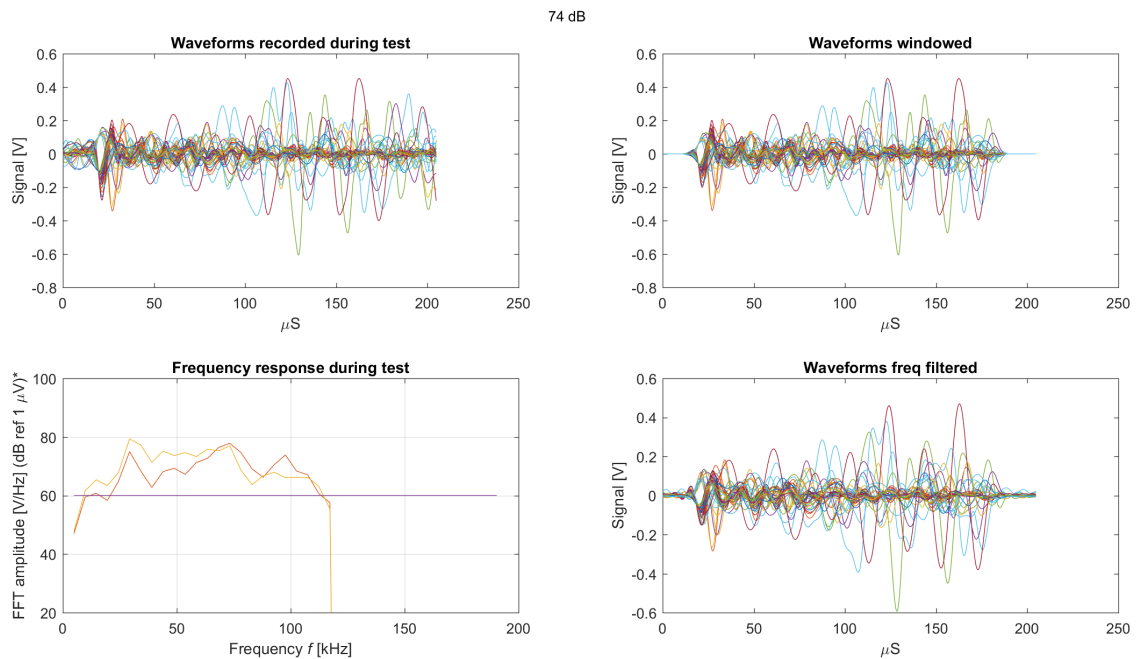
Figure 6.27: During another measurement on the wind turbine, the threshold was set to $74db_{ae}$. This time the effect of the yawing motion was not visible. Events occurred at an almost constant interval of 3 or 6 seconds between events.

Noise resulting from water droplets

While showering one can hear the water droplets hitting one's head, and the sound of water droplets hitting a water surface can also be heard. Similarly for the ultrasonic sensors in an offshore environment, these sensors might also pick up this noise. In order to assess the effect on the monitoring capabilities, the effect of water droplets on a water surface is studied. From literature, it appeared that rain is the largest contributor to noise from an environmental aspect [79]. Therefore, if the maximum effect of this type of noise can be determined for this application, other environmental sources will have less effect on the system performance.

The goal is to study the noise resulting from water droplets. As the sensors that are used are not designed for usage in a wet environment, the sensors that are submerged are wrapped inside a thin plastic bag to prevent water from entering the sensors. This does have an effect on the transmission of the signal, and therefore multiple tests are performed to eliminate this effect. The first test is performed using 4 sensors, without plastic bag, in dry conditions using a pencil lead break. Next, 2 of these sensors are wrapped inside a plastic bag, still, pencil lead breaks are applied as a source of acoustic emission. After this has been done, the plate is placed in a container filled with water, and pencil lead breaks are applied. Last, a shower head is aimed at the water, and generates noise. The resulting noise is measured and should give an indication of the noise that can be expected in harsh weather conditions.

Test setup

In this test, four Physical Acoustics PK6-I sensors are used, with specifications as shown in Appendix B. These are attached using magnetic hold downs to a metal plate with dimension 45cm by 40cm, while the thickness is 8mm. The sensors are connected via the USB-AE node to the laptop that is running the AEwin software.

The sensors are attached to the plate in a line with a 10 cm spacing, during all tests. Acoustic couplant gel is used to minimize losses in signal quality between the plate and the sensor. This is the basis for each of the different tests, and for the first test this is the setup that is being used. The second test aims at determining the effect of the plastic bag on the transmission of the signal. Therefore, sensors 3 and 4 are individually wrapped inside a thin plastic bag. Acoustic couplant gel is applied on the inside of the bag as well as on the outside, assuring that the decrease in signal quality is minimized from the metal plate up to the sensor. The second test is still performed in dry conditions. The third test takes it one step further, and has the two sensors that are wrapped inside a plastic bag submerged in water. The metal plate is placed vertically, such that the waterline is between sensors 2 and 3. The fourth and final test includes a source of noise resembling rain at sea. The rain is simulated using a shower head, at a height of 1 meter, positioned at 0.5 meter from the metal plate. The resulting acoustic noise is close to actual rain fall, with similar noise levels measured up to 20 kHz [95]. The frequencies of interest for this experiment are above 20 kHz, but the sound level at frequencies above 20 kHz remains constant or decreases slightly [96] [97], and therefor it is expected that this setup results in a realistic value for the noise that is to be expected in an offshore environment.

Test procedure

During these tests, a source of acoustic emission is required to either test the difference between different sensors or setups, or as the phenomenon of interest. The shower head provides noise during the fourth test, while during the other tests a pencil lead break provides the acoustic emission on the metal plate. The resulting signal at the sensors is studied afterwards to determine the effect of the different setups as well as the intended goal of these tests: finding a value that represents the actual noise resulting from environmental effects that can be expected if an acoustic emission monitoring system were to be installed offshore.

The first test makes use of pencil lead breaks, applied in line with the sensors at both ends and in the middle of the plate. The number of pencil lead breaks per location is set at five. During the second test, the pencil lead breaks are applied at the same locations, and five times at each location. During the third test, as part of the metal plate is submerged in water, only two locations have five pencil lead breaks applied each. During the fourth test, the shower head is a source of acoustic activity. The resulting noise levels are measured during time intervals of several minutes at varying threshold settings, assuring that an accurate value for the noise that is to be expected during offshore operation

is found.

The resulting signals are analyzed. During the first three tests, the signals are first checked whether an event is recorded at 4 sensors simultaneously. This is done by finding four signals that fall within the same small time slot, and checking whether the arrival time of the signal does lie within the expected margin. Together with this check, the intensity of the signal is required to exceed a certain threshold, in order to exclude reflections to be treated as normal signal. The remaining set of signals is then checked manually, to see if there are any outliers. With the subset of qualitatively good signals, the data of interest can be extracted. During most of the tests, the output for sensor 1 and 2 should be similar, while the output for sensor 3 and 4 will change, depending on whether the sensor is wrapped inside a plastic bag or submerged in water. To minimize variations, the performance of sensors 3 and 4 is compared between different cases by assuming that sensors 1 and 2 perform similar in different cases, as sensors 1 and 2 are placed at the beginning of test 1 and are not changed or moved in any way during the other tests.

Results

The tests were executed may 25th with the help of Erwin Boer from TNO. After analyzing the results, it appeared that signals were not detected at every pencil lead break in some cases. This is likely to be caused by reflections within the relatively small plate. Despite not capturing every signal, there still was enough data to perform the analysis and to determine the resulting noise from water droplets. In some cases a reflection was detected, but these were filtered out rather easily due to the decreased signal intensity of the reflections.

The first goal of the test was to determine the difference in sensitivity of the sensors to a signal that is travelling through the plate. This was done by comparing the attenuation in the signal, due to geometrical spreading to the attenuation of the signal that has been measured. It was found that the deviation from sensor to sensor in this setup was $-0.497 dB$ for sensor 1, $-2.648 dB$ for sensor 2, $+2.076 dB$ for sensor 3, and $+0.922 dB$ for sensor 4, with a positive sign indicating an overestimation in the measured signals, and a minus sign indicating an underestimation in the measured signals.

The second goal of the test was to determine the effect of adding a thin plastic layer between the sensor and the metal plate. This was found by comparing the results from the first and the second test. From the first test, 9 signals have been properly recorded, while during the second test 13 signals have been recorded properly. Unfortunately, during the first test, only 1 signal was recorded properly when the pencil lead was broken in the middle of the sample, therefore that part is removed from the tests, leaving 8 successful events that were matched with 6 successful events from the second test. The resulting attenuation was 3.8 dB, which is slightly more than measured in a different test, which may be caused by an increase in plastic layer thickness as a different plastic had been used.

The third test should find the attenuating effect of water on the signal transmission through the plate, as part of the signal can lead into the water. From the two times five pencil lead breaks that were applied, only four resulted in a detected signal at each sensor simultaneously. All of the four detected sets of signals occurred when the pencil lead was broken at the middle of the plate. This set has been compared with the set of signals obtained when a pencil lead was broken at the middle of the plate while the plate was not yet submerged. After removing the outliers, two sets of three signals each were remaining. The effect of the water on the attenuation levels of the signals was approximately -1dB at sensor 3 and -4dB at sensor 4.

With this information gathered, the effect of water droplets as a source of acoustic emission can be studied more accurately. The first noticeable feature is the amount of signals detected during a certain time span. The threshold was set at 40 dB first, which resulted in 5 731 signals recorded during a time span of just 3 minutes. The threshold was then increased to 50 dB, resulting in 10 101 recorded events during a time period of 7 minutes. When the threshold was set to 55 dB, a total of 705 signals were detected by the sensors during a time period of 9 minutes. During the measurement at 60 dB, only 20 signals were detected by the sensors during a time span of 9 minutes. At threshold settings of 65 dB and higher, no signals were recorded. The signals that were recorded during the tests can be compared with the pencil lead break test and between the various threshold settings. From figure 6.28 it can be seen that when the threshold was set at 55 dB, the measured peak values reached around 65 dB, while during pencil lead breaks, these values were around 100 dB. When the threshold was set at 60 dB, there were only 20 signals detected, of which three times the recorded time of arrival was very close, suggesting that those signals were originating at the same source. The timing of these
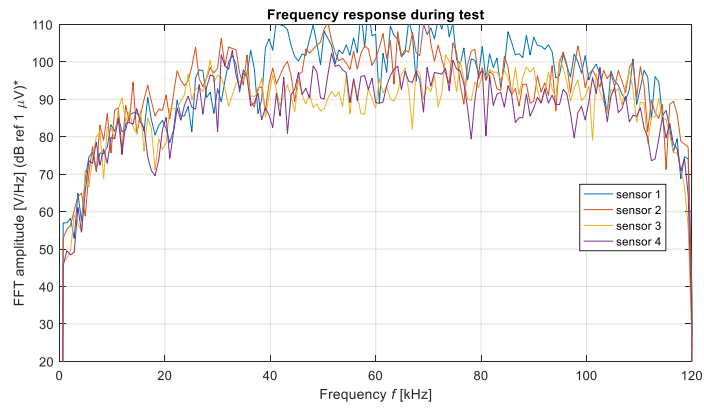
(a) Amplitude spectrum of pencil lead breaks applied at middle of the plate.
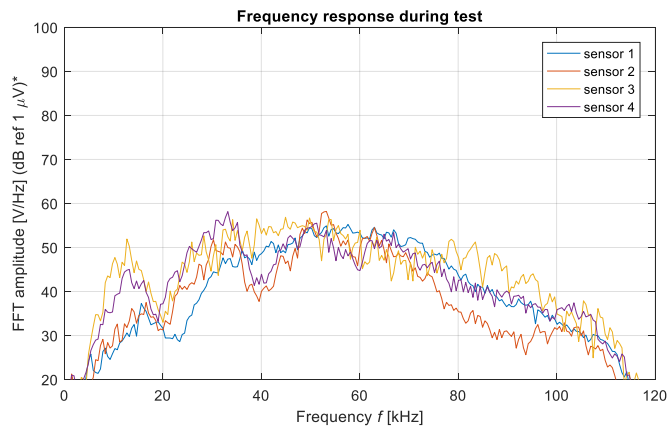
(b) Threshold setting of 50 dB.
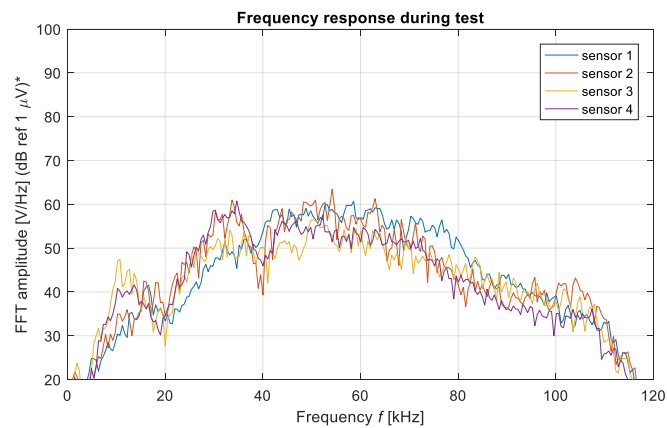
(c) Threshold setting of 55 dB.
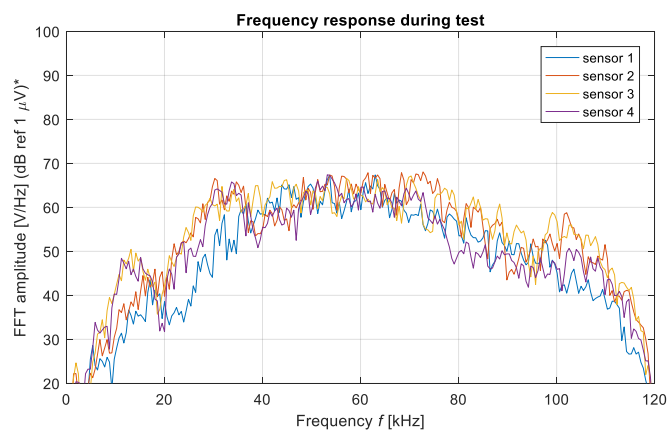
(d) Threshold setting of 60 dB.

Figure 6.28: Amplitude spectra for different threshold settings in comparison to those for pencil lead breaks. Sensors 1 and 2 are above the water level and not wrapped inside a plastic bag, sensors 3 and 4 are wrapped inside a plastic bag. The plate is submerged during the different threshold settings, but it is not submerged in case of the pencil lead breaks.
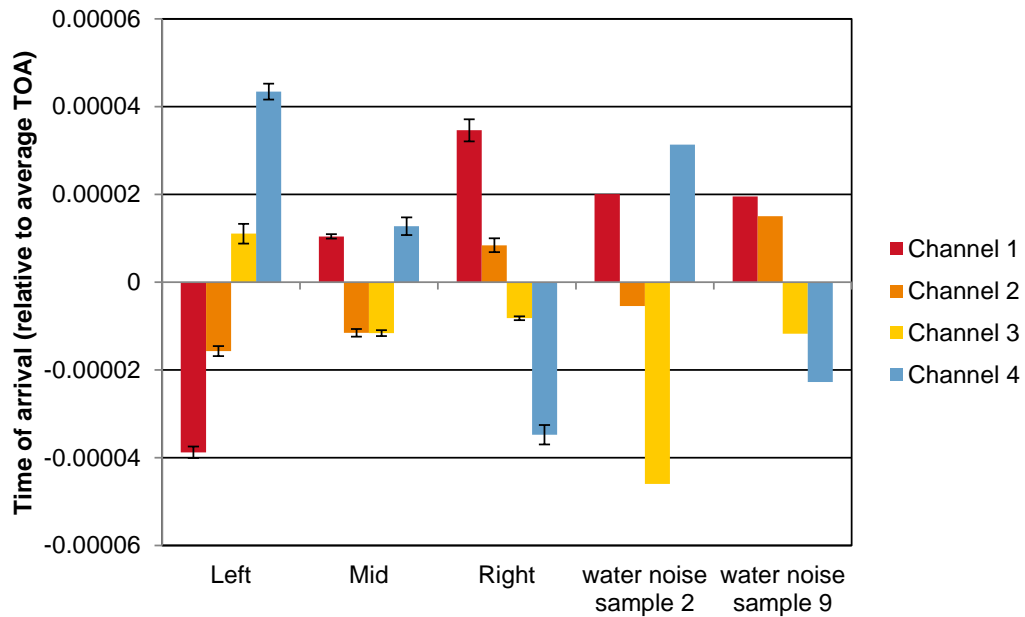
Figure 6.29: For all of the events recorded during the tests 1 to 3, the time of arrival has been compared. As the time of arrival is compared between the 4 sensors, the relative time of arrival is important. Therefore, the time of arrival is shown relative to the average time of arrival of the 4 signals recorded at one event. The arrival times for the three different locations of pencil lead breaks have been grouped. Within each of these groups the mean relative arrival time is shown, and the standard deviation of the recorded signals is calculated. The error bars indicate the standard error. Two instances of noise during the water drop test are also shown. It can be seen that the signals recorded during the water drop test, despite being very close to each other regarding their arrival times, are unlikely to come from within the plate, and can thus be filtered out of the data.

signals was different to those resulting from pencil lead breaks, as demonstrated in figure 6.29. This difference in timing allows for filtering of the recorded signals, to get rid of some of the noise. Based on these measurements the maximum noise level resulting from environmental sources is estimated to be approximately 57 dB, using the equipment as stated in section 6.7.1. Given that the peak amplitudes measured using a pencil lead break are well above 90 dB, this potentially allows for offshore operation of acoustic emission sensors, yet offshore testing is required as the in situ levels compared to the signal quality of fatigue crack growth may be better or worse.

Conclusion

A part that plays a large role in determining the coverage area of an acoustic emission monitoring system is noise. One of the different types of noise that can be expected offshore is environmental noise, of which rain has the highest intensity. The effect of wrapping 2 sensors inside a plastic bag was measured, which using the materials provided resulted in an attenuation of the signal of 3.8 dB. Placing the metal sample in water, having sensors 3 and 4 submerged in water, resulted in an extra attenuation of 1 dB for sensor 3, and 4 dB for sensor 4. Sensor 3 was 5 centimeters below the water level, and sensor 4 was 15 centimeters below the water level. The noise level that was measured during these tests was approximately 57 dB, while pencil lead breaks reached values of around 100 dB. Although there were a few events measured in which the amplitude of the noise reached a higher level, this only occurred four times over a time span of 9 minutes, and the arrival times of the signals could not result in a valid location. If such high levels in themselves could cause a problem, this type of noise could be filtered out. The results show a potential for acoustic emission monitoring in an offshore environment, and further testing on site should provide more detailed results on the actual combined environmental noise.

Practical Aspects of a Monitoring Network

Acoustic Emission Monitoring can facilitate a predictive or condition based maintenance strategy. Monitoring each wind turbine can become a costly business, and sampling may generate enough information to supply an operator for maintenance planning. The coverage area of an acoustic emission sensor node is limited. It is possible to get full coverage on a single wind turbine, but there may be smarter, more cost effective way of monitoring it. This chapter treats monitoring of a single wind turbine, followed by a proposed strategy for monitoring a wind farm, while the financial aspects for three scenarios are also discussed.

Coverage Area of an Acoustic Emission Node

An important aspect in acoustic emission monitoring of offshore wind turbines is the coverage area of the monitoring system. The coverage area depends on the attenuation of signal over distance, the source signal strength, the detection limit of the sensor, and the noise level on site. These aspects have been measured or simulated, in order to determine the individual effects. This section combines the individual measurements in order to estimate the coverage area of a single sensor node.

The first part that has been studied is the attenuation. This was done using numerical simulations. The numerical simulations allowed to determine the attenuation for multiple wall thicknesses for the frequency range of interest. The attenuation curve for a wall thickness of $60mm$ is shown in figure 7.1a. As mentioned previously, the frequency range of interest is bound between the high attenuation at low frequencies and the onset of higher order waves at higher frequencies. In case of a wall thickness of 60mm the lower bound is approximately $10kHz$, and the upper bound is approximately $25kHz$. The attenuation ranges from 6.5 dB/m to 4.5 dB/m in this frequency range, with 50% below 5 dB/m. This attenuation rate of 5 dB/m could therefore give a good approximation of the coverage area of a sensor. The signal source strength is typically 90 dB in steel structures. Combining the signal source strength, the attenuation as found in numerical simulations, and the geometrical spreading, results in an expected signal strength as a function of distance, as shown in figure 7.1b. Using this approach, the expected signal strength can be calculated for the different types of offshore wind turbine foundations.

The expected signal strength versus distance is only one part of the equation. In the figure shown, there is no lower threshold indicated for the signal strength and that would imply that the detection radius is infinite. The two most important factors that affect the lower threshold are sensor sensitivity and noise. Below a certain amplitude, the sensor is no longer capable of detecting the signal, which limits the detection radius of the sensor. In the case of Physical Acoustics PK6I sensors as used during the experiments, the detection limit is smaller than 10 dB. This is indicated by a horizontal line in figure 7.2, and the location where this line and the expected signal strength meet indicates the detection radius. Another factor that may limit the detection radius is noise. Noise can be frequency-dependent as well as wideband. It is assumed that the noise values that have been measured in water and at the wind turbine are uniformly distributed in frequency, and second, that they are representative for the noise that can be expected in an offshore wind turbine. The first assumption results in an underprediction for the
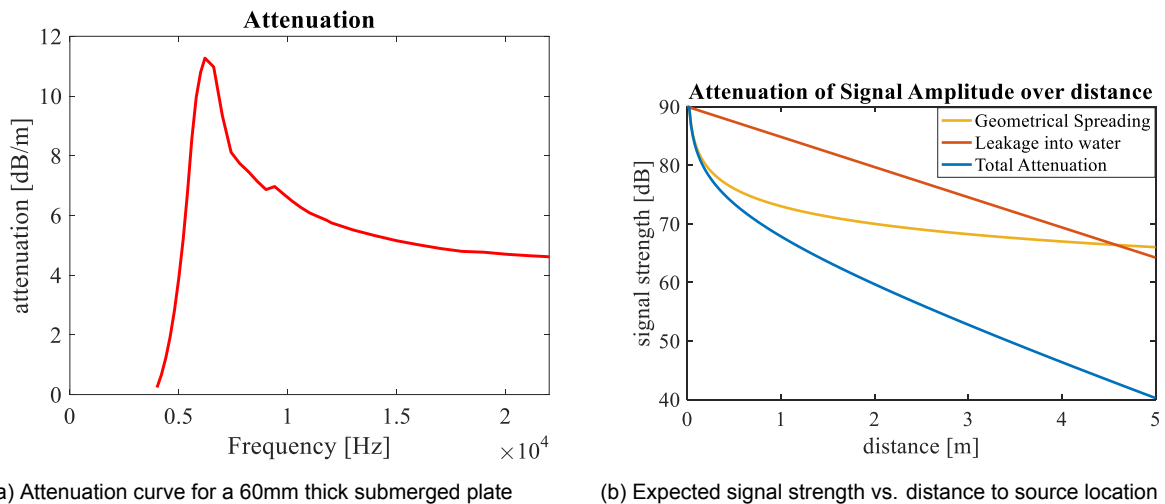
(a) Attenuation curve for a 60mm thick submerged plate

(b) Expected signal strength vs. distance to source location

Figure 7.1: The signal strength at a given distance can be calculated using the attenuation curve and the geometrical spreading. The attenuation varies with frequency, thus the coverage area should also vary with frequency. For ease of calculation, an attenuation value is chosen which represents the workable frequency domain of the attenuation curve.

detection range, and the effective noise may even be reduced by more advanced filter mechanisms. The second assumption has to be confirmed using onsite measurements, but given that there is no data indicating otherwise, the current measurements are the best available estimate. An uncertainty margin can be added to account for the limited amount of knowledge that is currently available. The noise that has been measured as a result of rotating equipment was $55dB$, while the noise level that has been measured as a result of water droplets measured $57dB$. This measurement is a worst case scenario, as it does not always rain, and the impact of water drops created by a shower head create more noise in comparison to actual rain [95].

There are a number of factors that may reduce or increase the detection range of the acoustic emission sensor even further as well as add more uncertainty. The connection between the surface and the sensor can affect the transmission of signal. Adding a small plastic layer of $20\mu m$ between the sensor and the structure reduced the transmission of signal by 3.8 dB. If an adhesive were to be applied at the interface of the sensor and the structure, the transmission of signal may be improved significantly [98][99]. Although the authors of these articles do not quantify the increase in transmission quality, it seems that the signal loss is decreased by approximately 10 dB. Any noise that comes from within the structure, such as mechanical noise is likely to show the same increase in amplitude, but it is more complicated to determine the effect on environmental noise. Another factor that could affect the detection range and capabilities of the monitoring system is time. With time, it is possible that the performance and coupling of the sensor decrease, while degradation of the structure increases. The decrease in performance of the sensor is likely to cause a decrease in the area that can be detected by the monitoring system. The degradation in performance can be measured by the sensors themselves, via an automated sensor test. If such performance loss occurs, there is a means to quantify it and depending on the requirements of the monitoring system the functioning is either acceptable, or a repair is required.

The effects of the factors mentioned that may influence the capabilities of the monitoring system are small to negligible. Some of the cases mentioned are only treated in a qualitative manner, while the effect for a number of cases could be quantified. For those cases, the effect is small, or could be offset by a countermeasure to maintain the same level of performance for the monitoring system. Based on the measurements, experiments and discussion, the margin for attenuation losses is estimated at $\pm 5\%$, and the margin for noise is estimated at $\pm 2.5dB$. The attenuation rate is estimated at 5 db/m for the monopile foundation and 13 dB/m for the jacket type foundation. The attenuation rate and the noise level meet at 2.4 meter in the case of a monopile foundation and at 1.2 meter in the case of a jacket type foundation, as shown in figure 7.3 by the solid line. Using the margins of uncertainty and the estimated attenuation and noise levels, the detection range is expected to lie between 1.9 and 3.1 meter in the case of a monopile foundation, and between 1.0 and 1.5 meter for a jacket type foundation,

Attenuation of Signal Amplitude over distance

Attenuation of Signal Amplitude over distance
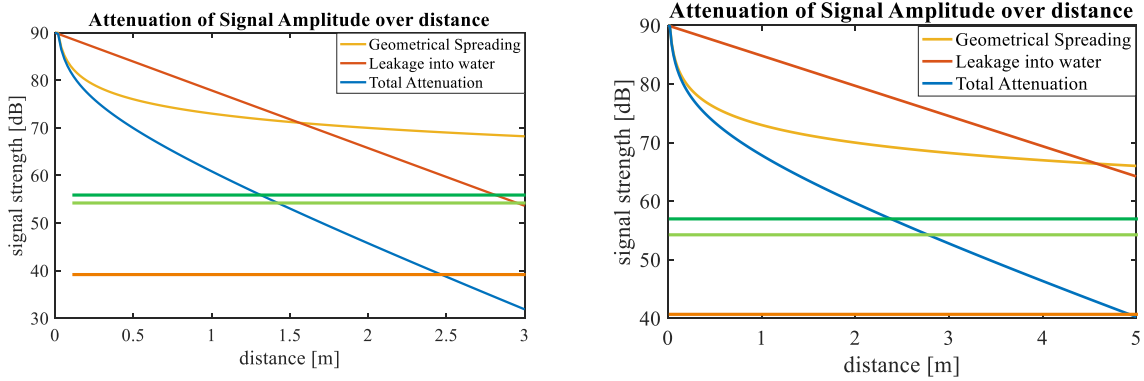
(a) Factors influencing detection range of 24mm thick submerged plate

(b) Factors influencing detection range of 60mm thick submerged plate

Figure 7.2: Combining the attenuation curve with the various noise levels (indicated by the horizontal lines), the top line being noise from water droplets and the most restrictive threshold, the estimated detection range can be calculated.

Attenuation of Signal Amplitude over distance

Attenuation of Signal Amplitude over distance
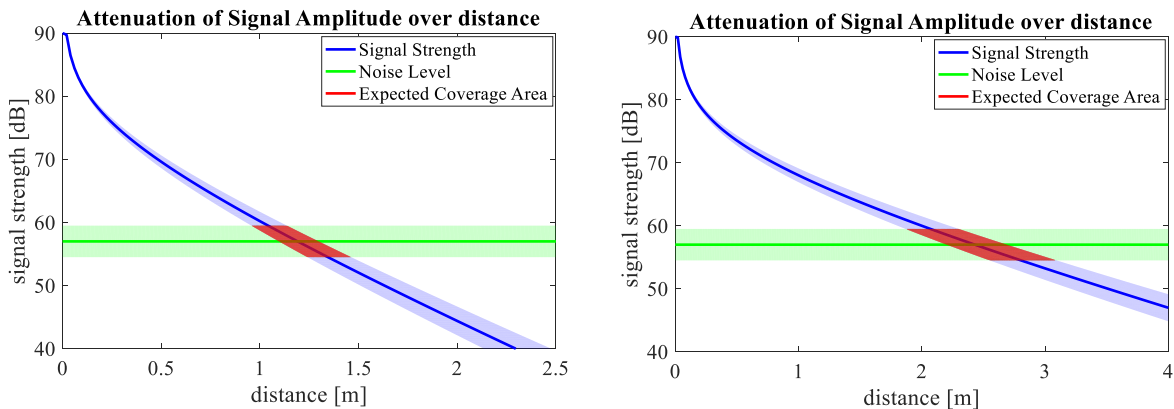
(a) Estimated detection range of 24mm thick submerged plate

(b) Estimated detection range of 60mm thick submerged plate

Figure 7.3: In order for the signal to be detected, it needs to be at least as loud as the noise, indicated by where the solid lines meet. The margins of uncertainty are indicated by the lighter areas. Combined, it results in a margin for the expected coverage area.

as shown in figure 7.3 by the red area.

Monitoring of a Single Wind Turbine

Fatigue crack growth can be detected using an acoustic emission monitoring system, when the location where it occurs is within range of the sensor node. If one would like to monitor a wind turbine, the areas of interest have to be covered by the sensor nodes. How many nodes are required to cover the complete foundation? Is it possible to use fewer sensor nodes to determine if fatigue crack growth is occurring?

Full Coverage of a Wind Turbine

To determine the number of sensor nodes required to have full coverage at a foundation, two parameters are required: the surface area to be monitored, and the coverage area of the sensor node. This is based on the case of a monopile and the assumption that there is no overlap in coverage area between sensor nodes, which is an overly positive assumption. The surface area A of the wind turbine can be calculated using

$$A_w = h_w * r_w * 2\pi \tag{7.1}$$
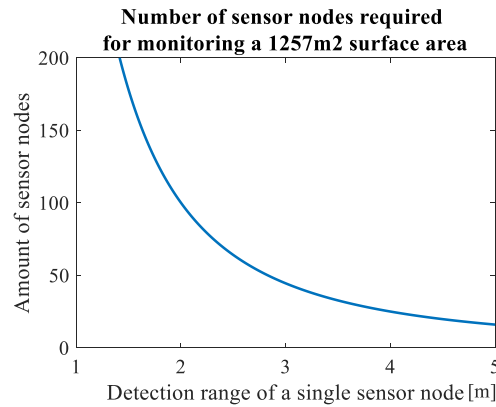
Figure 7.4: The number of sensor nodes required for covering a complete wind turbine foundations (monopile + transition piece, with a total area of $1257m^2$). At a detection radius of 2 meter, the number of sensor nodes required is approximately 100, and even at a detection range of 5 meter, at least 20 sensor nodes are required.

with index w indicating the wind turbine tower, h the height, r the radius of the monopile. The coverage area of the sensor node A_s can be found using the detection radius, r_s, of the sensor as follows:

$$A_s = \pi r_s^2 \tag{7.2}$$

A typical offshore wind turbine in the north sea is placed at a water depth of 25 meter, and with a transition piece that reaches up to 15 meter above the water level. The diameter is 5 meters, resulting in a total combined surface area of $1257m^2$. The number of nodes required for such a surface area is plotted against the detection range of a sensor in figure 7.4. The coverage area of a sensor node is, based on a detection radius of $2.0m$ for a wall thickness of $60mm$, approximately $13m^2$. It can be seen that the total number of sensor nodes required is fairly high. It is suggested to exclude areas that are unlikely to initiate fatigue crack growth.

Coverage of Potential Hotspots

Not every location on a wind turbine foundation has an equal risk of initiating fatigue crack growth. If an area is unlikely to be the source of fatigue crack growth, it may not be necessary to monitor that part of the structure. Identifying these areas can help in optimizing the sensor layout. Fatigue crack growth occurs when at a location the combination of loading and geometry cause the local stress to exceed the fatigue limit of the material. Using finite element analysis and simulations based on the loads a wind turbine experiences, the most vulnerable hotspots can be selected. Often, the wind loading that a turbine experiences is not distributed evenly among all wind directions, thus it is likely that the fatigue location can be predicted resulting in fewer sensor nodes required. For a wind turbine, a number of these locations have been identified, and are indicated in figure 7.5. The selection can be based on severity of damage if fatigue crack growth occurs, expected stress level, available budget, and accessibility, amongst others. Covering the base of the monopile, the boat landing, the grouting, and the power cable, requires approximately 6 to 9 sensor nodes, and can still give a good coverage of the most vulnerable areas.

In case of a jacket type foundation, the number of hotspots is increased, while the coverage area of a single sensor node is decreased. Every weld is a potential source of fatigue crack growth and, depending on the expected stress, may require monitoring. A single sensor node is expected to cover one K-joint, an example of which is given in figure 7.6. As a typical jacket consists of multiple joints, the number of sensor nodes required to monitor a full foundation may be increased in comparison to a typical monopile. However, after analyzing the structure for fatigue sensitivity, it may be sufficient to monitor only those joints that are expected to suffer from fatigue the earliest. It may be possible to assume that if no fatigue is detected at the weakest joint, the other joints are free of fatigue too. The grout is not expected to fail, as the amount of bending loads on the grout is limited in the case of a jacket. It may thus be acceptable to, only monitor the most vulnerable joints of a jacket, or even select only the most vulnerable locations overall, bringing the total number of sensor nodes to somewhere between 4 and 9.
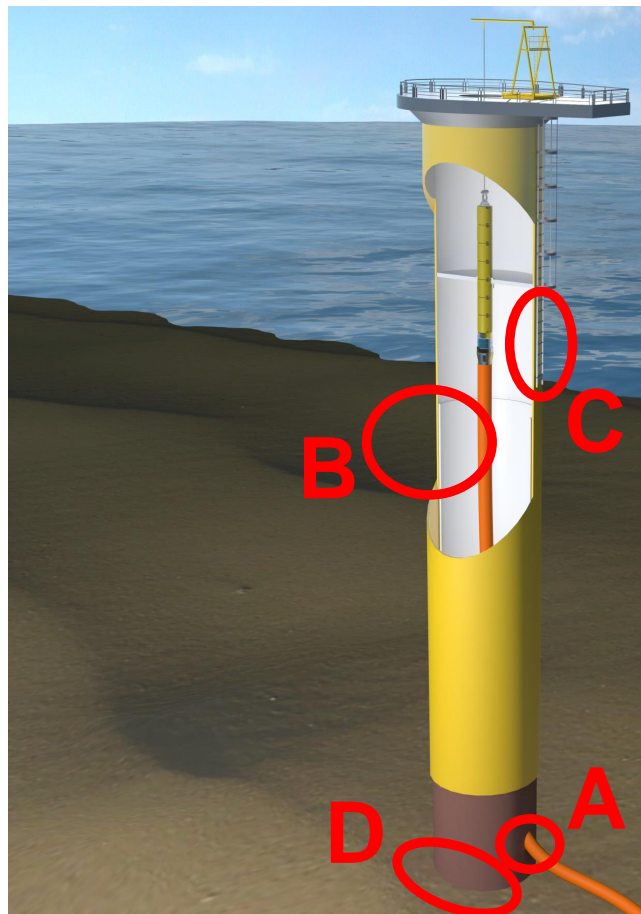
Figure 7.5: A number of locations on a wind turbine have a higher probability of initiating fatigue crack growth, as indicated in this figure. A: cable hole, B: end of grouting connection, C: boat landing, and D: the border at which the monopile meets the ground. Welds in general can also be an initiation point for fatigue crack growth. [picture altered from engineerlive.com]
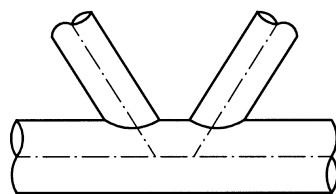
Figure 7.6: A schematic representation of a K-joint and how that would be applied in a jacket type foundation. [[100] & off-shorewind.biz]

Monitoring of a Wind Park

A wind park consists of multiple wind turbines. Each of these wind turbines could be monitored, but this may be cost ineffective. An alternative could be a fleet leader approach. This approach takes one or multiple wind turbines that are expected to encounter the largest loads. The loads may be deduced from wind speed data, which is recorded by each and every wind turbine. The measured wind speeds can be compared with the expectations in order to verify that indeed the wind turbines that experience the largest loads are selected. In case the wind turbines that have been selected are not experiencing the largest wind loads, it may also be possible to extrapolate data to other wind turbines [101]. Difficulties may lie in variations in positioning of different wind turbines, which may have an unforeseen effect on the loading within the wind turbine. A benefit of the acoustic emission monitoring system is that it can be retrofitted on a wind turbine when there is a suspicion of fatigue crack growth. The monitoring system can then quickly determine if, and where fatigue crack growth is occurring.

Using a fleet leader approach, the number of wind turbines that are monitored using an acoustic emission monitoring system can be kept low. For a similar monitoring system, two wind turbines were monitored in more detail using accelerometers and optical fiber strain gauges, while a less sophisticated monitoring system was monitoring a larger number of wind turbines [101]. For the acoustic emission monitoring system, it may be sufficient to install a network of sensors for accurate monitoring of the most probable locations for fatigue crack growth on two wind turbines. If wind speed data, or other less accurate measurements indicate that another wind turbine could be experiencing fatigue crack growth, the monitoring network could be expanded to determine when and where fatigue crack growth is occurring. Monitoring a wind park with 220 MW installed power, and providing the information required for a predictive maintenance strategy, may therefore require less than 18 sensor nodes.

Financial Analysis

These monitoring networks do come at a cost, as equipment and installation of the sensor network is required. Fortunately, the monitoring system also results in benefits. The benefits can be categorized in direct benefits, indirect benefits, and potential benefits. The direct benefits are a result of reducing the amount of visual inspections. The indirect benefits are a result of an improved maintenance strategy and the corresponding reduction in associated costs. The potential of what can be achieved using the monitoring system may be even larger, as structural health monitoring could be included in the design of wind turbine foundations.

Direct Benefits

Nowadays, it is common practice to periodically inspect the wind turbine foundation. This is done to detect fatigue crack growth. Inspection has to be done above sea level as well as below sea level. Inspections below the sea level require divers or a remotely operated vehicle, and detection is made more difficult by marine growth and reduced visibility underwater. Having an acoustic emission monitoring system, the amount of visual inspections could be greatly reduced. Currently, these inspections are usually performed yearly as in wind farm Egmond aan Zee [102]. The inspections require a diver or a remotely operated underwater vehicle (ROV), costing around 10,000 Euro per day [103]. A diver has more abilities than a ROV but can typically inspect one wind turbine per day, while a ROV can inspect 4 turbine foundations per day. The inspections include checks for physical damages, coating damages and untensioned bolts. No exact numbers for the division in work load between the different checks could be found, therefore it is assumed that inspection for fatigue cracks takes ten to twenty percent of total inspection time. For a wind farm similar in size to the Gemini wind park, which consists of 150 4MW wind turbines, it is expected that inspections of the foundation would cost between 250 k€/year and 750 k€/year, based on a study by GL Garrad Hassan [104]. Included in these inspections are foundation strength surveys, scour inspection, assessment of the paintwork, secondary steelwork, and the grouted connection. The cost of repair estimated for the foundation is expected to be between 125 k€/year and 750 k€/year. Acoustic emission monitoring will not prevent all of the inspection work, It is assumed that between 10% and 20% is spent on inspections of the wind turbine foundation. The direct reduction in monitoring cost is, based on these numbers, between 25 k€/year and 150 k€/year.
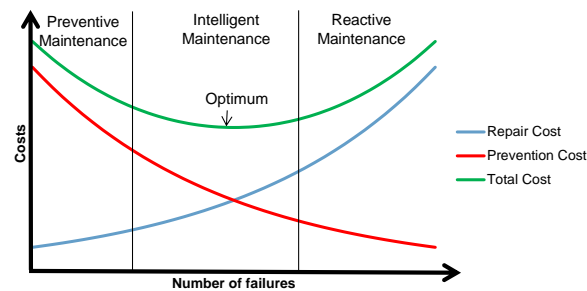
Figure 7.7: A preventive maintenance strategy has higher cost due to repairs being performed (long) before an actual failure. A reactive maintenance strategy results in down time, and potential damage as a result of a failure. In finding the optimum in operational and maintenance costs, parts should be replaced or repaired at the right time. This requires knowledge about the condition of various components. This can be gathered using condition monitoring systems, such as Acoustic Emission Monitoring. [108]

Indirect Benefits

The benefits of the monitoring system not only lie in a reduction of the amount of visual inspections, but the maintenance strategy could also benefit. If a wind turbine experiences a lot of down time, or components are replaced prematurely, operational costs may be higher than the ideal O&M costs could be, as shown in figure 7.7. Although O&M costs only account for approximately 25% of the total cost of wind energy, studies estimate that implementing a condition based maintenance strategy over a preventive or reactive maintenance strategy may save 20% in O&M costs [105] [106]. The share of maintenance performed on the foundation of offshore wind turbines could not be found. With wind farms reaching their design life time, determining the structural health of the foundation may play an important role when deciding between extension of wind farm operations or decommissioning of the wind farm. Conventional inspection methods have a certain detection limit, requiring a fatigue crack to have significant severity before it is detected. An acoustic emission monitoring system could in this case detect if there is fatigue crack growth occurring at all. If using acoustic emission monitoring a more accurate assessment of the structural health can be made, then this might have a positive effect on the levelized cost of electricity. Furthermore, acoustic emission monitoring could aid in reducing the number of tower collapses. Although the number of tower collapses is limited, only 62 accidents between 1997 and 2009 [107], a collapse results in a total loss of a wind turbine. It is difficult to say if and how many collapses acoustic emission monitoring could prevent, but it could contribute in early detection of severe damage. Looking at the overall indirect benefits, there are three main contributors: reduction in O&M cost, extension of wind farm life time, and prevention of collapses. It is difficult to quantify the actual effects of acoustic emission monitoring for these aspects, but it is clear that it results in a positive contribution.

Potential Benefits

The benefits may be larger than the direct and indirect benefits, as there is a potential for more benefits. These benefits are uncertain and depending on aspects that lie outside the scope of this monitoring system. Wind turbines are often overdesigned, due to uncertainties regarding the loading[109], the surrounding environment[19], or the approach used in designing a wind farm[110]. The acoustic emission monitoring system could provide information on the conditions in which fatigue cracks occur, and thereby provide knowledge that was not available before. With an increased knowledge on the performance of offshore wind turbines, the design of the wind turbine may be tailored to the specific environment, and the safety factor may be decreased. Both these measures are expected to result in weight savings, requiring smaller equipment and resulting in a cost reduction.

Cost of Various Scenarios

Before any monitoring can be done, the system has to be installed. There are a couple of scenarios analyzed for their associated cost. The total cost is derived from the sensor cost, the data acquisition cost, cost of installation, cost of monitoring, and possibly other costs too. The different options that are treated are: monitoring from the beginning of commissioning a wind farm, retrofitting a monopile

when fatigue crack growth is suspected, and monitoring using a remotely operated underwater vehicle, which may be possible in the future. The values given in this section are an indication of the expected cost and benefits, and prices when the technology is market ready may be different.

Install at Commissioning of Wind Farm
When structural health monitoring is incorporated in the design of a wind farm, it is likely that the sensors are installed during the commissioning of a wind farm. This allows for monitoring of one or multiple wind turbines during the life time of a wind farm, fatigue crack growth can be detected as soon as it occurs. In this scenario, it is likely that multiple sensor nodes are used on the turbines, in order to cover all of the potential fatigue hot spots. The number of sensor nodes required per wind turbine is estimated at six to nine in section 7.2.2. This scenario requires 24 to 36 sensors, costing approximately €500 each. The sensors are attached to a data acquisition system, which can cost €50,000 per four sensor nodes, or a wireless system may be used at €10,000 per sensor node. As it is assumed that during installation a boat is available for transport of equipment and personnel, the added cost for installation of the sensors is estimated at €7,000 assuming that an installation team costs €2,500 per day and can install four sensor nodes per day, plus €2,000 in transport costs. A weatherproof computer system with modem is also required to transfer data to shore, for which the cost is estimated at €5,000. Lastly, the software and support required for operation has to be accounted for too. The software and support costs are estimated at €1,000 for now, but could be reduced in the future as the goal is to have a fully automated and autonomous system. Summing up the costs, the total cost per wind turbine for such an acoustic emission monitoring system would lie between €85,000 and €135,000, for a monitoring network consisting of six to nine sensor nodes.

Retrofitting of Wind Turbine
Currently, many wind farms are already in operation. Some of these wind farms may be suitable for extension of their operations after their designed life time. A structural assessment has to ensure that the wind turbine is able to withstand this extension, and an inspection for fatigue cracks is often part of this assessment. Another option could be that an operator suspects fatigue crack growth and would like to determine if fatigue crack growth is occurring at a certain location. For this scenario it is assumed that a boat has to be chartered in order to install the equipment, costing €5,000 per day. The cost of installation is €2,500 per day, with a minimum of one day, while up to four sensors can be installed per day. The sensor cost per node is €2,000, and one data acquisition unit costs €10,000. The hardware and software to store, process, and send the data to the operator costs €5,000, and €1,000 respectively. The total cost of installing one sensor for monitoring of a certain area on a wind turbine is €25,500. Per four installed sensor nodes, the cost could be €61,500, if all are installed at the same wind turbine.

Monitoring by Remotely Operated Underwater Vehicle
A futuristic scenario, yet technically not impossible, would be to have a ROV perform acoustic emission monitoring. As mentioned in section 7.4.4, an operator may be interested in determining whether fatigue crack growth is occurring at a certain location. This can be performed by installing a permanent sensor, but if an operator has a number of locations within a wind farm for which the structural health has to be determined, a mobile ROV could visit these locations. Such a ROV is reusable, and can monitor a different wind turbines within a single wind farm, or with the help of a transporter vehicle visit multiple wind farms. In order for fatigue crack growth to occur, a wind turbine has to operate at high load, while for the rover to move from one wind turbine to another requires low currents. As strong winds often cause significant current, the number of locations the ROV can visit during a year is limited by the number of cycles. It is assumed that there are 12 cycles per year, allowing for 12 different locations to be monitored. Although the cost of a ROV at €500,000 is higher than the other scenarios, the ROV has the advantage of being mobile. Assuming that the ROV operates mostly autonomously, requiring €10,000 per year for directing the vehicle to a different location, while the expected life time of a the ROV is 10 years, the yearly cost is approximately €60,000. At the same time, the number of locations monitored is larger than the previous scenarios. Although permanent installation of an acoustic emission monitoring system may result in more information on a wind turbine over its life time, the ROV scenario has the potential of being a cost-effective solution when short term monitoring is sufficient.

Cumulative Cash Flow
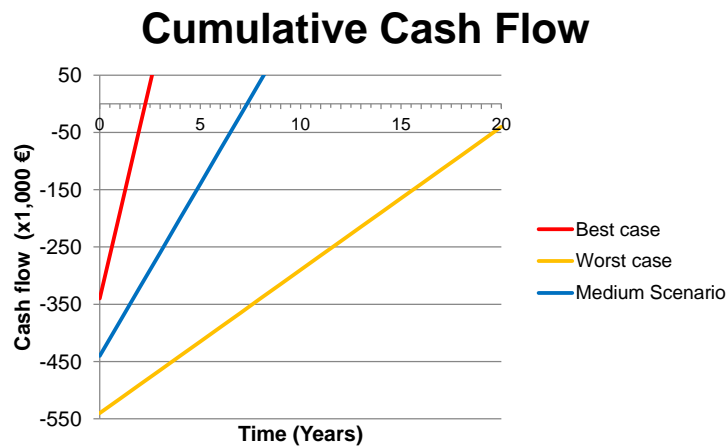
Figure 7.8: Cumulative cash flow diagram as a result of Acoustic Emission Monitoring for wind turbine operators. The best case scenario assumes that the cost of each monitoring system is low, at €85,000, while the savings as a result of monitoring are estimated at €150,000 yearly. Break-even is achieved after 25 months. The worst case scenario assumes that the cost of the monitoring system is €135,000 each, while the savings are only €25,000 per year. In this case, break-even is achieved after 21 years. The medium scenario is somewhere in between, with €110,000 investment cost, and yearly savings of €60,000. Break-even is achieved in slightly over 7 years.

Payback time of investment

For an operator the two most important factors are whether the system can function as intended over the life time of a wind turbine, and whether the system is profitable for the operator. Due to the uncertainty in the cost savings, the time it takes for this system to pay back its investment cost has a large margin. For a wind farm of 150 4MW wind turbines, the cost savings were estimated at between €25,000 and €150,000, while the cost of covering the most important areas on a wind turbine was estimated between €85,000 and €135,000. Installation of the monitoring system on each wind turbine would not be cost effective, but installation on a single turbine is not likely to give enough statistical meaning to the results. For such a wind farm as described before, four monitored wind turbines are probably sufficient to perform the monitoring as intended, and reach the cost savings as described. In figure 7.8, the cumulative cash flow diagram from the perspective of the operator is shown, in which the revenue is determined by the cost savings due to reduced inspections. It is expected that having more wind turbines equipped with a monitoring system results in a more accurate prediction for the wind farm as a whole, and cost savings on inspections are expected to increase. In order to improve the cost estimates, detailed operational data from wind farm operators is required, specifying how much resources are spent per task.

8
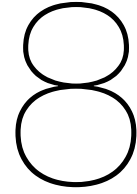
Discussion and Recommendations

This thesis has treated different aspects of acoustic emission monitoring in an attempt to determine whether acoustic emission monitoring of offshore wind turbine foundations is feasible. The experiments that have been performed often resulted in getting a step closer towards the end goal. Sometimes, the experiment did not give the desired results, and the cause for deviation had to be studied. Either way, the methods used and the results require interpretation regarding the accuracy and the usability of the results that have been gathered. After discussing the experiments and their results, an outlook is given of the remaining steps. There are several steps remaining before an acoustic emission monitoring for offshore wind turbines could be commercialized. These steps include tests that can be performed to prove functioning of the system in an offshore environment, together with recommendations on focus points during these tests.

Discussion

In this section, the different experiments are discussed. The numerical simulations are treated first.

The results from the numerical simulation are expected to be accurate up to 10%. The model has been compared with other research, by Watkins et al. [94], and within a certain frequency range the results nearly coincided. According to Watkins, their method is accurate up to $\pm5\%$, while the results from simulation deviated 5% too. The frequency range in which the results are accurate is ranging from peak attenuation up to the onset of higher order wavemodes. At frequencies below peak attenuation, the (near)-zero frequencies cause a disturbance in the results. At the onset of higher order wavemodes, the model loses accuracy as the distribution between the different wavemodes, and the different wavemode velocities result in too many variables. This is not a problem for this application, as the acoustic emission monitoring system is using the same frequency range for operation. In determining the coverage area, the attenuation is one of three main factors, the others being the source signal amplitude and the noise level.

The noise level could not be measured at an offshore wind turbine foundation, but two experiments have been performed in order to get an estimate for the noise that is to be expected on site. The noise measurement on the wind turbine captured noise resulting from rotating equipment. Some incidental high intensity signals have been picked up at 80 dB, which is high but was only incidental. Noise from rotating the wind turbine head reached 54 dB, typically once every minute, for a total of 30 seconds. Furthermore, the noise with these aspects was between 40 and 45 dB. There are some remarks that should be considered when interpreting the results. In this case, only a single wind turbine has been monitored, for a couple of hours, in light weather conditions (just above the cut-in wind speed). The results are valid for this single wind turbine in this set of conditions, but there are a number of variables at play that may influence the outcome. The noise level may vary between different manufacturers or even types from the same manufacturer. The state of the wind turbine is unknown, e.g. does it have any repairs or defects that could change the noise levels? The age of the wind turbine could also play an effect in the noise levels, as when wear sets in the noise spectrum and intensity may change. As mentioned, the wind speed was around 5 m/s, while most wind turbines generate electricity up until a wind speed of 25 m/s, and may be subject to even higher wind speeds during stormy weather. The effect

of higher wind speeds on emission of ultrasonic noise has not been studied yet, but is unlikely to cause a decrease in noise. This especially is of interest as it is expected that fatigue crack growth occurs at high wind speeds, and thus loading, rather than at lower wind speeds. On a positive note, it is expected that modern wind turbines are quieter compared to older wind turbines, as technology advances and manufacturing tolerances decrease, allowing for a more precise production of components. The noise measured at the wind turbine does potentially limit the coverage area of the monitoring system, but with the current measurements it is expected that a monitoring system will function as intended. However, a more thorough analysis of multiple wind turbines, in multiple conditions could provide proof for this statement.

Another contributor to the noise in offshore wind turbine foundations comes from the environment. These sources can be ships, animals, and weather effects. Of these types of noise, it was found that rain would have the highest intensity of the sources that produce monotonous noise, with the exception of boat engines. With the help of equipment in the laboratory, rain can be simulated, and the resulting noise as measured by the sensors is studied. The results have shown that there is indeed some noise resulting from the water droplets, peaking at 57 dB, similar in severity to when the wind turbine rotor is yawing. There were some events detected of high intensity, but as demonstrated in that section, those particular events are not expected to influence the detection capabilities of the monitoring system as they can be filtered out due to incompatible arrival times. There are a number of uncertainties in the results, which may influence the noise level as detected by the sensors. The first factor is the setup used; although the shower head which was used in the tests does come close to actual rain, there are differences that may have a positive or negative effect on the results. In comparison to light rain, the water droplets created by the shower head are likely to create more noise [95]. The velocity of water droplets in the test setup has not been measured, nor has the water drop size been measured. A water droplet with a diameter of 1-2mm has a terminal velocity of 6 to 9 m/s [111]. As the water exiting the shower head is pressurized (tap water), it is assumed that the velocity of the water droplets is reasonably close to the terminal velocity, and deviations due to the velocity are expected to be negligible. The noise resulting from waves hitting the structure has not been studied. According to Ainslie et al. the noise resulting from waves is supposed to be of lesser intensity than rainfall [79]. However, it is unclear if this is also valid for waves hitting a structure. The laboratory setup does not allow for testing of different types and sizes of waves, and therefore leaves a gap as to whether the statement made by Ainslie et al. remains valid in this case. The frequency at which waves hit the structure during a storm is relatively low. The natural frequency of waves is typically around 0.1Hz, while the natural frequency of a monopile embedded in clay is closer to 0.5Hz[112]. If one assumes that fatigue crack growth is more likely to be caused by the oscillation of a wind turbine than by waves hitting the structure, this is not expected to limit the functioning of the monitoring system. If this assumption does not hold, it is expected that onset of fatigue crack growth may be lost in noise caused by the waves hitting the structure, but as the crack develops, crack growth is then also expected to occur when the structure is not hit by waves. Based on these results, it is not expected that the capabilities of the setup are limited more than they would have been by the mechanical noise resulting from the wind turbine rotor yawing.

Other aspects of acoustic emission monitoring have also been studied. In order to reduce the amount of data stored on site, an add-on was developed allowing the QBF software to operate at set intervals. During the testing of this add-on, no problems have been encountered. The interval used during the test was short, and the number of repetitions of the analysis was limited. Error handling can be added to increase the certainty that the program will continue to function over a longer period of time. Important to note is that in case the program would stop working, no data is lost, as it is just not processed any more. A remote restart may be used in such a case to continue processing of the data. It can be concluded that the processing of acquired data can be done autonomously and locally, reducing storage and/or bandwidth requirements, and if any unforeseen error may occur, it is not expected that data will be lost and a restart is likely to fix the problem, at least temporarily.

With the remote autonomous operation demonstrated, the next step was determining the influence of curvature and surface quality on the transmission of signal. The results indicate the effect of curvature is small to negligible, at less than 2 dB for the jacket type foundation, while the surface condition plays significant role in transmission of the signal, as the signal amplitude was decreased by 20 dB. The quality of these results is considered to be reliable. In the curvature test, the largest factors that may influence the results are the surface quality, varying input by pencil lead break, and non-constant distance between the sensor and the point of pencil lead break. An imperfect surface quality results in

a worsened transmission of signal, and thus the results found for the effect of curvature may be slightly pessimistic. However, the decrease in signal transmission was small. The input by the pencil lead break used in the experiment may vary slightly, as no fixture has been used for application of the pencil lead break or the distance between the sensor and the point of application of the pencil lead break. A ruler has been used for indicating the distance between the location for the pencil lead break and the sensor, which may result in some variation in signal transmission quality. If one were to assume that the location at which the pencil lead break is applied can vary by up to 5mm on a total of 280mm, the difference in signal transmission due to geometrical spreading between 277.5mm and 282.5mm equals 0.1 dB, and should therefore have a negligible effect on the results. The lack of using a fixture for application of the pencil lead may lead to a variation in amplitude of the signal. A difference of 5 degrees in angle of application results in a variation of applied force of between 5 and 10 percent [113]. To limit the amount of variation as much as possible, a geometry set triangle was used to maintain the same input angle between tests, but the length of the pencil lead was harder to control. This is likely to have caused some variation, of which the severity is hard to determine. By repeating the pencil lead break a number of times, the variation is reduced, and the signal amplitude typically had a standard deviation of less than 1 dB, indicating a constant input signal has been applied. The results from the experiment are believed to be reliable, as possible variations have been quantified whenever possible and only had a small to insignificant effect. There is no reason to assume that the curvature of a wind turbine foundation may limit the capabilities of an acoustic emission monitoring system, but the surface quality can result in significant changes in signal transmission.

Lastly, the experiments that were performed on the T-joint are treated. The structure in the laboratory is comparable to jacket type foundations, which have a smaller radius than monopile foundations. At a relative error between 5 and 10 percent, there is some uncertainty in the precise location at which fatigue crack growth occurs, but this does not decrease the functionality much. The first goal of the monitoring system is to detect fatigue crack growth, and this is not in any way affected by the accuracy in localization of the signal source. The second goal is to locate fatigue crack growth, and although the error is between 5 and 10 percent, this means that, for a case where the estimated source is at one meter away from the sensors, the actual source lies within a circle with radius of 5 to 10 cm. Hereby periodical visual inspections can be replaced with visual inspections focused on the suspected areas, whenever fatigue crack growth is detected, allowing for a condition based maintenance strategy. As the goal of the monitoring system is to reduce the number of periodical visual inspections, the error in localization is small and not expected to limit the functionality of the monitoring system. Following the localization accuracy test, the T-joint was monitored for a fatigue test. The intent of this test was to detect fatigue crack growth on the test sample as it was being fatigue loaded for a different experiment. The hydraulic load cell resulted in too much noise, preventing fatigue crack growth from being detected. As this setup was used for a different test that had priority over the acoustic emission monitoring, the amount of modifications that could be made was limited, and the noise could not be mitigated. Such a situation, with this amount of noise, would not exist in offshore wind turbine foundations.

Recommendations

This thesis brings acoustic emission monitoring of offshore wind turbine foundations closer, but before it can be regarded as a technique for practical use, some steps still need to be taken. These steps include more thorough analysis of noise, as well as laboratory and on site demonstrators. Furthermore, when performing acoustic emission monitoring, a number of aspects need attention.

- The first step on this list is to perform the fatigue test using a setup in which the noise is mitigated. The fatigue test that was performed as part of this thesis was suffering from the noise created by the hydraulics. This test can be seen as a demonstrator of the monitoring system in a controlled environment. Optionally, the test setup should be submerged in water, to include the possible effect of water on the acoustic emission signals at the crack locations. By performing this test, all the fatigue-related elements of the monitoring system as implemented offshore would be included.

- The next step logically follows from the first step: performing noise measurements at wind turbines and in an offshore environment. The environmental noise should ideally be monitored during a period of a year, to cover all four seasons. During winter, the weather conditions are harsh, which may result in higher noise levels. The environmental noise measurements are expected

to be independent of wind turbine manufacturer and type. The mechanical noise, resulting from rotating parts, may be dependent on manufacturer and wind turbine type. Determining this noise may require to perform a new test for each new type if no data for that type of wind turbine is available. When measurements on multiple wind turbines have been performed, it may be possible to define a number of variables that influence the mechanical noise. These variables may include parameters such as wind speed, installed power capacity, manufacturer, age, etc. With noise levels determined after these tests, the coverage area of the monitoring system can be determined, and the specifications of the system can be adjusted to the needs.

- With the coverage area known, the locations at which sensors are placed have to be determined. It is possible to cover all the surface area of a wind turbine foundation, but fatigue typically starts at one or a few spots. If these weak spots could be identified, a monitoring system may only have to be installed at those locations. It could be assumed that if there is no fatigue occurring at a weak spot, then fatigue is not expected at areas that are less prone to fatigue. This information could perhaps be supplied by accurate finite element assessments as well as by wind park operators that have long-term experience with wind turbines.

- With these questions answered, and these tests performed, the last step would be to install the monitoring system on an actual wind turbine. This should preferably be on a wind turbine of which is known that fatigue crack growth has started to occur. A sensor node can be placed in the vicinity of an anticipated crack. Such a test combines all the knowledge that has been gathered up to that point, and would be the last test before the monitoring system can be deemed market ready.

- The connection between the sensor and the surface is another important part in the functioning of an acoustic emission monitoring system. Further research on easy-to-install sensors with lower sensitivity to the surface condition is deemed valuable in order to minimize the installation cost and time.

9

Conclusion

This thesis has elaborated on the feasibility of acoustic emission monitoring in offshore wind turbine support structures. It has done so by studying the emission of ultrasonic signals from fatigue crack activity, the attenuation rate and noise level required for calculation of the coverage area of a sensor, as well as by studying the localization accuracy, and the effect of surface quality and curvature on the transmission of signal. Numerical simulations have been performed using a spectral element method, studying the attenuation of signal in fluid-solid interaction. This has been done for wall thicknesses ranging from 12mm up to 60mm, with steel as the solid and water as the liquid. The frequency range that is of interest for acoustic emission monitoring is bound by high attenuation at low frequencies, and by the onset of higher order wavemodes at high frequencies. For a wall thickness of 24mm, this results in a frequency range of 25 - 63 kHz and an attenuation rate of 13 db/m on average, while a wall thickness of 60mm results in a frequency range of 10 - 25 kHz and an attenuation rate of 5 db/m on average.

In order to assure proper functioning of the acoustic emission monitoring system at an offshore setup, the effect of curvature, surface treatment, and the remote autonomous processing of data are tested. The analysis software can be run at set intervals, allowing for a reduced storage or bandwidth need, which is useful at a remote location with limited access to shore. The transmission of signal between the surface and the piezoelectric sensors, for studying the curvature and surface treatment effect, has been performed using pencil lead breaks as an input signal. Rust could reduce the signal transmission with 20dB. The sensors function best when the surface is smooth, which can be achieved by grinding and/or sanding any rust. The effect of curvature is small, and expected to lie well below 2dB for a jacket type structure, with typical diameter of 0.5 to 2 meter, and even less for a monopile structure, with typical diameter of 3 to 8 meter.

Next up in studying how the acoustic emission monitoring system would function in an offshore environment is the localization accuracy of the quasi beamforming method on a T-joint sample. Fatigue crack growth in a T-join section occurs at the weld. Pencil lead breaks were applied at four locations along the weld to produce a signal that could be used to determine the location, similar to what would occur during fatigue crack growth. The accuracy of the quasi beam forming in localization of the signal source location lay between 5 and 10%, and the signal was detected in 83% of the inputs. The fatigue test that followed was hindered by noise caused by the hydraulic system. This type and amount of noise is not representative for offshore conditions. The two most notable sources of noise that have to be taken into account are noise from rotating parts, e.g. the wind turbine itself, and rain noise, when applicable. The noise resulting from rain has been simulated in the laboratory using a shower head and a water tank, and the noise that has been recorded was about 57 dB. The noise resulting from the wind turbine itself has different characteristics. The average noise level during normal operation was in the range of 40 to 45 dB. The adjustment of the wind turbine to the wind direction results in a constant noise with an amplitude of 54 dB. During the measurements, this happened once every minute, with a duration of 30 seconds. A different type of noise, possibly from the wind turbine head, had also been recorded, with a high intensity of 80 dB but this noise was less frequent. The interval measured varied; sometimes the interval was 3 seconds, sometimes it was 6 seconds. The source of this was not further studied or localized. However, it is not expected to compromise the monitoring

capabilities of the monitoring system, as it is expected that this incidental noise can be filtered out.

With the attenuation rate and noise levels determined, the coverage area of a sensor has been determined. This has been done for both monopile type foundations, with an assumed wall thickness of 60mm as well as for jacket type foundations for which the wall thickness was assumed to be 24mm. The noise level is similar in each case, and estimated at 57 dB. The attenuation rate was estimated at 5 dB/m for the case of a wall thickness of 60mm, and 13 dB/m for the case of a wall thickness of 24mm. Combined with the geometrical spreading that results in an estimated coverage radius of 2m and 1.2m. With a margin of uncertainty regarding the noise level of ±5dB and uncertainty in the attenuation rate of ±1 dB/m, the coverage radius is expected to lie between 1.7 and 3.0 meter for a monopile foundation, and between 1.0 and 1.7 meter for a jacket type foundation.

Covering a full wind turbine foundation using sensor nodes with such a coverage radius would require many sensors, and may not be the most cost effective solution. Wind turbines have been used in offshore conditions since 1991 and this has resulted in experience regarding the locations that are most prone to fatigue. Using this knowledge, it is possible to assume that if fatigue crack growth occurs, it will occur at any of these locations. Covering these locations requires between six and nine sensor nodes in case of a monopile type foundation, while a jacket type foundation can have the most vulnerable locations covered by between four and nine sensor nodes. The wind turbines are often located in large wind farms. Monitoring of each wind turbine is a possibility, but a fleet leader approach can be a more efficient alternative. This approach uses measurements on a subset of the total number of wind turbines. The subset that is chosen is often subject to the largest loads, which is verified by low level measurements at each wind turbine such as wind velocity. When the fleet leaders are not experiencing wear or damage, it is assumed that the other wind turbines are free from damage too. When the fleet leaders do experience damage or wear, the data that has been gathered can be combined to make a prediction regarding the state of the other wind turbines. Further inspections may be required to confirm the state of the wind farm, but due to the localization capabilities of the acoustic emission monitoring system, this process can be sped up.

The cost and benefits of the monitoring system are an important factor for the potential user. The cost has been determined for three scenarios, being at the commissioning of a wind farm, retrofitting, or a mobile remotely operated underwater vehicle (ROV). The cost for the first two scenarios is assumed to be purely installation costs, as the monitoring system is supposed to operate autonomously. The cost for the first scenario, installation at commissioning of the wind farm, using six to nine sensors, lies between €85,000 and €135,000 for each wind turbine at which the monitoring system is installed. The cost for the second scenario, retrofitting of a wind turbine was priced similarly at €61,500 per four installed sensor nodes. The ROV-scenario would require a high initial cost in the order of €500,000, including the robot, sensors, and other equipment. The ROV allows for 12 locations to be inspected each year, and costs approximately €10,000 per year in order to move and setup the system. With an estimated life time for the ROV of 10 years, that would amount to €60,000 per year. The benefits that are to be expected are a result of improved operations and maintenance. It is estimated that for a typical wind farm of 600 MW, the yearly benefits are between €25,000 and €150,000, due to a reduction in the number of inspections. More accurate monitoring also allows for better planning of maintenance which results in lower costs, although that has not been quantified. A typical wind farm has a life expectancy of 25 years, similar to what is assumed for the sensors. Installing a sensor network on each wind turbine would be too costly. A fleet leader approach may be a more cost effective solution. For this approach only few wind turbines are selected, in order to generate an accurate representation of the structural health of the wind farm. If for such a wind farm 4 wind turbines would have to be monitored in order to reduce the amount of inspections as predicted, the return on investment time would lie around 8 years. Looking at the far future, the knowledge obtained using acoustic emission monitoring could be used for further improvements in offshore wind turbine design, resulting in life cycle cost savings. Based on this thesis, acoustic emission monitoring of offshore wind turbines is feasible and further research towards implementation in wind farms is justified.

A
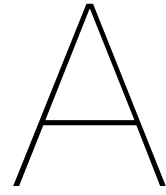
Wind Energy Locations
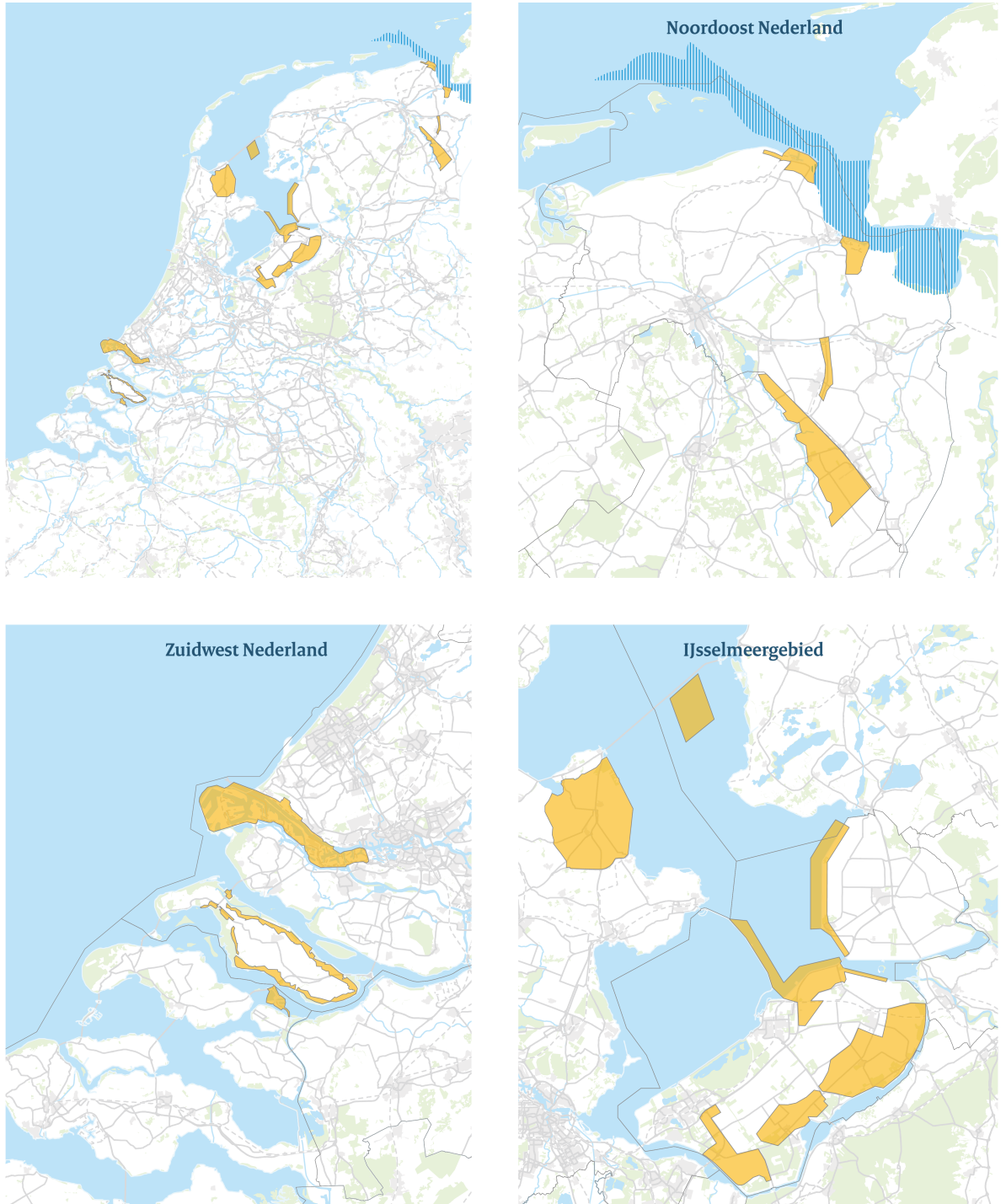
Kaart 1: Gebieden voor grootschalige windenergie

◼ Gebieden voor Grootschalige Windenergie

▦ Eems Dollardverdraggebied

Figure A.1: The locations that have been appointed in the Netherlands for onshore wind energy.

Elementen van de routekaart

▨ Aan te wijzen gebieden, minimaal 10 NM uit de kust
▮ Aangewezen gebieden
▢ Indicatief kabeltrace
◆ Indicatief hubplatform

Overige informatie

▮ Andere aangewezen gebieden
▮ Bestaande parken en parken in aanbouw
---- Nautische 12 mijl

Figure A.2: The locations that have been appointed in the Netherlands for offshore wind energy.
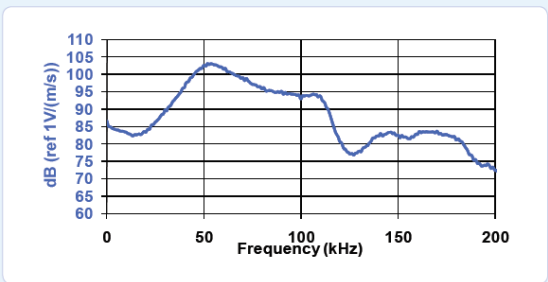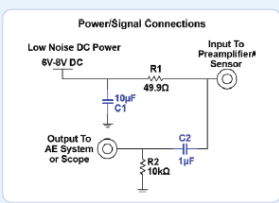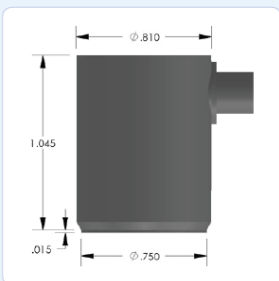
B

Specifications Physical Acoustics - PK6I

MISTRAS
A World of NDT Solutions | *Products & Systems Division*

PHYSICAL ACOUSTICS CORPORATION

PK6I Sensor

Medium Frequency Integral Preamplifier Resonant Sensor

DESCRIPTION AND FEATURES

The PK6I sensor is a medium frequency, resonant, acoustic emission sensor with an integral, ultra low noise, low power, filtered, 26dB preamplifier, which can drive up to 200 meters of cable. This sensor represents an improvement in both noise and low power consumption performance, with noise level below 3 uV and power consumption of 25 mW. The PK6I features a strong stainless steel, integrated body structure. The sensor has smaller size and the same frequency response as the R6I sensor.

The integrated Auto Sensor Test (AST*) capability allows these sensors to pulse as well as receive. This feature lets you verify the sensor coupling and performance at any time before, during or after the test.

APPLICATIONS

The PK6I sensor has been designed to be used with the Pocket AE, a small handheld AE system, or with the Sensor Highway II, an outdoor rated, on-line monitoring system.

OPERATING SPECIFICATIONS

Dynamic
Peak Sensitivity, Ref V/(m/s) .... 106 dB
Operating Frequency Range .... 35-65 kHz
Resonant Frequency, Ref V/(m/s) ....~55 kHz
Directionality ....+/- 1.5 dB

Environmental
Temperature Range .... -35 to 80ºC
Shock Limit ....500 g
Completely enclosed crystal for RFI/EMI immunity

Physical
Dimensions...0.812"OD X 1.06"H
20.6 mm OD X 27 mm H
Weight ....45 grams
Case Material... Stainless Steel
Face Material.. Ceramic
Connector..SMA
Connector Locations...Side

Electrical
Gain .... 26 dB
Power Requirements ....4-7 VDC @ 5 mA
Operating/Max Current... 5/35 mA
Noise Level (RMS RTI)...<3 µV

ORDERING INFORMATION AND ACCESSORIES

PK6I PK6I
Cable (specify cable length).......................1234-SMA/BNC-X
Magnetic Hold-Down MHPK15I
Amplifier Subsytem AE2A, AE5A

Sensors include
NIST Calibration Certificate & Warranty

* AST — Auto Sensor Testing feature allows AE systems to control the sensor as a pulser and a receiver at the same time. It can therefore characterize its own condition as well as send out a simulated acoustic emission wave that other sensors can detect, so the condition of the nearby sensors also can be tested.

Power/Signal Connections

Low Noise DC Power 6V-8V DC
R1 49.9Ω
C1 10µF
Input To Preamplifier/ Sensor
Output To AE System or Scope
C2 1µF
R2 10kΩ

WORLDWIDE HEADQUARTERS:
195 Clarksville Rd •
Princeton Jct, NJ 08550 • USA
T: +1.609.716.4000 • F: +1.609.716.0706
E-MAIL: sales.systems@mistrasgroup.com

CANADA	T: +1.403.556.1350	**HOLLAND**	T: +31.010.245.0325	**RUSSIA**	T: +7495.789.4549
CHINA	T: +86.10.5877.3631	**INDIA**	T: +91.22.2586.2444	**SCANDINAVIA**	T: +46(0)31.252040
FRANCE	T: +331.498.26040	**JAPAN**	T: +81.33.498.3570	**S. AMERICA**	T: +55.11.3082.5111
GERMANY	T: +49.040 2000.4025	**MALAYSIA**	T: +60.9.517.3788	**UK**	T: +44(0)1954.231.612
GREECE	T: +30.210.2846.801-4	**MIDDLE EAST**	T: +973.17.729.356		

Figure B.1: Specifications of the PA PK6I which has been used frequently during the research for acquiring acoustic emission data. Specifications of individual sensors might deviate slightly from the as designed specifications.

C
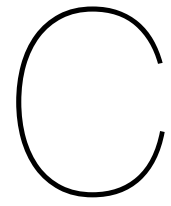
USB AE Node specifications

MISTRAS

One Source for Asset Protection Solutions

| PRODUCTS & SYSTEMS DIVISION | PRODUCT BULLETIN |

1283
USB AE Node

AE Input
Link Out
Parametric 1
Link In
PHYSICAL ACOUSTICS CORPORATION
A Member of MISTRAS
A World of NDT Solutions
Parametric 1-4 and I/O
Alarm/Hit/Power

USB AE Node

The USB AE Node is a full-featured, low-cost Acoustic Emission System that plugs conveniently into the USB port of a user's PC or laptop. The AE System has all the capabilities, features and performance users can expect from their larger Acoustic Emission systems combined with portability and accessibility that USB connectivity provides. The system can be expanded to 4 channels (synchronized).

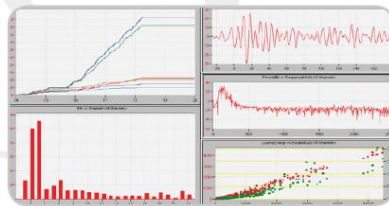### EASY LAPTOP & PC CONNECTION; LOW-COST AE SYSTEM; FREE LABVIEW/C++ DRIVER

The USB AE Node is a single channel Acoustic Emission (AE) Digital Signal Processor with full AE hit-and-time-based features, including waveforms. Through the USB Connector, the AE Node is easily interfaced to a Notebook or PC running Windows 7, 8 and XP™ and Physical Acoustics Corporation's (PAC) well known AEwin™ or AEwin Lite™. The USB AE nodes can be connected to available USB ports of a notebook which also supplies the power needed to operate the USB AE Node.
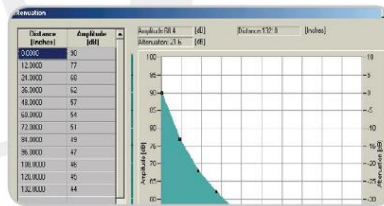
The AE Node can accept single ended or differential sensors amplified by an internal low noise preamplifier. Additionally, PK Series low power integral preamp sensors can be used for long distance connections.

AEWIN FOR USB AE NODE SOFTWARE
Extracted Hit Features:

- Time of first threshold crossing
- Peak amplitude
- Energy
- Envelope strength
- Duration
- Rise time
- Counts
- True Energy
- RMS
- ASL
- Counts to peak
- Parametrics (1-2)

Time-Based Features:

- Parametrics (1-4)
- ASL
- RMS
- True Energy
- Waveform Collection

FEATURES
- Powered and operated through USB Port
- Rugged surface mount (SMT) construction
- Built-in internal preamplifier and power for external preamplifiers
- 18 bit resolution, 20MHz sampling frequency
- With analog and programmable digital filters
- Waveform and Location Options
- Free LabView/C++ driver available for customer program development

SPECIFICATIONS
AE Input: ....1 Channel/USB node (4 nodes/system)
Sampling Frequency: ....20 MHz
AE Digitizing: ....18 bits
Parametric Inputs: ....CH 1, +/- 10V, 16 bits
　　　　　　　　　　　　　　　　CH 2-4, 0-10V, 16 bits
Digital I/O: 2
Preamplifier: ....Built-in
OS: ....Win XP, VISTA, Win 7, and Win 8
Case Size: ....L 5.25"x W 3.25"x H 1.25"
　　　　　　　　　　　　　　　　(133 x 83 x 32mm)
Weight: ....0.5 lbs. (0.23kg)
Power Requirements: ....USB Powered (5V)
　　　　　　　　　　　　　　　< 100 mA/running
Power Consumption: ....< 0.5 watt

For more information:
Please call **1-609-716-4000** or visit us on the web at **www.mistrasgroup.com.**
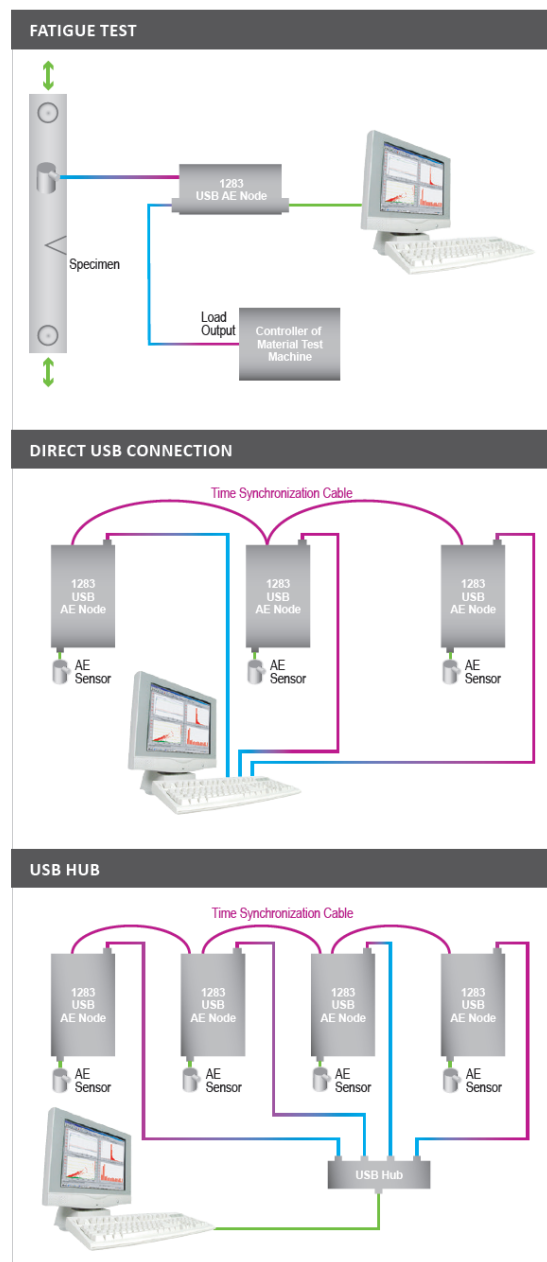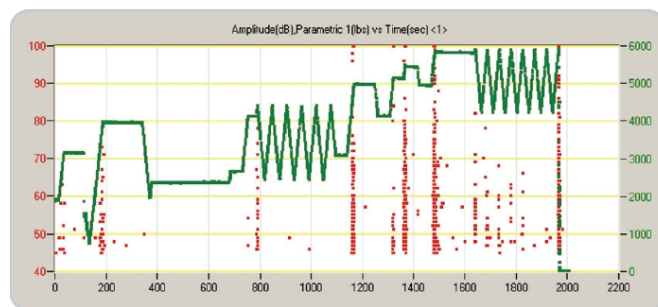
www.mistrasgroup.com

Figure C.1: Specifications of the USB AE node, which is used to record the data from the sensor and store it on the computer.

Application of USB AE Node to Fatigue and Tension/Compression Tests

Fatigue and tension/compression tests have been widely conducted in industries, universities and research institutes. Although strain gauge is widely used in the test to monitor strain or stress change of materials, initial cracks or internal structure failure is hardly identified with strain monitoring or visual inspection. Defects might have already been generated in the tested materials well before they are visually observed.

Although it is well known that acoustic emission (AE) technology can be used to monitor initiation of cracks or internal defects, applications of AE technology to fatigue and tension/compression tests was limited because of the cost and complexity of an AE system. Now, with a newly innovated USB AE node, a single channel AE system is just palm size. It can be readily plugged into a USB port of a laptop or a desktop PC to perform AE test without using external power and preamplifier. AE test can be as convenient as a mouse click.

Cracks or internal defects can be identified soon after they are initiated. In addition, a load sensor or cycle counter can also be connected to a parametric channel of the USB AE node (Figure 1) to make historical trending record in conjunction with the AE so that the load magnitude, testing time or fatigue cycle of crack initiation can be recorded in the same time and displayed in the same graph (See graph below). Free LabView/C++ driver is available for customers to develop their own application programs.
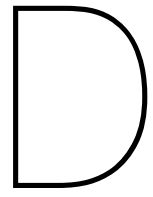
FATIGUE TEST

DIRECT USB CONNECTION

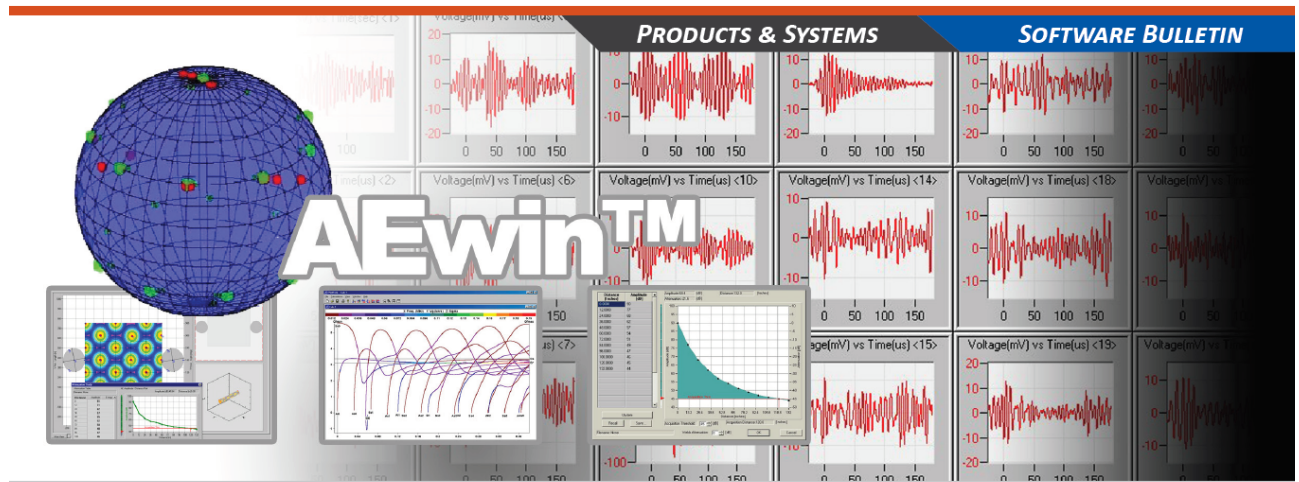**USB HUB**

Figure C.2: Specifications of the USB AE node, which is used to record the data from the sensor and store it on the computer.

D

AEwin software

MISTRAS

PRODUCTS & SYSTEMS   SOFTWARE BULLETIN

AEwin™

AEwin™ | Comprehensive, Versatile & Friendly AE Software

AEWIN™ FEATURES OVERVIEW

AEwin™ is a Windows™ compatible (XP, Windows 8, and Windows 7) software for real-time "simultaneous" Acoustic Emission (AE) feature and waveform processing, display, fast storage and replay. Used for true, real-time operation and control with your MISTRAS AE Systems (Express-8, PCI2, SAMOS, SH II, SH III, AE USB Node, Wireless AE Node).

AEwin™ also features complete compatibility with MISTRAS' standard data file format (DTA), allowing you to replay and analyze your previously collected AE files and framework for easily adding graphs and additional graph screens and user controllable tool bars including: setup icons, acquisition control, line listing, status and statistics. Includes real-time connectivity with Industrial Control Systems (Modbus, OPC)

GRAPHIC CAPABILITIES
- Exceptional 2-D and 3-D graphing capabilities that allow the setup of multiple graphs on a screen, limited only by the screen resolution
- Toggling between multiple screens by selecting a user-labeled tab

- Mouse-driven "Data Selection" features that allows designation of hits, waveforms and events from graphs for detailed analysis and filtered export
- Ability to set up and individually size (on screen) many different types of graphs including; 2-D line graphs, histograms, point plots, waveforms, FFTs, overlays, multiple plots on a single graph and color options
- Arrange multiple graphs on a screen
- Expandable to full screen with zooming and panning for close-up analysis
- Full cursor readout capability
- Alarms triggered by graph data

LOCATION & CLUSTERING OPTION
- 1, 2 and 3 dimensional location modes
- Allows setup of multiple location groups
- Provides mouse-oriented sensor placement and editing features
- Allows selection of type of structure (plate, vessel, etc.) for setup, viewing & location
- Incorporates attenuation profiling into location software (to view a sensor coverage map and provide source amplitude info)
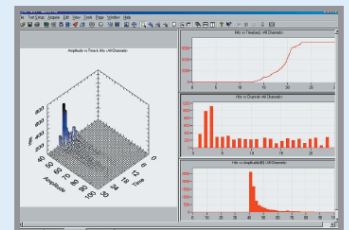
Above: AEwin's 3-D graphing capability allows the graph to be rotated freely, using the mouse.
Below: A typical activity screen with both AE features and waveforms, processed with a simple mouse clickz for any specific hit.

Visit our website for an office near you
www.mistrasgroup.com

Local Presence, Global Reach!

www.mistrasgroup.com

Figure D.1: AEwin is the software that is used to determine the acquisition settings and correspondingly to process and store the results. This bulletin gives an overview of the capabilities of the software.

E
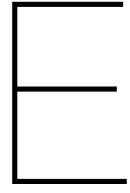
Vestas V90 Specifications

V90-3.0 MW
Facts and figures

POWER REGULATION pitch regulated with variable speed

OPERATING DATA

Rated power	3.0 MW
Cut-in wind speed	3.5 m/s
Rated wind speed	15 m/s
Cut-out wind speed	25 m/s
Re-cut in wind speed	20 m/s
Wind class	IEC IA and IEC IIA
Operating temperature range	standard range:
	-20 °C to 40 °C
	low temperature option:
	-30 °C to 40 °C

SOUND POWER

(Mode 0, 10 m above ground, hub height 80 m,
air density 1,225 kg/m³)

4 m/s	97.9 dB (A)
5 m/s	100.9 dB (A)
6 m/s	104.2 dB (A)
7 m/s	106.1 dB (A)
8 m/s	107.0 dB (A)
9 m/s	106.9 dB (A)

ROTOR

Rotor diameter	90 m
Swept area	6,362 m²
Nominal revolutions	16.1 rpm
Operational interval	8.6 - 18.4 rpm
Air brake	full blade feathering with
	3 pitch cylinders

ELECTRICAL

Frequency	50/60 Hz
Generator type	4-pole doubly fed generator

GEARBOX

Type	two planetary stages and one helical stage

TOWER

Type	tubular steel tower
Hub heights	65 m and 80 m (IEC IA)
	105 m (IEC IIA)

BLADE DIMENSIONS

Length	44 m
Max. chord	3.5 m

NACELLE DIMENSIONS

Height for transport	4 m
Length	9.65 m
Width	3.65 m (3.85 m installed)

HUB DIMENSIONS

Max. diameter	3.6 m
Max. width	4.2 m
Length	4.4 m

Max. weight per unit for transportation	70 metric tonnes

Figure E.1: The specifications for the Vestas V90 wind turbine on which noise measurements were performed.
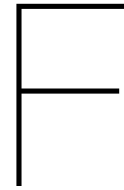
Results from Localization Test

The following pages show the results from the localization experiment on a T-joint section, as described in section 6.4. For each test there is a figure showing all the estimated source locations for events that passed all the criteria, with the sensor locations indicated by the blue dots within the blue square. The red square indicates the location at which the pencil lead breaks have been applied. Each black '+' indicates one estimated source location. The second figure for each test (except test 4, it's the third figure in that particular case) shows the cumulative estimate for that test. Blue indicates a low probability for the source to be located there, while (dark) red indicates a high probability of the source being located there.

Test series = 0 , dt = 0.2 μs, window = [150 400] μs, min. correlation = 0.7, (o) is S0, (+) is A0
max. Δt error = [10] μs, BP filt. coefs = [10   20   90 100] kHz, $[c_{A0}$ $c_{S0}]$ = [3200 4500] m/s,

Figure F.1: Test 1. Location of identified events.

Figure F.2: Test 1. Cumulative estimated source location of signal

Test series = 0 , dt = 0.2 μs, window = [150   400] μs, min. correlation = 0.7, (o) is S0, (+) is A0 max. Δt error = [8] μs, BP filt. coefs = [10   20   90   100] kHz, [c$_{A0}$ c$_{S0}$] = [3200   4900] m/s,

Figure F.3: Test 2. Location of identified events.

Figure F.4: Test 2. Cumulative estimated source location of signal

Test series = 0 , dt = 0.2 μs, window = [150 400] μs, min. correlation = 0.7, (o) is S0, (+) is A0
max. Δt error = [10] μs, BP filt. coefs = [10   20   90 100] kHz, [c_{A0} c_{S0}] = [3200 4500] m/s,

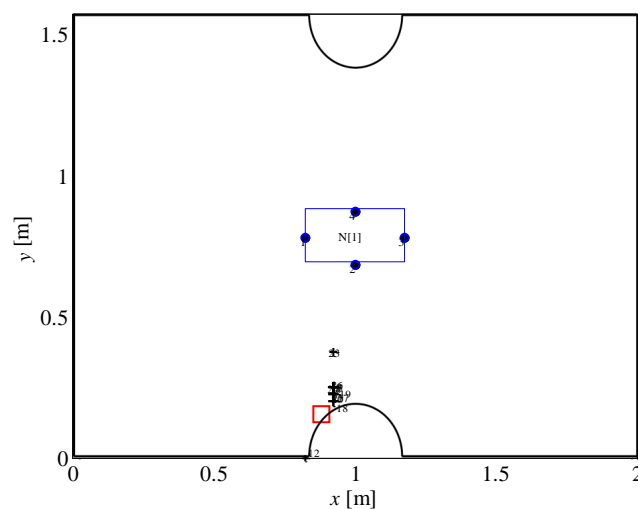Figure F.5: Test 3. Location of identified events.
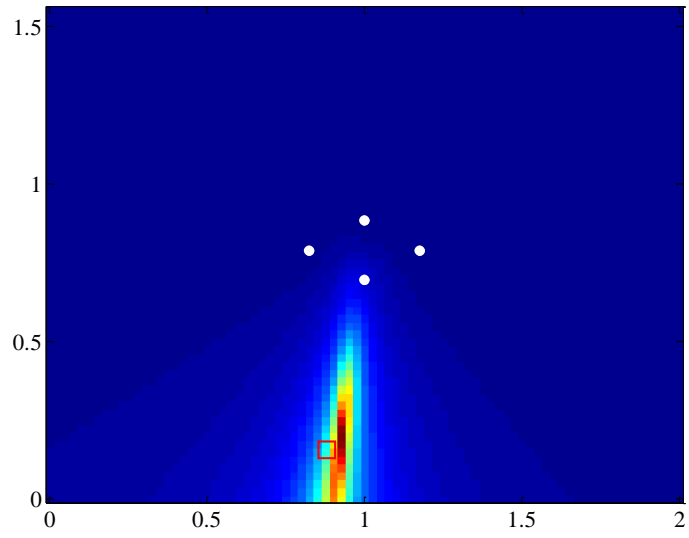
Figure F.6: Test 3. Cumulative estimated source location of signal

Test series = 0 , dt = 0.2 μs, window = [150 400] μs, min. correlation = 0.7, (o) is S0, (+) is A0
max. Δt error = [10] μs, BP filt. coefs = [10   20   90   100] kHz, [c_{A0} c_{S0}] = [3200 4500] m/s,

Figure F.7: Test 4. Location of identified events without dispersion correction.

Test series = 0 , dt = 0.2 μs, window = [150 400] μs, min. correlation = 0.7, (o) is S0, (+) is A0
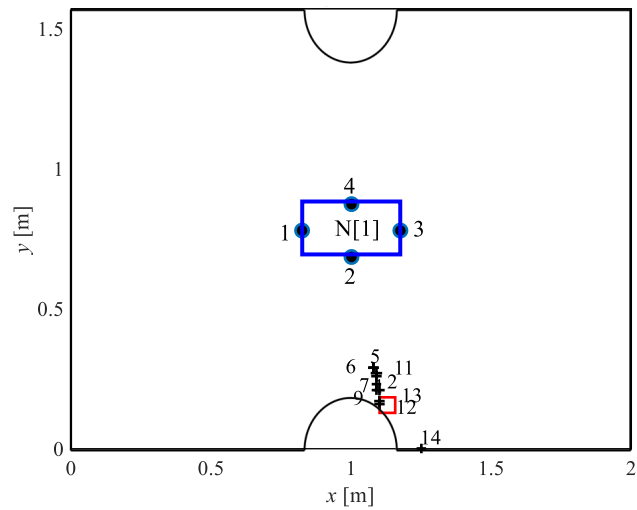max. Δt error = [10] μs, BP filt. coefs = [10   20   90 100] kHz, [c_{A0} c_{S0}] = [3200 4500] m/s,
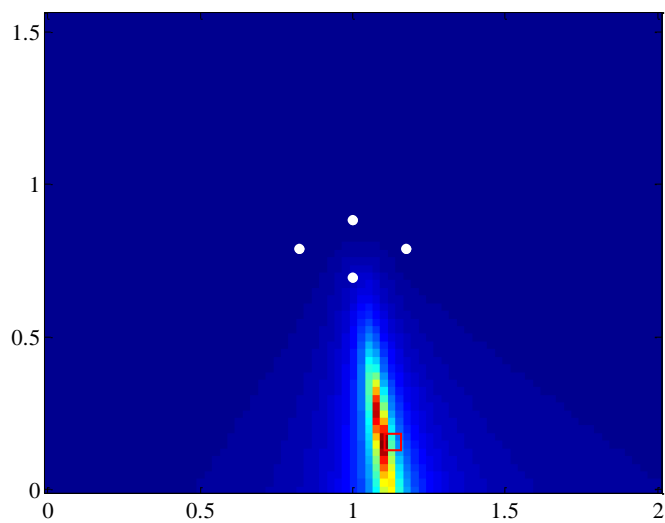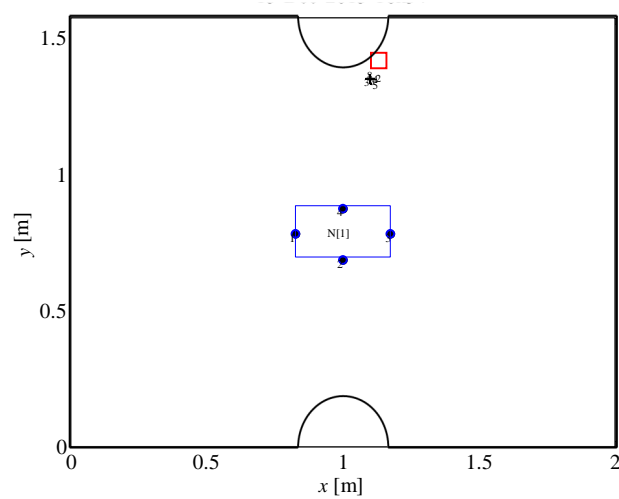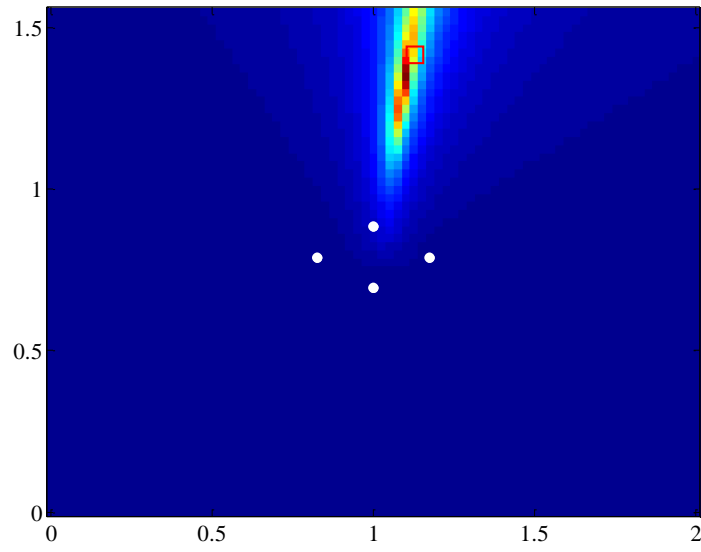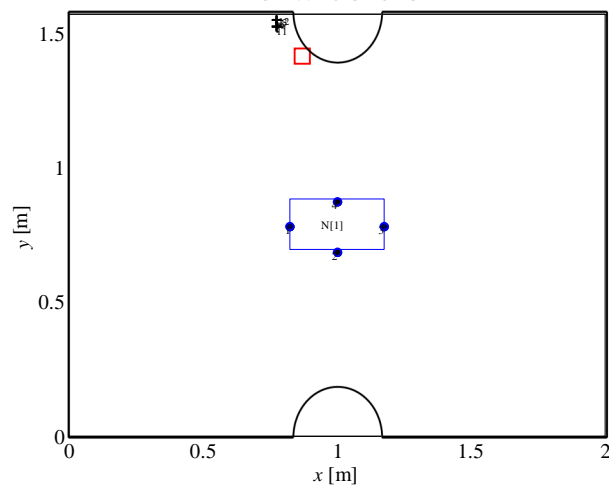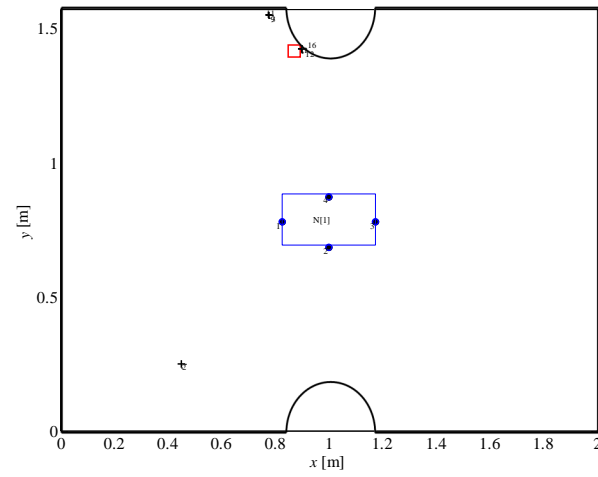

Figure F.8: Test 4. Location of identified events with dispersion correction.

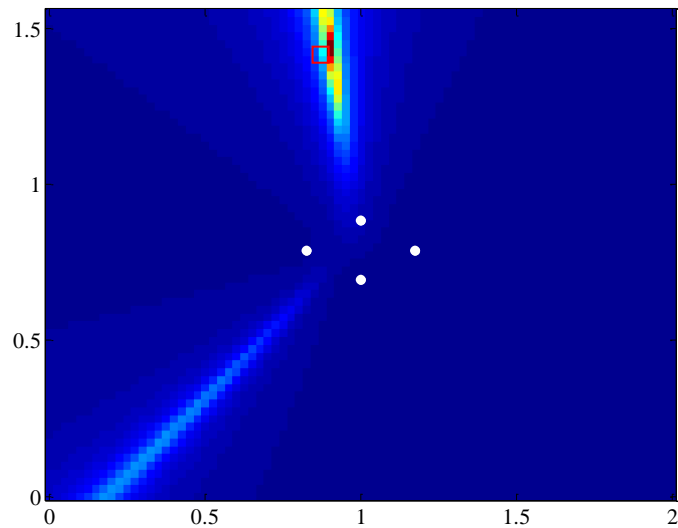
Figure F.9: Test 4. Cumulative estimated source location of signal

Bibliography

[1] J. Norskov, "Wind turbines reached record level in 2014," 1 2015.

[2] I. E. Agency, "Key world energy statistics 2014," tech. rep., 2014.

[3] U. E. I. Administration, "International energy statistics."

[4] G. W. E. Council, "Global wind report - annual market update 2014," tech. rep., 2014.

[5] N. Research, "World wind energy market update 2015," tech. rep., 2015.

[6] T. E. W. E. Association, "Wind in power - 2014 european statistics," tech. rep., 2015.

[7] L. Yuanyuan, "China increases target for wind power capacitiy to 1,000 gw by 2050," 1 2012.

[8] U. D. of Energy, "Wind vision: A new era for wind power in the united states," tech. rep., 2013.

[9] R. voor Ondernemend Nederland, "Monitor wind op land," 2015.

[10] C. B. voor de Statistiek, "Cbs statline - windenergie; elektriciteitsproductie, capaciteit en win-daanbod per maand," 9 2015.

[11] H. Kamp and M. S. van Haegen, "Kamerbrief over windenergie op zee," 2014.

[12] N. W. E. Associatie, "Windenergie opwekken nederland feiten | nwea."

[13] C. B. voor de statistiek, "Windenergie op land; productie en capaciteit per provincie," 6 2015.

[14] R. voor Ondernement Nederland, "Provinciaal beleid windenergie," 12 2014.

[15] H. Kamp, "Kamerbrief over kosten windenergie op zee," 2015.

[16] G. G. Hassan, "A guide to uk offshore wind operations and maintenance," tech. rep., 2013.

[17] B. L. L. S.M., "Externe notitie - kosten wind op zee 2015," 2015.

[18] N. R. E. Laboratory, "2013 cost of wind energy," tech. rep., 2015.

[19] B. Associates, "Future renewable energy costs: offshore wind," tech. rep., 2014.

[20] B. Valpy and P. English, "Future renewable energy costs: Offshore wind," tech. rep., 2014.

[21] E. W. E. Association, "Economics of wind energy," tech. rep., 2009.

[22] E. Rosenbloom.

[23] M. Bolinger and R. Wiser, "Understanding trends in wind turbine prices over the past decade," tech. rep., 2011.

[24] UPWIND, "Design limits and solutions for very large wind turbines," tech. rep., 2011.

[25] R. A. Rivas, J. Clausen, K. S. Hansen, and L. E. Jensen, "Solving the turbine positioning problem for large offshore wind farms by simulated annealing," *Wind Engineering*, vol. 33, no. 3, pp. 287–297, 2009.

[26] J. den Boon, J. Sutherland, R. Whitehouse, R. Soulsby, C. Stam, K. Verhoeven, hogedal M., and T. Hald, "Scour behaviour andscour protection for monopile foundations of offshore wind turbines," tech. rep., 2015.

[27] L. Frédéric, M. TAKARLI, and F. DUBOIS, "Acoustic emission technique (aet) for failure analysis in wood materials," in *ICF13*, 2013.

[28] J. ibn Ḥayyān, R. Russell, and .-. Holmyard, Eric John, *The works of Geber*. London : Dent, new ed. / with introduction by e.j. holmyard ed., 1928.

[29] J. Czochralski, "Die metallographie des zinns und die theorie der formänderung bildsamer metalle.," *Metall und Erz*, pp. 381–393, 1916.

[30] C. Heiple, S. Carpenter, and M. Carr, "Acoustic emission from dislocation motion in precipitation-strengthened alloys," *Metal Science*, vol. 15, no. 11-12, pp. 587–598, 1981.

[31] G. Speich and R. Fisher, "Acoustic emission during martensite formation," in *Acoustic Emission*, ASTM International, 1972.

[32] E. Scheil, "Über die umwandlung des austenits in martensit in gehärtetem stahl," *Zeitschrift für anorganische und allgemeine Chemie*, vol. 183, no. 1, pp. 98–120, 1929.

[33] F. Kishinouye, "An experiment on the progression of fracture," *Journal of acoustic emission*, vol. 9, no. 3, pp. 177–180, 1990.

[34] B. Muravin, "Acoustic emission science and technology," *Journal of Building and Infrastructure Engineering of the Israeli Association of Engineers and Architects*, 2009.

[35] Lokilech, "Pedalarm," 2007.

[36] T. Roberts and M. Talebzadeh, "Acoustic emission monitoring of fatigue crack propagation," *Journal of Constructional Steel Research*, vol. 59, no. 6, pp. 695 – 712, 2003.

[37] H. Wadley, C. Scruby, and J. Speake, "Acoustic emission for physical examination of metals," *International Metals Reviews*, vol. 25, no. 1, pp. 41–64, 1980.

[38] K. Holford, "Acoustic emission–basic principles and future directions," *Strain*, vol. 36, no. 2, pp. 51–54, 2000.

[39] J. A. Hudson, *The excitation and propagation of elastic waves*. CUP Archive, 1980.

[40] J. L. Rose, *Ultrasonic waves in solid media*. Cambridge university press, 2004.

[41] C. Willberg, S. Duczek, J. M. Vivar-Perez, and Z. Ahmad, "Simulation methods for guided wave-based structural health monitoring: A review," *Applied Mechanics Reviews*, vol. 67, no. 1, p. 010803, 2015.

[42] I. A. Viktorov, *Rayleigh and Lamb waves: physical theory and applications*. Plenum press, 1970.

[43] N. Nemati, B. Metrovich, and A. Nanni, "Acoustic emission assessment of through-thickness fatigue crack growth in steel members," *Advances in Structural Engineering*, vol. 18, no. 2, pp. 269–282, 2015.

[44] P. L. Pahlavan, J. Paulissen, R. Pijpers, H. Hakkesteegt, and R. Jansen, "Acoustic emission health monitoring of steel bridges," (Nantes, France), pp. 1163–1170, 2014.

[45] T. Lay and T. C. Wallace, *Modern global seismology*, vol. 58. Academic press, 1995.

[46] C. Scruby and H. Wadley, "An assessment of acoustic emission for nuclear pressure vessel monitoring," *Progress in Nuclear Energy*, vol. 11, no. 3, pp. 275–297, 1983.

[47] P. L. Pahlavan, R. Pijpers, H. Hakkesteegt, R. Jansen, and W. Peelen, "Fatige crack identification and lifetime prediction for steel brdige deck structures," (Stanford,), 2015.

[48] L. Rogers and R. Monk, "Detection and monitoring of cracks in offshore structures," (Houston), pp. 35–46, Offshore Technology Conference, 1987.

[49] F. P. G. Márquez, A. M. Tobias, J. M. P. Pérez, and M. Papaelias, "Condition monitoring of wind turbines: Techniques and methods," *Renewable Energy*, pp. 169–178, 2012.

[50] P. Paris, M. Gomez, and W. Anderson, "A rational analytic theory of fatigue," *The Trend in Engineering*, pp. 9–14, 1961.

[51] P. Paris and F. Erdogan, "A critical analysis of crack propagation laws," *Journal of Basic Engineering*, pp. 528–534, 1963.

[52] A. Evans, M. Linzer, and L. Russell, "Acoustic emission and crack propagation in polycrystalline alumina," *Materials Science and Engineering*, pp. 253–261, 1974.

[53] A. Kahirdeh and M. Khonsari, "Energy dissipation in the course of the fatigue degradation: Mathematical derivation and experimental quantification," *International Journal of Solids & Structures*, pp. 74–85, 2015.

[54] *Damage testing, prevention and detection in aeronautics*. 2006.

[55] J. Mayrosh, "Experimental study of the attenuation of acoustic emission signals in welded steel structures. - theses and dissertations," tech. rep., 2001.

[56] P. A. Gaydecki, F. M. Burdekin, W. Damaj, D. G. John, and P. Payne, "The propagation and attenuation of medium-frequency ultrasonic waves in concrete: a signal analytical approach," *Measurement Science Technology*, pp. 126–134, 1992.

[57] J. Hazzard, S. Maxwell, and R. Young, "Micromechanical modeling of acoustic emissions," (Trondheim), pp. 519–526, Society of Petroleum Engineers, 1998.

[58] J. Hazzard and R. Young, "3d numerical modelling of acoustic emissions," (Toronto), 2002.

[59] M. Silk and K. Bainton, "The propagation in metal tubing of ultrasonic wave modes equivalent to lamb waves," *Ultrasonics*, pp. 11–19, 1979.

[60] R. F. d. Lucena and F. Taioli, "Rayleigh wave modeling: A study of dispersion curve sensitivity and methodology for falculating an initial model to be included in an inversion algorithm," *Journal of Applied Geophysics*, pp. 140–151, 2014.

[61] D. K. Tromp, C. Barnes, and J., "Wave propagation near a fluid-solid interface: a spectral element approach," *Geophysics*, vol. 65, no. 2, pp. 623–631, 2000.

[62] A. M. Zelenyak, M. A. Hamstad, and M. G. Sause, "Finite element modeling of acoustic emission signal propagation with various shapes waveguides," (Dresden), 2014.

[63] M. Hamstad, "Acoustic emission signals gerated by monopole (pencil-lead-break) versus dipole sources: Finite element method and experiments," *Journal of Acoustic Emission*, pp. 92–106, 2007.

[64] T. L. Richards, "Finite element analysis of structural-acoustic coupling in tyres," *Journal of Sound and Vibration*, pp. 235–243, 1991.

[65] R. Bernhard and J. Huff, "Structural-acoustic design at high frequency using the energy finite element method," *Journal of Vibration and Acoustics*, pp. 295–301, 1999.

[66] R. Bernhard and S. Wang, *Energy Finite Element Method*, pp. 287–306. Berlin, Heidelberg: Springer Berlin Heidelberg, 2008.

[67] M. Tanaka and Y. Masuda, "Boundary element method applied to certain structural-acoustic coupling problems," *Computer Methods in Applied Mechanics and Engineering*, pp. 225–234, 1988.

[68] S. H. Schot, "Eighty years of sommerfeld's radiation condition," *Historia mathematica*, vol. 19, no. 4, pp. 385–401, 1992.

[69] L. Rodríguez-Tembleque, J. A. González, and A. Cerrato, "Partitioned solution strategies for coupled bem-fem acoustic fluid-structure interaction problems," *Computers and Structures*, pp. 45–58, 2015.

[70] G. Liu, K. Dai, and T. Nguyen, "A smoothed finite element method for mechanics problems," *Computational Mechanics*, pp. 859–877, 2007.

[71] J. Dennis, A. Fournier, W. F. Spotz, A. St.-Cyr, m. A. Taylor, S. Thomas, and H. Tufo, "High resolution mesh convergence properties and parallel efficiency of a spectral element atmospheric dynamical core," *The Internation Journal of High Performance Computing Applications*, pp. 225–235, 2005.

[72] D. Komatitsch and J.-P. Vilotte, "The spectral element method: An efficient tool to simulate the seismic response of 2d and 3d geological structures," *Bulletin of the Seismological Society of America*, pp. 368–392, 1998 1998.

[73] E. Keen and L. Rogers, "Location of discrete sources of acoustis emission in complex tubular joints," (London), pp. 2984–3000, Pergamon Press, 1987.

[74] L. Dong, X. Li, and G. Xie, "An analytical solution for acoustic emission source location for known p wave velocity system," *Mathematical Problems in Engineering*, 2014.

[75] S. Spencer, "Closed-form analytical solution of the time difference of arrival source location problem for minimal element monitoring arrays," *Journal of the Acoustical Society fo America*, pp. 2943–2954, 2010.

[76] E. Robert and D. Jurg, "Acoustic emission source detection using the time reversal principle on dispersive waves in beams," pp. 87–92, Research Publishing, 2013.

[77] G. C. McLaskey, S. D. Glaser, and C. U. Grosse, "Beamforming array techniques for acoustic emission monitoring of large concrete structures," *Journal of Sound and Vibration*, pp. 2384–2394, 2010.

[78] C. U. Grosse, "Acoustic emission localization methods for large structures based on beamforming and array techniques," (Nantes), 2009.

[79] M. Ainslie, C. d. Jong, H. Dol, G. Blacquière, and C. Marasini, "Assessment of natural and anthropogenic sound sources and acoustic propagation in the north sea," tech. rep., 2009.

[80] W. Hufenbach, H. Richter, A. Langkamp, and R. Böhm, "Application of acoustic emission analysis for damage investigations in fibre and textile reinforced composites," in *Conference on Damage in Composite Materials: Non Destructive Testing and Simulation (CDCM06), Stuttgart*, vol. 18, Citeseer, 2006.

[81] L. Rogers and K. Stambaugh, "Application of acoustic emission technology for health monitoring of ship structures," *Ship Structure Committee*, 2014.

[82] T. Heindsmann, R. H. Smith, and A. Arneson, "Effect of rain upon underwater noise levels," *Acoustic Society of America*, pp. 378–379, 1955.

[83] C. Long, P. Lepper, and J. Flint, "Ultrasonic noise emissions from wind turbines: potential effects on bat species.," (London), pp. 907–913, Institute of Acoustics, 2011.

[84] A. Prosperetti and H. N. Oğuz, "The impact of drops on liquid surfaces and the underwater noise of rain," *Annual Review of Fluid Mechanics*, pp. 577–602, 1993.

[85] H. Medwin, J. A. Nystuen, P. W. Jacobus, L. H. Ostwald, and D. E. Snyder, "The anatomy of underwater rain noise," *The Journal of the Acoustical Society of America*, vol. 92, no. 3, pp. 1613–1623, 1992.

[86] C. D. Scofield, *Oscillating microbubbles created by water drops falling on fresh and salt water: amplitude, damping and the effects of temperature and salinity.* PhD thesis, Monterey, California. Naval Postgraduate School, 1992.

[87] J. Mitchell and L. Rogers, "Monitoring structural integrity of north sea production platforms by acoustic emission," (Houston), pp. 111–115, Offshore Technology Conference, 1992.

[88] T. Hayashi and D. Inoue, "Calculation of leaky lamb waves with a semi-analytical finite element method," *Ultrasonics*, vol. 54, no. 6, pp. 1460 – 1469, 2014.

[89] S. Marburg, *Discretization Requirements: How many Elements per Wavelength are Necessary?*, pp. 309–332. Berlin, Heidelberg: Springer Berlin Heidelberg, 2008.

[90] G. Seriani, E. Priolo, J. Carcione, and E. Padovani, "High-order spectral element method for elastic wave modeling," in *SEG Technical Program Expanded Abstracts 1992*, pp. 1285–1288, Society of Exploration Geophysicists, 1992.

[91] D. Komatitsch and J. Tromp, "Introduction to the spectral element method for three-dimensional seismic wave propagation," *Geophysical Journal International*, vol. 139, no. 3, pp. 806–822, 1999.

[92] D. Komatitsch and J. P. Vilotte, "The spectral-element method: an efficient tool to simulate the seismic response of 2D and 3D geological structures," vol. 88, no. 2, pp. 368–392, 1998.

[93] E. Faccioli, F. Maggio, R. Paolucci, and A. Quarteroni, "2d and 3d elastic wave propagation by a pseudo-spectral domain decomposition method," *Journal of seismology*, vol. 1, no. 3, pp. 237–251, 1997.

[94] R. Watkins, W. Cooper, A. Gillespie, and R. Pike, "The attenuation of lamb waves in the presence of a fluid," *Ultrasonics*, vol. 20, no. 6, pp. 257–264, 1982.

[95] A. Mohanty, S. Fatima, and M. Chandravanshi, "Effect of bubble size on underwater noise spectra," *Measurement*, vol. 60, pp. 258 – 266, 2015.

[96] J. A. Scrimger, D. J. Evans, G. A. McBean, D. M. Farmer, and B. R. Kerman, "Underwater noise due to rain, hail, and snow," *The Journal of the Acoustical Society of America*, vol. 81, no. 1, pp. 79–86, 1987.

[97] J. A. Nystuen, "Rainfall measurements using underwater ambient noise," *The Journal of the Acoustical Society of America*, vol. 79, no. 4, pp. 972–982, 1986.

[98] J. L. Quiroga, J. E. Quiroga, and R. Villamizar, "Influence of the coupling layer on low frequency ultrasonic propagation in a pca based stress monitoring," (Cartagena), NDTnet, 2015.

[99] S. Colombo, A. Giannopoulos, M. Forde, R. Hasson, and J. Mulholland, "Frequency response of different couplant materials for mounting transducers," *NDT& E International*, vol. 38, no. 3, pp. 187 – 193, 2005. Structural Faults and Repair.

[100] A. Nazari, Z. Guan, W. Daniel, and H. Gurgenci, "Parametric study of hot spot stresses around tubular joints with doubler plates," *Practice Periodical on Structural Design and Construction*, vol. 12, no. 1, pp. 38–47, 2007.

[101] W. Weijtens, N. Noppe, T. Verbelen, A. Iliopoulos, and C. Devriendt, "Offshore wind turbine foundation monitoring, extrapolating fatigue measurements from fleet leaders to the entire wind farm," *Journal of Physics*, vol. 753, 2016.

[102] M. de Jong, "Adaptations to a marine climate, salt and water owez_r_111_20101020," *Results corrosion inspections Offshorewind farm Egmond aan Zee*, vol. 2009, 2007.

[103] V. Davey, O. Forli, and G. Raine, *Non-destructive Examination of Underwater Welded Structures*. Woodhead Publishing online, Woodhead Publishing Limited, 1999.

[104] G. G. Hassan, "A guide to uk offshore wind operations and maintenance," tech. rep., 2013.

[105] A. May and D. McMillan, "Condition based maintenance for offshore wind turbines : the effects of false alarms from condition monitoring systems," in *Safety, Reliability and Risk Analysis: Beyond the Horizon* (R. D. J. M. Steenbergen, ed.), pp. 783–789, CRC Press, September 2013.

[106] Y. Bot and D. Azoulay, "Asset maintenance simulation: The case-study of an offshore wind farm," in *2015 Annual Reliability and Maintainability Symposium (RAMS)*, pp. 1–6, Jan 2015.

[107] J.-S. Chou and W.-T. Tu, "Failure analysis and risk management of a collapsed large wind turbine tower," *Engineering Failure Analysis*, vol. 18, no. 1, pp. 295 – 313, 2011.

[108] P. Tchakoua, R. Wamkeue, M. Ouhrouche, F. Slaoui-Hasnaoui, T. A. Tameghe, and G. Ekemb, "Wind turbine condition monitoring: State-of-the-art review, new trends, and future challenges," *Energies*, vol. 7, no. 4, pp. 1–36, 2014.

[109] N. Cosack, *Fatigue Load Monitoring with Standard Wind Turbine Signals*. PhD thesis, Faculty of Aerospace Engineering and Geodesy of the Universitat Stuttgart, 2010.

[110] IRENA, "Innovation outlook: Offshore wind," tech. rep., 2016.

[111] P. Wang and H. Pruppacher, "Acceleration to terminal velocity of cloud and raindrops," *Journal of Applied Meteorology*, vol. 16, no. 3, pp. 275–280, 1977.

[112] S. Adhikari and S. Bhattacharya, "Vibrations of wind-turbines considering soil-structure interaction," *Wind and Structures*, vol. 14, no. 2, p. 85, 2011.

[113] M. Sause, "Investigation of pencil lead breaks as acoustic emission sources," *Journal of Acoustic Emission*, pp. 184–196, 2011.